2003

Development of an FRP Reinforced Hardwood Glulam Guardrail

Joshua Keith Botting

DEVELOPMENT OF AN FRP REINFORCED HARDWOOD GLULAM GUARDRAIL

By

Joshua Keith Botting

B.S. University of Maine, 2001

A THESIS

Submitted in Partial Fulfillment of the

Requirements for the Degree of

Master of Science

(in Mechanical Engineering)

The Graduate School

The University of Maine

December, 2003

Advisory Committee:

William Davids, Assistant Professor of Civil Engineering, Advisor

Donald Grant, Chairman and R. C. Hill Professor of Mechanical Engineering

Michael Peterson, Associate Professor of Mechanical Engineering

DEVELOPMENT OF AN FRP REINFORCED HARDWOOD GLULAM GUARDRAIL

By Joshua Keith Botting

Thesis Advisor: Dr. William Davids

An Abstract of the Thesis Presented
in Partial Fulfillment of the Requirements for the
Degree of Master of Science
(in Mechanical Engineering)
December, 2003

This study focuses on the development of an aesthetically pleasing, cost-effective, timber guardrail system, which utilizes low-grade New England hardwoods such as red maple and beech. This required that several issues be addressed, including structural modeling, rail section design, rail fabrication, evaluation of durability, rail-to-rail field splice connection design, and the evaluation of guardrail system performance under impact loading.

The use of glulam beams in infrastructure is increasing rapidly with the reduced availability and increase in cost of high grade solid sawn timber. New techniques allow for increased material usage while maintaining a high strength product. Selective stacking of laminates, using finger jointed lumber, and using a brickwork layup were all techniques which were used to increase utilization of lower grade lumber. To enhance the system performance, the glulams are reinforced with fiber reinforced polymer (FRP). Using these techniques a glulam guardrail was developed, which is relatively light, durable, and should be capable of passing the

NCHRP Report 350, Test Level 3 crash test. The guardrail was evaluated through modeling and quasi static bending and tension testing.

To evaluate the effectiveness of the design under the Test Level 3 crash test, the test and rail system was modeled using the Barrier VII dynamic impact program. This demonstrated that the guardrail system is not only under large bending loads, but also encounters large tensile forces. This tension force will need to be transferred between rail sections by use of a splice connection, if the rail is to perform effectively. Glulam beams are not traditionally used for applications where it is necessary to transfer large tensile forces between members. Designing a high-strength bolted connection between both wood and composite members is inherently difficult due to their tendency to fracture. A solution was developed where steel connection plates were bonded to the ends of the rail sections during fabrication so that the field connection only requires bolting the rail to a steel splice plate.

The reinforced glulam maple guardrail system was tested in four ways to assess its performance. The first was an eccentrically loaded tension test, which was designed to test the rail splice connection. The second test was a simply supported three point bending test. From this test the modulus and section properties for the guardrail beams were determined. The third test which was performed was a combined bending and tension test to determine the response of the rail under actual impact loading conditions. Using the experimentally determined modulus, a model of the beam under combined bending-tension was used to design a reaction frame. This reaction frame induced tension in the rail by restraining the shortening of the rail due

to bending. The durability of the rail and splice design was evaluated for exterior exposure using the ASTM D1101-A delamination test.

The major conclusions of the study are that the FRP-reinforced hardwood glulam guardrail appears to be capable of passing an actual crash test, and that the rail is a cost effective alternative to existing timber guardrail systems.

ACKNOWLEDGEMENTS

I would like to thank those who have helped with this study. I would like to thank both of the R.E.U. students who have assisted me: Stephen Cotton for performing the background work for this study and Chad Gibson for assisting in the fabrication and splice connection design. I would also like to thank fellow graduate students Matthew Richie and Eric Cassidy for their assistance in fabricating the beams.

I would like to thank the New England Transportation Consortium for their generosity in funding the research which I have done. I would also like to thank Don Forest of Gordon Composites for his assistance on this project and Mark Quarantiello of Sovereign Specialty Chemicals for donating all of the SIA E2119 epoxy used in this study. I would also like to thank Robert Kaseguma and Floyd Spencer from Unadilla Laminated Products of Unadilla, New York, for cutting finger joints in the large lumber used in this project. Further, I would like to thank James Alexander, Jr. for his assistance in the development and fabrication of the combined bending and tension fixture.

I would like to thank my committee for their support. Most of all I would like to thank my advisor William Davids, for his ideas, support, knowledge, and most of all patience throughout the last two and a half years.

TABLE OF CONTENTS

LIST OF TABLES

LIST OF FIGURES

Chapter 1

INTRODUCTION

1.1 Background

Guardrails are a common sight along roads and highways, and are designed to protect motorists from certain dangers along the roadside. The most commonly used guardrail is the steel W-beam. The W-beam is used because it is inexpensive, its behavior is well understood, it is durable, and it is easily installed. However, steel W-beam rail is considered an eyesore by some motorists. This is especially true along scenic highways, where wooden guardrails are thought to be a much more aesthetically pleasing alternative to steel rails.

This study focuses on the development of an aesthetically pleasing, cost-effective, timber guardrail system which utilizes low-grade New England hardwoods such as red maple and beech. In order to be accepted for highway application, the rail must be capable of passing the NCHRP test level 3 crash test (NCHRP, 1993), and be easily installed using a standard post spacing of 1.83-m. These obstacles required that several issues be addressed, including structural modeling, designing the rail section, fabricating the rail specimens, evaluating the durability of the rail design, developing a rail-to-rail field splice, and assessing the guardrail system performance under impact. The remainder of this chapter will provide an overview of these issues and an outline of this thesis.

1.2 Guardrail Overview

The design of traditional guardrail systems is a challenging problem. There are many factors to consider while designing the system. The types of hardware and soil properties are critical factors which determine the performance of the system. The problem is further complicated by the use of wood in the rail systems. However, there are several commonly used wooden rail systems on highways today.

Two wooden guardrail systems were examined: logs with embedded steel channels, and the Merritt Parkway guardrail system, also known as the steel backed timber rail, which consists of a solid sawn beam of southern pine with a steel backing plate. In both of these wooden rail systems, the steel is used to carry the tension developed in the rail under vehicular impact. However, drawbacks exist in all wooden guardrail designs currently in use. In the guardrail systems that use logs with embedded steel channels, the logs can add a variable of uncertainty to the system. The shape and size variations inherent in the logs can cause a vehicle to deflect above or below the barrier more easily. Further, the cost of replacing the relatively large solid sawn timbers, such as in the Merritt Parkway system, when damaged is increasingly rapidly, while the availability of large clear sections of structural softwood is decreasing rapidly.

The proposed guardrail system that is developed in this thesis uses a reinforced glulam rail section fabricated from readily available mixed hardwoods (primarily red maple) and reinforced with FRP, as shown in Figure 1.1:

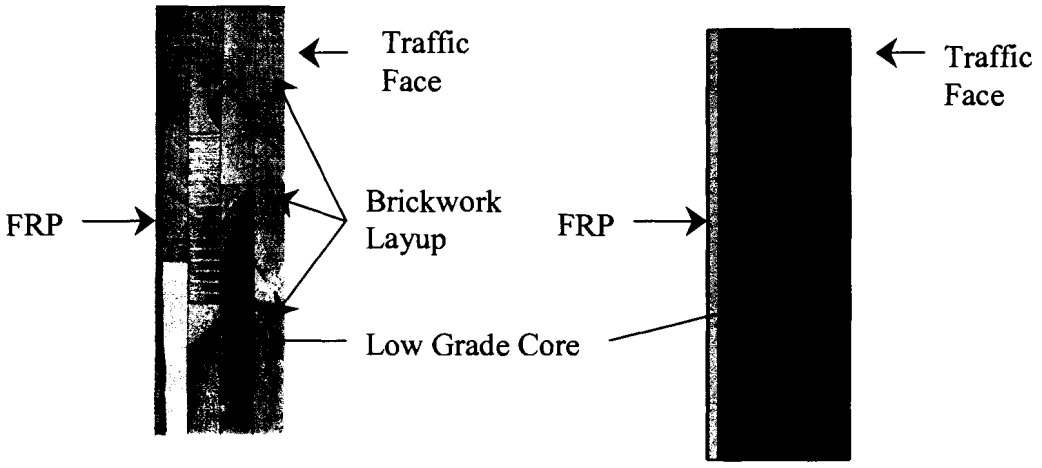

Figure 1.1 Glulam Guardrail Cross-Section

The guardrail rail sections were designed, modeled, and fabricated in 3.658-m lengths. A splice connection was also designed to join adjacent rail sections. This splice connection was included in the modeling of the guardrail system. The wooden side of the reinforced guardrail faces traffic. The post spacing which was used was 1.83-m. The rail was mounted with the center of the rail 635-mm above the grade. The system layout is displayed in Figure 1.2. Once the system layout was established, the next step was to model the system.

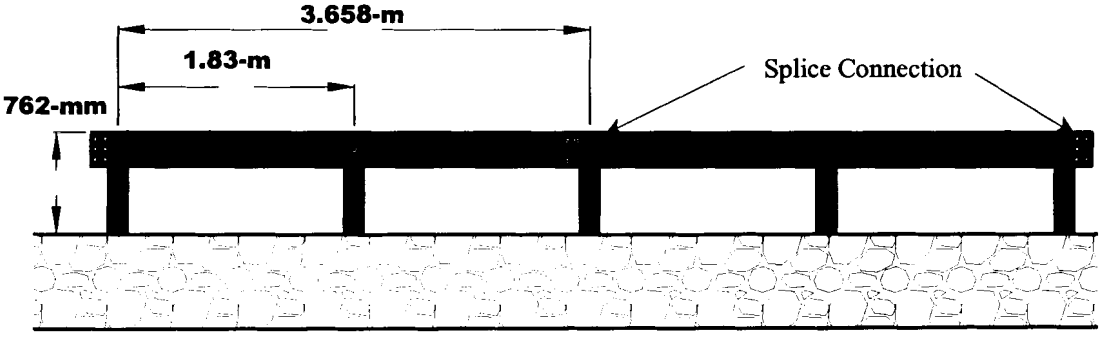

Figure 1.2 Glulam Guardrail Layout

The successful development of this guardrail required that several major issues be addressed. First, the structural response of the guardrail under vehicular impact had to be determined. The critical design parameters are the rail ductility and

tensile capacity. The modeling of the guardrail is covered in Chapter 2. Second, the rail cross-section had to be sized, and issues regarding fabrication of this rail had to be addressed as discussed in Chapter 3. Chapter 4 discusses the bending tests conducted to access the flexural characteristics of the rail. Chapter 5 focuses on the design and testing of the bolted field splice connection that is critical for transferring the tension between adjacent 3.658-m sections of rail. Chapter 6 presents the development and results of the critical flexure-tension tests that were designed to produce loads similar to those experienced by a guardrail under vehicular impact. Finally, Chapter 7 presents a summary of the work performed and the conclusions reached in this study.

Chapter 2

GUARDRAIL MODELING

2.1 Introduction

This chapter provides an overview of guardrail systems currently in use and the techniques used to model guardrail systems. First, the types of guardrail systems are discussed followed by a detailed discussion of existing wooden guardrail systems. Then the method of modeling the FRP-reinforced glulam guardrail cross-section is discussed. Finally, the modeling of the guardrail system under vehicular impact is discussed and the expected peak axial loads on the guardrail are estimated. The axial load induced due to vehicular impact is critical for the designing the guardrail splice connection as discussed in Chapter 5.

2.2 General Overview

Guardrails are a common sight along highways. The purpose of a guardrail is to redirect errant traffic safely away from obstacles without causing injury to the occupants. There are many variations on the basic design of a guardrail system. The three major components of a guardrail system are the soil, post-blockout, and the rail itself. The combination of these components determines the behavior of the system under vehicular impact (Patzner, 1998). This study focuses solely on the development of the rail section.

2.3 Guardrail Systems

The two major types of flexible beam guardrail systems are steel and wooden beams. The majority of the guardrails currently used along highways are steel beams.

There are two basic types of steel guardrail: the W-beam and the Thrie beam. These steel beams act as tension ribbons when impacted, as discussed later in the chapter.

Wood is a common material for use in roadside barriers. However, wood is most commonly used in guardrail systems in blockouts and posts. Wood is attractive for its use in posts due to its relatively large cross-section and low strength as compared to a steel post. The increased surface area allows the post to develop larger soil reactions, while the lower strength causes the post to snap and reduce snagging potential which is not possible with steel posts. However, wood is not commonly used for guardrail beams. Plain wood is not an effective material for use in rail sections due to its low load capacity and brittle failure mechanism. However, wood is attractive for use in guardrail systems for its aesthetic value. There are several variations of wooden guardrail systems. A key element of the wooden guardrail systems currently in use is that they all use a steel backing, which provides ductility and transfers tensile loads through the systems. Two such systems are discussed in this section: the Merritt Parkway and the IRONWOOD systems.

2.3.1 Guardrail Failure Criterion

In order to compare the types of guardrails it is important to understand how a guardrail system functions. During an impact, energy passes from the vehicle into the rail, from the rail through the blockouts, into the post, and into the soil. A single post cannot transfer all of the energy of the system into the soil. Instead, all of the posts in the system and the terminals transfer a portion of the energy into the soil. There are several different failure methods which can occur under vehicular impacts. Guardrails and the failure criterion which apply to them are designed specifically to pass the

NCHRP 350 Test Level 3 crash test. Guardrails are not designed to withstand high speed perpendicular impacts. Most of the impacts which occur at high speeds do not impact the rail at large angles. Therefore, the purpose of a guardrail is to redirect errant vehicles back onto the road without causing significant injuries to the occupants of the vehicle. If the vehicle ruptures the system, the guardrail has failed. If the guardrail system is too stiff, the vehicle will decelerate too rapidly causing injury to the occupants. If the guardrail system deforms such that the vehicle is not allowed to return to traffic, then the guardrail fails. This is known as a pocketing failure and usually results high decelerations resulting in occupant injury (Patzner,1998). Pocketing generally occurs when the system is not stiff enough. The most dangerous failure method of a guardrail system is snagging. Snagging occurs when part of the vehicle, usually the bumper or wheel, impacts a post and the post does not fail. By snagging a post, the vehicle can be caused to flip over the barrier. If the vehicle does not flip, there is also danger of large impulse forces on the occupants due to impacting the posts. The posts are designed such that during a crash the loads in the posts approach their capacity in the area of the impact so that if the vehicle does impact the post directly, the post will snap with minimal additional force. The behavior of the guardrail system is controlled by the stiffness of the rail, post, and soil.

2.3.2 Steel Guardrails

In steel guardrail systems the rail primarily performs as a tension ribbon. The three most commonly used types of steel guardrail systems are the W-beam, Thrie beam, and cable. When compared with the loads which are encountered during a

vehicular impact, the bending stiffness of all three steel barrier systems is very low. Further, there is essentially no bending stiffness in the cable guardrail systems. In addition, at the area of impact the W-beam and Thrie beam rails are crushed which reduces the effective moment of inertia and effectively the bending stiffness. Due to the relatively low bending stiffness and the ductility of the steel, these systems act as tension ribbons. The majority of the energy from the impact is transferred to the post and ultimately into the soil, through tensile forces in the guardrail system. Cable guardrails are not commonly used due to their large snagging potential. The W-beam is the most commonly used guardrail system. The depth of the W-beam rails is 305-mm. The Thrie beam is a deeper version of the W-beam, with a depth of 506-mm. Both the W-beam and Thrie beam are available in various thicknesses depending on the application. The typical installed cost of the W-beam 3C is $44/m (Maine Department of Transportation, 2003), which varies slightly depending on the length and degree of curvature in the rail.

2.3.3 Merritt Parkway Guardrail System

Wooden guardrail systems are used in many applications to provide a more aesthetically pleasing alternative to the traditional steel guardrails. The concept which is used in most of the currently available wooden guardrails is steel reinforced timber rail. This concept is used on the Merritt Parkway Guardrail (MPG) system, also known as the steel backed timber guardrail (Lohrey, 1997). The MPG system uses a 306-mm by 152-mm solid rough sawn southern pine or douglas fir wooden section with a 152-mm by 9.5-mm steel backing plate bolted to the wooden section. The wooden beam exists for aesthetic purpose and also acts as a bumper to catch the

vehicle and transfer the loads into the steel backing. The wood is not efficiently utilized in the guardrail. The steel backing behaves similar to a W-beam. The 9.5-mm thick steel backing adds considerable mass to the system, 42 kg for the 3.658-m rail section. The mass of the wooden section of the rail is approximately 100 kg for the 3.658-m rail length. In addition to the Merritt Parkway Guardrail being heavy, it is also more than three times as expensive as the W-beam, with an installed cost of $150/m (Maine Department of Transportation, 2002).

2.3.4 IRONWOOD Guardrail System

The IRONWOOD guardrail system is another steel backed timber guardrail system that is similar in concept to the Merritt Parkway Guardrail system. The IRONWOOD system consists of a 200-mm diameter round timber of iron wood with a 6-mm thick steel channel embedded in and bolted to the timber. The IRONWOOD guardrail system passed the NCHRP Report 350 Test Level 3 crash test (New York State Department of Transportation, 2000). The IRONWOOD system uses the rounded timber to catch the vehicle and transfer the energy of impact into the steel channel. In this system the wood is not used as a structural element of the guardrail, instead it is used primarily as a bumper and for aesthetic purposes. The IRONWOOD system costs $180/m (New York State Department of Transportation, 2000).

2.4 Transformed-Section Analysis

In order to determine the properties of the reinforced timber rail cross-section, a transformed section analysis was used to determine the stiffness and the capacity of the rail cross-section design. The maple was assumed to have a linearly-elastic stress-strain response in both tension and compression. While wood will yield under

compression, no acceptable prediction of the yielding, experimental or empirical, was found to quantify the extent of yielding or yielding behavior of red maple. Therefore, for the initial stiffness and capacity analysis, the effect of compressive yielding of the glulam was neglected. The properties which were used in the transformed section analyses were those published in the Wood Handbook (Wood Handbook, 1999) for red maple at 12% moisture content, an elastic modulus of 11.3 GPa, and a modulus of rupture of 92 MPa. The modulus of rupture is maximum tensile stress in the wood at a bending failure (Wood Handbook, 1999). The wood is assumed to be linearly-elastic until failure. The FRP was treated as linearly-elastic in both tension and compression. The modulus which was used for the FRP was the average tensile elastic modulus for the Gordon Composites GC-67-UB unidirectional E-glass bar stock, 40 GPa. The tensile strength which was used for the FRP was the average tensile strength for the GC-67-UB, 950 MPa (Gordon Composites, Inc., 2001). The yield moments which were calculated as the moment which caused the first tensile failure in the wood.

2.5 Guardrail Modeling

Since the 1960's a number of guardrail modeling programs have been developed in order to evaluate the behavior of guardrails systems, or individual guardrail hardware items under vehicular impact. The current generation of guardrail modeling uses explicit nonlinear dynamic finite element software such as LS-DYNA3D (Patzner, 1998). Such models are often used in the development of guardrail terminals. The finite element models use detailed models of the impact vehicle, the soil, the posts, and the rails. Even with these complicated models, it is

still not possible to exactly model a reinforced glulam beam. The 3D nonlinear stress-strain response of wood is not well understood. It is computationally costly to model the system using the appropriate material models in 3D finite element packages (Patzner, 1998). In addition, modeling the system using LS-DYNAD3D or other comparable software would require additional time, expertise, and computer hardware. For these reasons, a three-dimensional model was not used to model the reinforced glulam guardrail system.

In order to evaluate the design of a reinforced glulam guardrail design, the guardrail systems were modeled using a dynamic finite element modeling program, Barrier VII (Powell, 1973) developed at the University of California, Berkeley. Barrier VII is a commonly used finite element program which is used to evaluate guardrail systems (Taun,1989; Rosson, 1996). Barrier VII is a simple two-dimensional finite-element modeling tool which incorporates flexural elements to model the guardrail, springs to model the posts, springs and dampers for modeling the soil, and is ideal for modeling the geometry of the system. The Barrier VII program also assumes an elastic plastic response of the rail section with a final failure point. This can be representative of the behavior of reinforced glulams with large amounts of reinforcement, due to the compressive yielding of the wood. The NCHRP Report 350 also recommends the use of Barrier VII for initial modeling of guardrail systems (NCHRP, 1993). Due to the simplicity of implementation and its wide acceptance, the Barrier VII program was used to model the guardrail system.

2.5.1 Barrier VII

The Barrier VII program is a finite element program which models a vehicle impacting a deformable rail system. The Barrier VII program will allow several different types of rail elements, beams, cables, posts, springs, dampers, and hinges. Barrier VII models the interaction of the vehicle, barrier, posts, soil, tires, and the vehicle sliding along the rail. The vehicle is modeled as a mass body with springs which interact with the barriers. The system is modeled as a dynamic, inelastic, geometrically nonlinear, large deformation, two-dimensional structural analysis problem. This program is best used for situations when roll and pitch of the vehicle are negligible, which is assumed to be the case for the model used to validate the reinforced glulam guardrail. Barrier VII is useful for predicting the maximum loads on the components of the barrier system (NCHRP, 1993).

2.5.2 Crash Test

The crash test which was modeled was the NCHRP Report 350 Test Level 3-11 (NCHRP, 1993). The 3-11 test uses a 2000P vehicle, which is a 2000 kg pickup truck, typically a ¾ ton model which is one of the top two models in sales for the model year. This test was chosen as a basis for the worst case scenario for all of the available Test Level 3 (TL-3) tests. The vehicle strikes the barrier at a speed of 100 km/hr and an angle of 25°. This test is intended to test the structural integrity of the rail section.

2.5.3 System Model

The system which was modeled was 47.5-m long, which is greater than the minimum length of 30-m specified for a TL-3 crash test. The minimum

recommended length of guardrail which should be modeled is 45.7-m (Calcote, 1978). W6X15 steel posts 1.8-m long and spaced 1.8-m on center were assumed in the analysis. The terminal post at one end of the system was anchored, and the other end post was free to displace in the soil. The soil spring stiffness which was used in Barrier VII was 440 kN/m (Calcote, 1978). All of the Barrier VII models use a damping multiplier for rigid body rotation of 1.4. This damping factor was found to increase the stability of the model. The vehicle impacts the rail near the center, 22.86-m from the end, half way between the two central posts. The reinforced glulam rail sections were modeled as 3.505-m beams connected to the post, with 76-mm long by 13-mm thick steel plates connecting the rail sections to the post and adjacent rail sections at either end of the beams. This steel plate models the splice connection which is discussed in Chapter 5. The moment capacity and bending rigidity of this steel plate is significantly smaller than the reinforced rail sections, and therefore the plates effectively act as a yielding hinge in the system which reflects the actual behavior of the splice connection. All of the rail elements are assumed to have an elastic-plastic response by Barrier VII.

2.5.4 Element Length Convergence Study

In order to determine the appropriate size of the reinforced glulam beam elements used to model the system, a convergence study was performed with several different element lengths. The convergence study was performed using the properties of the 114-mm deep cross-section with 3% FRP reinforcement. The modulus which was used for the section was 11.3 GPa (Wood Hand Book, 1999). The yield moment which was used in Barrier VII for the element length convergence study was 73 kN-

m. This yield moment was based on a transformed section analysis, where the yield moment was found as the moment which induced a tensile failure in the wood. The moment of inertia, which was used in the element length convergence was $41.2*10^6$ – mm^4. The transformed area of the reinforced glulam which was used in the Barrier VII element length convergence study was 0.032 m^2. These properties were developed using a transformed section analysis, as discussed previously. A post spacing of 1.83-m was used in all of the modeling. The layout of the system is seen in Figure 2.1:

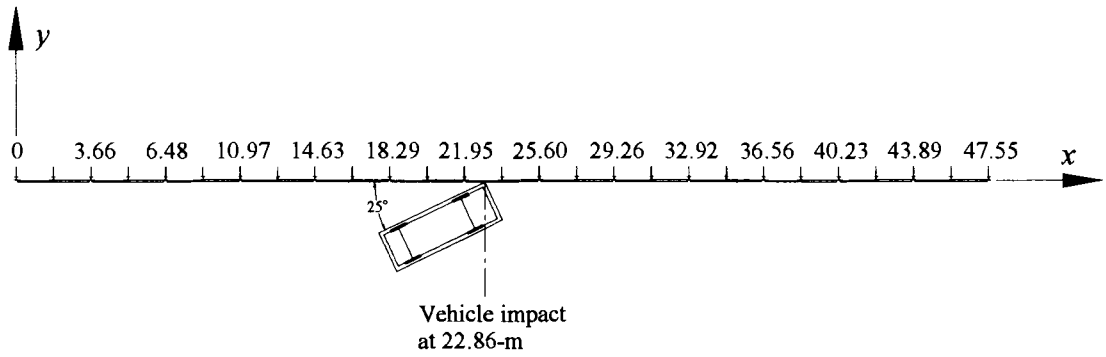

Figure 2.1 Guardrail System Layout (all dimensions in meters)

The largest simulation which was successfully run involved 339 nodes, and 365 elements. Four different guardrail element lengths of 914-mm, 457-mm, 228.5-mm, and 152-mm were used. The guardrail element lengths are the lengths of the majority of the elements in the system, but there is a 76-mm shorter transition element at each end of the rail section to incorporate the splice connection. The 914-mm node spacing for a typical 3.658-m rail is displayed in Figure 2.2:

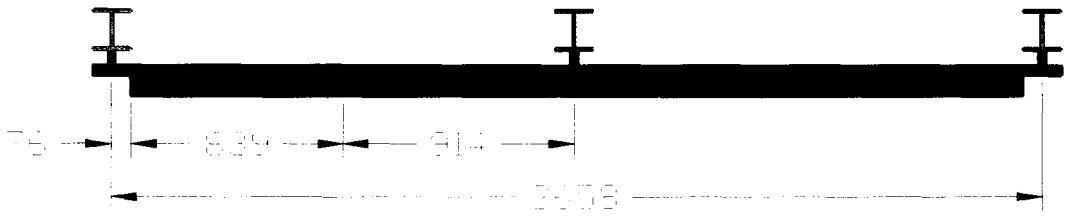

Figure 2.2 914-mm Element Layout (all dimensions in mm)

A typical element layout for the 457-mm element length is displayed in Figure 2.3:

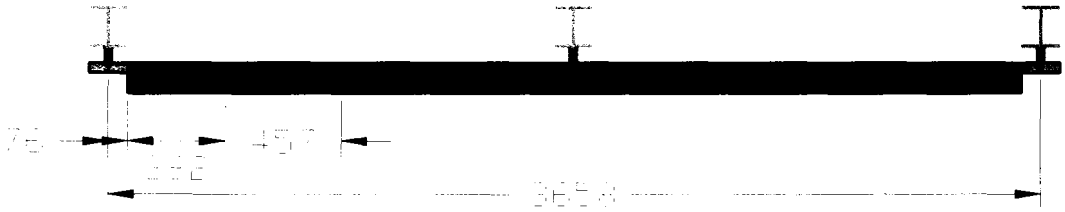

Figure 2.3 457-mm Element Layout (all dimensions in mm)

A typical element layout for the 228.5-mm element length is displayed in Figure 2.4:

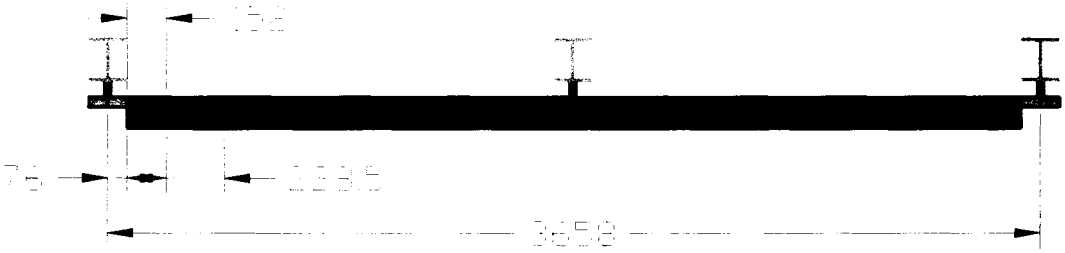

Figure 2.4 228.5-mm Element Layout (all dimensions in mm)

A typical element layout for the 152-mm element length is displayed in Figure 2.5:

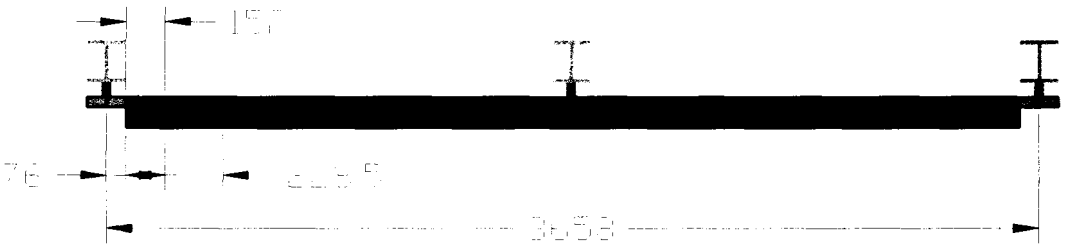

Figure 2.5 152-mm Element Layout (all dimensions in mm)

In order to incorporate smaller elements into the system without greatly increasing the number of elements and the run time of the program, an additional trial was run using

152-mm elements from x coordinates of 18.288-m to 32.918-m and 457-mm elements for the remaining length of the system. At element lengths of less than 152-mm, the model became numerically unstable.

The vehicle impacts mid-span between posts at 22.86-m from the beginning of the guardrail system at 25°, to approximate the worst case-loading scenario on the rail section. The time step which is used in the element length convergence study is 0.0001 s. The x direction displacements for the rail at 23.774-m are compared to demonstrate the convergence of the system. The node at 23.774-m is the first splice-post connection after the impact point. The effect of the difference in element length is cumulative, and is therefore more apparent toward the end of the simulation. There is a variation in the duration of the impact for the varying element length, therefore the results are only compared between the beginning of the simulation and 0.3 sec. The results of the element length convergence study for the x displacement at 23.774-m are shown in Figure 2.6:

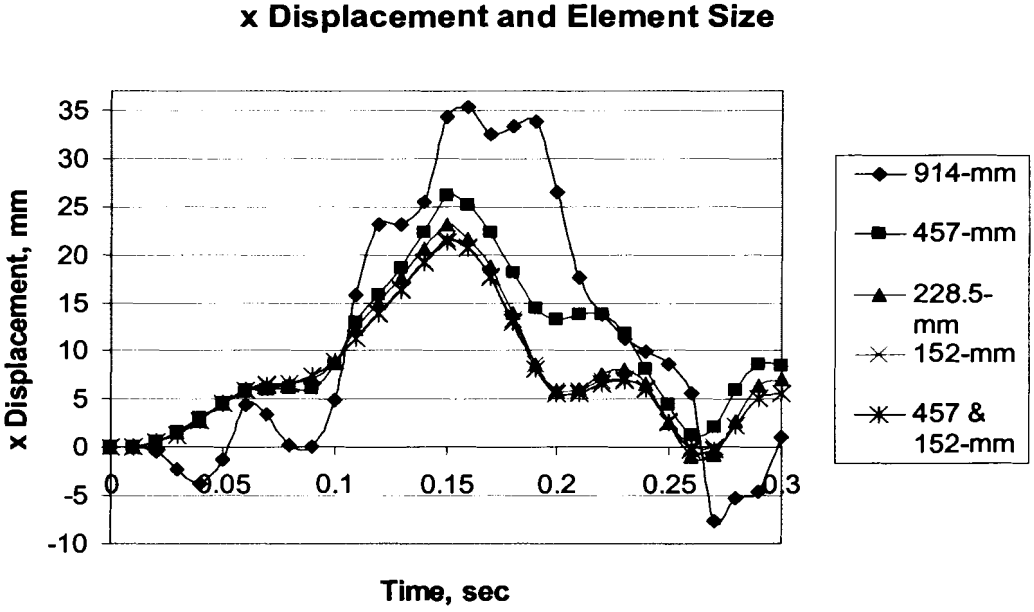

Figure 2.6 x Direction Displacements Through Time

The solution clearly converges with an element length of 152-mm in the area of impact. There is very little difference between the models with an element length of 152-mm for the entire system and the model with 152-mm elements only in the area of impact. The model with 228-mm elements across the entire length varied only slightly from the model using the 152-mm elements. Barrier VII terminates when the vehicle has been out of contact with the barrier for 600 time steps. The 600 time steps were subtracted from the time at the end of the test to determine the duration of the impact. The duration of impact was also affected by the element length used in the model. Figure 2.7 shows the relation between guardrail element length and duration of the impact:

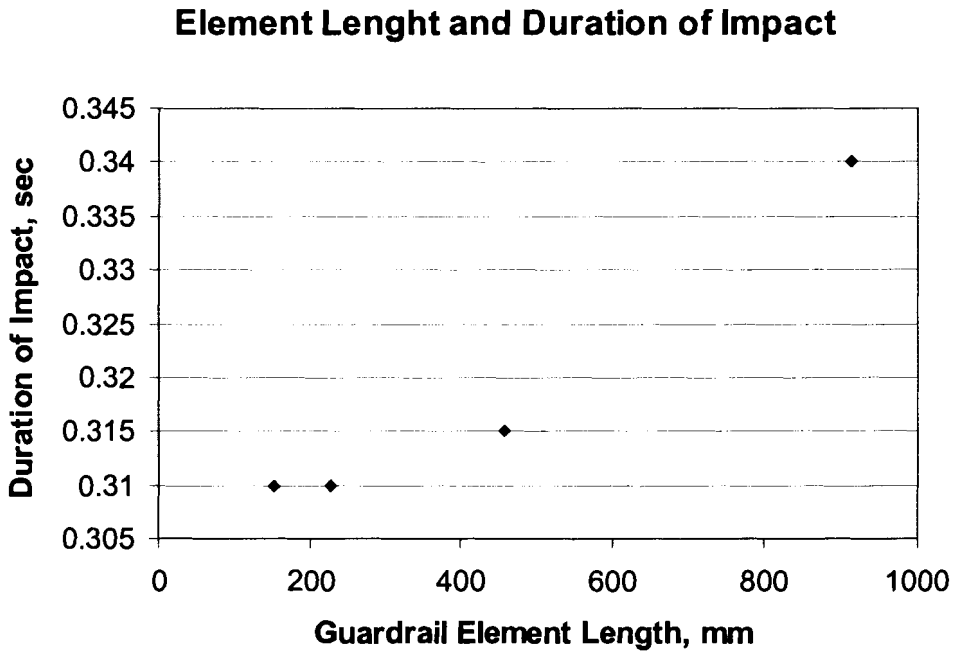

Figure 2.7 Convergence of Impact Duration and Element Length

The duration of impact clearly converges to a time of 0.31 sec. This value occurs with the element lengths of 152-mm and 228-mm. The model with 457-mm elements with 152-mm elements near the impact region also has a duration of impact of 0.31

seconds. Based on the convergence studies, the element size which was used to perform the analysis of the system was selected to be the split system with the 152-mm elements from x coordinates of 18.288-m to 32.918-m and 457-mm elements for the remaining length of the system.

2.5.5 Time Step Convergence Study

In addition to the size of the elements used to model the system, a convergence study was performed to determine the most appropriate time step. The recommended time step for Barrier VII is usually between 0.01 s and 0.005 s (Powell, 1973). However, it is recommended to use smaller time steps when the stiffness of the system and speed of the vehicle are increased. The stiffness of the reinforced glulam guardrail system is higher than that of the standard W-beam and further, the TL-3 crash test speed of 100-km/hr is relatively high. Therefore, smaller time steps were investigated. Further, at time steps greater than 0.001 seconds the system became unstable and the vehicle loses contact with the barrier suddenly. Therefore, five time steps were used in the convergence study, 0.00001 s, 0.00005 s, 0.0001 s, 0.0005 s, and 0.001s. The convergence analyses showed that the duration of the impact did not vary for any of the time steps considered, and the time step does not affect the behavior of the Barrier VII model within the limits considered. However, the larger time steps show more noise than the smaller time steps. This is most apparent when looking at the axial force in the guardrail splice connection, at the first splice after the impact point, which is a critical design parameter, as shown in Figure 2.8:

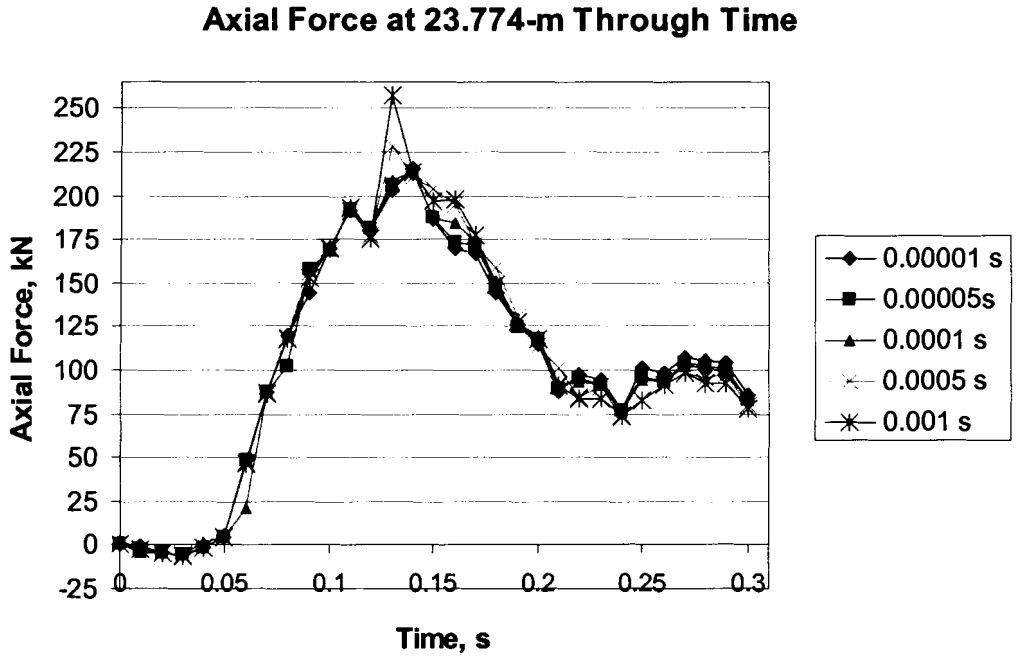

Figure 2.8 Axial Force at 23.774-m for Various Time Steps

Figure 2.8 shows that at time steps of greater than 0.0001 the axial load spikes at 0.13 s and appears to over-estimate the force in the splice. However, there is very little change in the maximum force predicted for the remaining time steps. Based on the time step convergence analyses, a time step of 0.0001 s was used to do the analysis of the reinforced glulam guardrail system.

2.5.6 Reinforced Guardrail Analysis

Barrier VII analyses were performed on three reinforced glulam cross-section designs. The original design was a 152-mm thick glulam with 3% reinforcement by volume. A lighter design consisting of a 114-mm thick glulam with 3% reinforcement by volume was also considered. The final design modeled was a 76-mm thick glulam with a 3.5-mm thickness of reinforcement (4.7%). Each of these cross-sections was analyzed with the transformed section method using the properties which were previously discussed in this chapter to get the flexural stiffness, and yield

moments. The properties, which were used in the Barrier VII modeling are reported in Table 2.1:

Beam	Bending Rigidity, MN-m^2	Moment of Inertia, 10^6 mm^4	Transformed Area, m^2	Yield Moment , kN-m	Weight per m, kg
152-mm	1.105	97.7	0.0428	130	20.8
114-mm	0.467	41.3	0.0321	73	15.6
76-mm	0.155	13.7	0.0225	40	10.4
W-beam	0.191	0.95	0.0013	8	10.3

Table 2.1 Cross-Section Properties

The bending rigidity displayed in Table 2.1 is E. The yield moments given in Table 2.1 for the reinforced glulam cross sections are the moments at the first predicted failure of a tension lamination. The analyses indicate that the rails yield in bending at the impact point in all cases considered. Therefore, the rail section must retain additional capacity after failure. Through the analysis it became apparent that a large axial force is induced in the rail as shown in Figure 2.9:

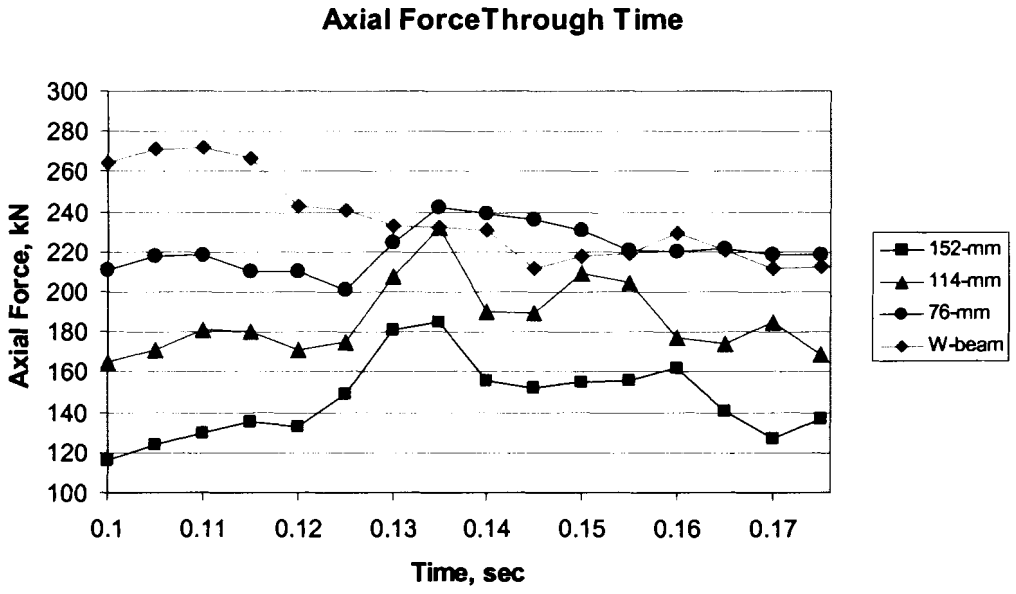

Figure 2.9 Maximum Axial Force in the Splice Connection Through Time

Figure 2.9 shows the maximum force in the splice connections through the time when the forces are the highest. The results are also displayed for a 12 gauge W-beam guardrail tested under the same system configuration as the reinforced rail sections. The force values which are displayed for the W-beam guardrail are the maximum force in the rail since there are no splices modeled for the W-beam. As the beam stiffness decreases, the axial forces increase and the deflections of the rail increase as well. See Table 2.2:

Cross-Section	Maximum Axial Force, kN	Maximum Longitudinal Displacement, mm	Maximum Lateral Displacement, mm	Maximum Acceleration, g
152-mm	185	33.782	432.308	11.5
114-mm	209	37.846	488.95	10.31
76-mm	242	50.292	572.262	11.05
W-beam	271	93.472	626.872	11.17

Table 2.2 Summary of Barrier VII Analysis

The lateral displacements which are reported in Table 2.2 are the total displacements of the rail in the *y*, lateral, direction, not the displacements of the rail relative to the posts. The accelerations which are reported in Table 2.2 are the resultant of *x* and *y* accelerations on the vehicle due to the impact with the rail. The vehicle accelerations for all of the reinforced glulam cross sections are less than the accelerations predicted for the W-beam rail under the same crash test, which is a good indicator of acceptable crash test. The lateral displacements of the wood-FRP rail systems are also less than those for the W-beam, which is indicative of acceptable performance.

2.6 Conclusions

By using a transformed section analysis and the Barrier VII modeling tool, analyses were performed on several reinforced guardrail sections. These analyses predict that the rail sections will reach the flexural capacity at the area of impact and that large tensile loads are induced in the rail section due to impact. The vehicle accelerations and lateral displacements which occur during the vehicular impact are comparable to those for the same rail system using a standard W-Beam guardrail. The 76-mm deep reinforced hardwood glulam guardrail cross-section behaves similar to the standard steel W-beam and therefore should be capable of passing the NCHRP 350 Test Level 3 crash test. The critical result of the analyses is that the guardrail section and splice connection must be capable of carrying a tensile force of approximately 240 kN. This large tensile force is the major design constrain on the development of the reinforced hardwood glulam guardrail which results in the development of a specialized splice connection to transfer the force between adjacent rail sections.

Chapter 3

REINFORCED GUARDRAIL SECTION DESIGN, FABRICATION, AND DURABILITY TESTING

3.1 Introduction

Modeling with Barrier VII, as discussed in Chapter 2, has shown that during a vehicular impact, a guardrail system experiences combined bending and tension loading. This chapter presents the design of a reinforced rail section to carry both bending and tension loads.

As discussed in Chapter 2, existing steel-backed timber guardrails such as those used on the Merritt Parkway utilize a heavy, solid timber section with a steel backing plate. The timber acts as a bumper and the steel plate serves as a continuous tension ribbon. The objective for this chapter is to develop an FRP-backed wooden glulam rail that performs adequately under the NCHRP Test Level 3 crash test conditions. The remainder of this chapter focuses on the development of the guardrail cross section, including geometry and material selection.

3.2 Reinforced Cross-Section Design

In order to design the cross-section, the guardrail must be sized, the species of wood must be selected, the amount and type of reinforcement must be selected, and the size and number of lamination must be defined.

The FRP-reinforced rail section discussed in this chapter is similar to the Merritt Parkway Guardrail rail section discussed in Chapter 2. However, the design

of the FRP reinforced glulam uses low-grade hardwood laminations instead of the expensive and heavy solid sawn timber and FRP tensile reinforcement in lieu of steel.

3.2.1 Sizing of Guardrail

The guardrail must be capable of catching all types of vehicles with bumpers of varying heights. The IRONWOOD rail section discussed in Chapter 2 uses a 200-mm diameter round timber to catch the vehicles. The Merritt Parkway Guardrail (MPG) rail and the standard steel W-beam both use a section depth of 305-mm to catch vehicles. The reinforced hardwood guardrail system designed uses a glulam of depth 254-mm, which is intermediate between that of the Merritt Parkway Guardrail and the IRONWOOD rail systems. This value was deemed to be appropriate to account for a variance in mounting height, which is not available with the IRONWOOD system, and to reduce the size, cost, and weight of the glulam section.

3.2.2 Reinforcement

In order to design the glulam cross-section, the type of FRP used in the reinforced glulam needed to be selected. There are many different types of FRP which have been evaluated for bonding to wood. These types can be divided into two main categories: prefabricated and wet layup. The wet layup of FRP application consists of applying a fabric of fibers across the surface that is being reinforced and applying resin to the fabric through various means. There are two main types of wet layup: hand layup and vacuum assisted resin transfer (SCRIMP, VARTM, ect.). The hand layup consists of applying the resin to the fabric by using hand rollers to force the resin into the fabric. The vacuum assisted methods use a vacuum to pull the resin into the fabric. These methods result in a good FRP-wood bond but require an

additional cost in the fabrication to attach the FRP. Also, good quality control on FRP fabricated with wet layups can be difficult to achieve due to the inherent difficulty of achieving the vacuum on the part being fabricated as well as maintaining fiber orientation during both hand layup and vacuum impregnation.

An additional option is prefabricated FRP sheets. The quality control for prefabricated sheets of FRP is very high. However, one drawback to the prefabricated sheets is that they require additional steps to attach FRP to the wood. Based on other work performed at the University of Maine (Lopez-Anido, 2001), it has been shown that it is possible to bond the FRP to softwoods using a Hydroxymethylated Resorcinol, (HMR), primer and FPL-1 epoxy. Although the HMR and FPL-1 reinforcement system had not previously been used with hardwood glulams the prefabricated FRP attached with the FPL-1 epoxy was chosen to reinforce the glulam guardrail.

There are many different types of prefabricated FRP reinforcement which can be used to reinforce glulam. A unidirectional E-glass epoxy Gordon Composites laminate was selected based on other work performed at the AEWC Center. The laminate selected was the Gordon Composites GC-67-UB Unidirectional Fiberglass Bar Stock (Gordon Composites, Inc., 2001). The bar stock was selected based upon the dimensions of product which were required.

3.2.3 Species Selection

The species of wood to be used for the glulam was limited to the native species of eastern hemlock, red pine, red maple, and spruce-pine-fir. The species which were selected were red maple and mixed hardwoods. The hardwoods were

selected based on ongoing research conducted at the University of Maine by Engineered Materials of Maine, which produces structural hardwood glulam beams using mixed hardwoods with a phenol-resorcinol-formaldehyde (PRF) resin system. A brickwork lay-up was chosen for the guardrail system because it allows the use of multiple narrower pieces of wood to develop the full rail height of 254-mm. The reduced material size reduces the cost of the material which is needed to manufacture the guardrail sections. The use of a brickwork glulam also allows for the selective stacking of laminates, with a low quality core and a higher quality facing of the glulam. Further, the red maple is an under utilized species, and the wood that is used is low-grade material ripped from random width and length material which is essentially a waste product from hardwood mills.

3.2.4 Lamination Scheme

A guardrail system requires a balance of strength and stiffness. The guardrail must not rupture under an impact, must not form a pocket which can trap the vehicle, but must also be flexible enough to protect the occupants of the vehicle. If a guardrail is too stiff, it will not deflect sufficiently and will cause rapid decelerations of the vehicle occupants. The stiffness of the system is controlled by three factors: rail, post, and soil. Based on the Barrier VII modeling discussed in Chapter 2, a cross-section 152-mm deep by 254-mm wide was selected with 3% reinforcement by volume on the non-traffic face. This depth of 152-mm was the same as that of the Merritt Parkway Guardrail system. However, this 152-mm thick rail would be heavy, 20.8 kg/m, since maple is more dense than the southern pine or douglas fir used in the Merritt Parkway Guardrail. A 114-mm deep cross-section with 3% reinforcement by

volume was designed to be lighter than the 152-mm cross section, 15.6 kg/m. An initial test specimen was fabricated using the 114-mm deep cross-section. The FRP was ordered in 3.5-mm by 127-mm bars, 3% by volume of the 114-mm cross-section. While initial durability testing of the 114-mm cross section proved successful, the cross-section was further reduced to 76-mm deep in order to reduce weight, increase material usage, and reduce the stiffness of the system in order to cause the system to behave more like a tension ribbon than a rigid barrier. The 76-mm deep cross-section has a mass of 10.3 kg/m, which is comparable with the weight of the W-beam rail.

The reinforcement that was used on the 76-mm deep cross-section was the 3.5-mm thick reinforcement which was ordered for the 114-mm deep rail section. This 3.5-mm reinforcement is 4.7% by volume of the 76-mm cross-section. The FRP reinforcement consisted of two separate 127-mm wide sheets, since a single 254-mm by 3.5-mm thick sheet could not be purchased at the time of fabrication. The stiffness and approximate yield moment of the cross-sections were calculated by a transformed section analysis as discussed in Chapter 2. The calculated properties for the cross-sections considered are presented in Table 2.1. The moment capacities which are displayed in Table 2.1 for the reinforced glulam cross sections are the moment at the first predicted tensile failure. These analyses predict that the bending rigidity of the 76-mm cross-section is less than the bending rigidity of the steel W-beam, with four times the moment capacity. The reduced bending rigidity is beneficial to the guardrail system because the less rigid rail causes the system to attain smaller bending stresses and behaves more like a tensile ribbon, similar to the steel W-beam.

3.2.5 Brickwork Lamination Design

The glulam portion of the rail system consisted of four 19-mm laminations. The laminations were sorted into two categories based on their quality: face laminations and core material. Laminations with edge knots less than 1/3 of the cross-section and with a slope of the grain of less than 12.5% were classified as face laminations; any board which did not meet these criteria was used as core material. Placing the highest quality laminations on the faces of the glulam ensures that the highest quality laminations are in the area of maximum flexural stress and will also improve the wood-FRP bond. The brickwork lay-up was achieved by using combinations of two and three boards as shown in Figure 3.1:

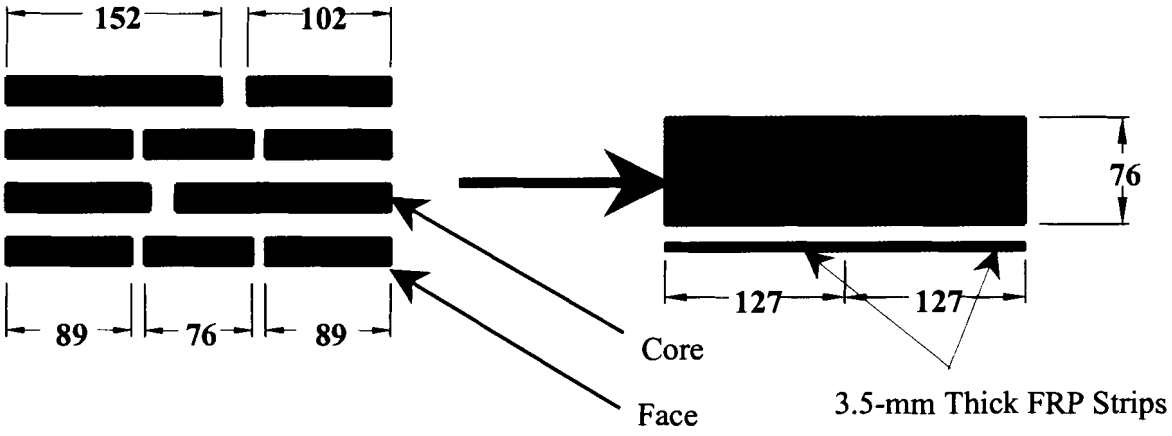

Figure 3.1 Glulam Brickwork Layout (all dimensions in mm)

The brickwork layups use random sequences of these board combinations. In the brickwork layups no seams were allowed to overlap on adjacent layers. The glulams were fabricated to 260-mm wide and saw cut to give the 254-mm dimension.

3.3 Reinforced Glulam Fabrication

The guardrail sections were fabricated in 3.658-m lengths. However, the wood for the glulams was purchased in random widths and lengths seconds from O &

R Lumbra, Inc. in Milo, Maine. The first step in the process was to plane the wood surface and saw the wood to width. The wood was then graded and sorted. The next step in the fabrication process was to cut finger joints into the wood. In order to create 3.658-m boards, multiple pieces of wood were finger jointed together to form a continuous piece of lumber. Finger jointing at the AEWC Center proved to be difficult due to quality and size issues with the finger jointer. The finger joints cut at the AEWC were poorly cut, and did not align well. Further, it was not possible to finger joint boards wider than 120-mm. The boards wider than 120-mm were finger jointed by Unadilla Laminated Products in Unadilla, New York. The remaining finger joints were cut in-house at the AEWC Center. The finger joints were joined using the Ashland ISOSET UX-100 adhesive in the finger joint press at the AEWC Center. Once the boards were finger jointed the next step in the fabrication process was to laminate the boards together.

The boards were laminated in the cold clamps in the AEWC center. The hardwood glulams are fabricated under higher pressure than traditional glulams. Due to the inconsistency in the thickness of the planed boards, the boards required additional compression to eliminate the slight gaps. The clamping pressure which was used was approximately 2758 kPa. The resin was applied as a constant coating of $0.0341 g/m^2$. The resin was applied with the resin applicator. The laminates were manually stacked as seen in Figure 3.2:

Boards In Resin Applicator Coated Boards

Stack Cold Clamps

Figure 3.2 Resin Application

The beams were fabricated in pairs. Once the boards of the glulam were coated with resin and stacked, they were flipped on edge so that the force was applied perpendicular to the bond line. A strip of plastic was placed between the two beams and on the outside of the cold clamps. The two 51x157-mm box steel sections and two 19-mm by 157-mm steel bars were stacked on both sides of the beam to distribute force across the outside of the beams. This setup is shown in Figure 3.3:

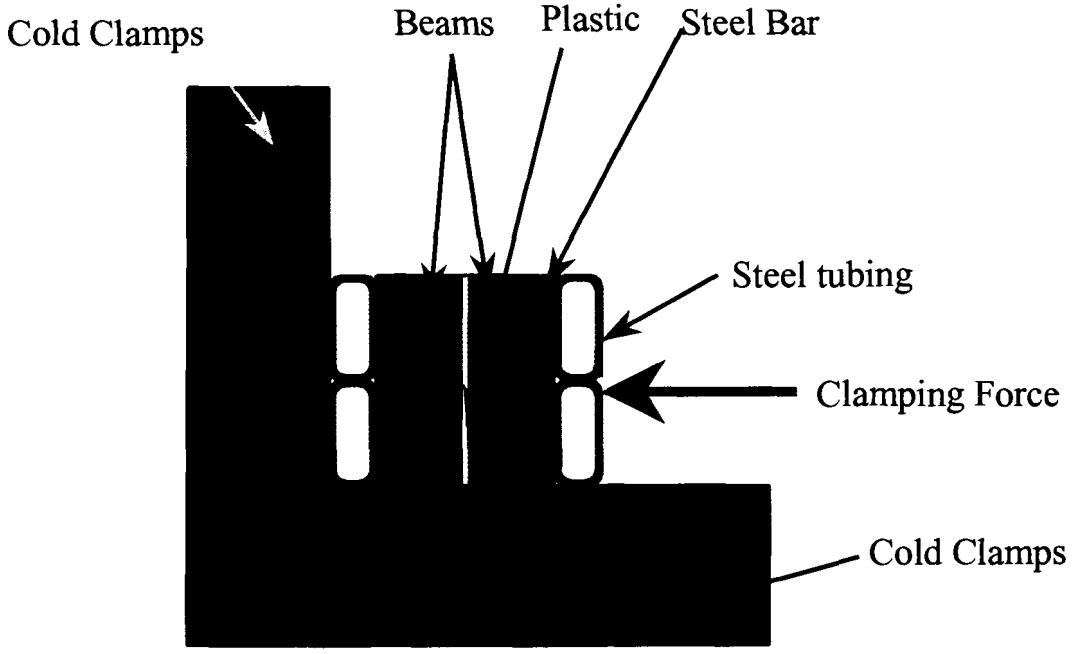

Figure 3.3 Cold Clamp Setup

Once the beams were in place, they were clamped in the cold clamps with 36 –25.4-mm diameter rods which are connected through the 51x51-mm tubing with long 51-mm nuts torqued to 332 N-m of torque. Lateral bracing was also used to compress the depth of the beams, to minimize gaps, and to ensure alignment of the boards. Lateral bracing was used at the third points of the beams. The beams were then cured under room temperature conditions for a minimum of eight hours.

3.4 Bonding FRP to the Glulam Rail

In order to bond the FRP to the glulam it was necessary to treat the surface of the glulam with a coupling agent to allow the FPL-1 to bond to the wood. Hydroxymethylated resorcinol (HMR) was the coupling agent which was used. Once the glulams were fabricated, they were trimmed to size, planed, and primed with HMR primer. The surface was planed to create a fresh surface and remove excess resin on the surface. The HMR primer was applied in a coat of 147 g/m^2. The HMR

was mixed and applied in accordance with the AEWC Center work instruction WI-01-05. The HMR was applied and cured for 16-21 hours before the application of FPL-1.

FPL-1 epoxy was used to bond the FRP to the primed wood. The FPL-1 epoxy was formulated in accordance with AEWC Center work instruction WI-01-05. The spread rate used was 538 g/m^2. The FPL-1 epoxy was applied by hand in an even coat across the treated surface of the beams. The FRP strips were wiped down with acetone to remove contaminates, then the FRP strips were placed on top of the FPL-1 covered surface. The beams were then flipped and clamped with the FRP faces together and a strip of plastic between the FRP strips to prevent FRP strips from bonding together. Approximately 345 kPa of clamping pressure was applied to the bond surface using the cold clamps with 14-25.4-mm rods torqued to 136 N-m. The beams were then allowed to cure for a minimum of eight hours before unclamping.

Five 3.658-m specimens were fabricated through this process. These specimens were cut to length for the tests described in Chapters 4-6. The specimens were cut in a two-stage process, since the FRP very rapidly dulls the saw and because a wood saw is not designed to cut FRP. First, the FRP and approximately 4-mm of the wood was cut with a diamond abrasive blade in two blade widths, then the remaining wood was cut with a wood blade and trimmed to be even with the FRP.

3.5 Durability Testing

Before further structural testing could be performed, the durability of the reinforced glulam guardrail section needed to be qualified. Therefore, a set of durability and delamination tests was performed. These tests are important to qualify

the behavior of FRP-glulam bond in adverse environmental conditions. The test which was used to qualify the durability of the bonding of the wood to the FRP was the ASTM D1101 (ASTM (a), 2002) delamination test. ASTM D1101 was also used to qualify the durability of the splice connection as discussed in Chapter 5. The ASTM D1101 test is a quality control test to determine the integrity of wood-to-wood bond.

The ASTM D1101 test is not for qualification of adhesive performance, the ASTM 2559 (ASTM (b), 2002) test is for qualifying adhesives. However, the ASTM D1101 test was selected because it offered several advantages over the ASTM 2559 test. First, the ASTM 2559 test calls for the fabrication of specialized specimens on which to perform the test, which would require additional time and expense. The ASTM D1101 test is performed on a section of production run material, as a quality control test. The use of the actual designed cross-section was beneficial because of the large width of the cross-section and the reduction in time and materials associated with fabricating specialized specimens. There were also problems with the ASTM 2559 test and testing the reinforced glulam sections. The FPL-1 epoxy has a glass transition temperature less than the temperatures at which steam is applied in the ASTM 2559 test. For these reasons, the effect of the ASTM 2559 test on the FPL-1 epoxy bond is unclear. The ASTM D1101 test was used also to test the durability of the splice connection discussed in Chapter 5.

The ASTM D1101 Test Method A test consists of a wetting cycle and a drying cycle. The wetting cycle supersaturates the wooden portion of the specimens by submerging the specimens in water, pulling a vacuum for five minutes to remove

the air from the wood, and then a pressure cycle where the vessel is pressurized to 552 Kpa to force water into the wood structure. After the vacuum and pressure cycle, the specimens are dried in an oven at 60 °C for 24 hours. This wet-dry cycle is repeated three times to conclude the test. Between each wetting and drying cycle, the specimens are observed to denote any delamination in either of the bonds in the specimens.

Through all of the testing which was performed, there was minimal delamination of the FRP from the wood. The first set of ASTM D1101 tests were run on a 114-mm cross-section and qualified that the sections performed well. While there was an area of debonding, this area was not a bond failure since it was initially void of epoxy due to an error in the fabrication procedure. No further epoxy voids were observed in the 76-mm specimens.

Further durability testing of the rail cross-section was performed on 76-mm deep rail sections. Ten tests were run on specimens cut from the same billets as the tension test specimens (see Chapter 5). These tests showed minimal quantifiable delamination, less than 2.5-mm. In all cases the FRP separated in the middle, due to the use of two separate sheets, and cracked at the gaps between pieces of wood, due to stress concentrations. The areas of debonding were localized to these cracked areas. ASTM D1101 disregards delamination in the areas of damaged wood and checking. ASTM D1101 is written for the testing of wood-to-wood bonding, and is not written for wood-FRP bonding, so the delamination in the area of the gaps was also neglected.

3.6 Cost Analysis

In order to estimate the cost of the reinforced hardwood glulam guardrail system, the fabrication process was analyzed. The implementation of the guardrail system was broken into three areas: raw materials, fabrication, and installation.

The raw materials consist of the components used to manufacture the guardrail, the glulam, reinforcement, FPL-1 epoxy, splice plates, and SIA E2119 epoxy. This estimate is based on a commercially available glulam. However, no 254-mm by 76-mm commercially available maple glulams were found on the market. Engineered Materials of Maine currently produces a 241-mm by 89-mm glulam for $14.50 per meter. The volume cost of this glulam was applied to the 254-mm by 76-mm glulam giving a cost of $13.00 per meter. While the treatment of the reinforced glulam was not addressed in this study, the cost of preservative treatment for structural lumber is estimated at 20% of the cost. The cost of the treated glulam is estimated at $15.65 per meter.

Reinforcement is provided by Gordon Composites as two 127-mm by 3.5-mm bars, which is approximately $37.20 per meter. In order to fabricate the splice connection for each steel rail section two 254-mm by 152-mm by 13-mm thick steel plates, one 76-mm by 76-mm steel plate to attach the rail to the intermediate post, and one 305-mm by 25.4-mm by 13-mm plate are required. These plates will also need to be predrilled. Therefore, the price was set to $2.20/kg to account for machining of the plates.

The SIA E2119 cost $20.20 per liter when purchased in 18.9-liter pails. The cost for SIA adhesives epoxy was calculated for the same quantities as discussed in

Chapter 5 with the same spread rate used for the 76-mm by 76-mm by 13-mm steel plate in the center of the rail. The cost of the FPL-1 epoxy was estimated at $33.00 per kg from work at the AEWC.

The cost associated with the fabrication of the beams comes in three different processes: bonding the FRP to glulam, bonding the steel plates to the FRP, and drilling holes through the SIA adhesive and reinforced glulam. The labor costs of installing the guardrail beams were based on a rate for a three man crew of laborers, $33.40 per man hour (Ogershock, 2002). It was estimated that with a cold clamp setup similar to the ones used to fabricate the test specimens, five man hours would be required to reinforce twelve 3.658-m glulams. For installation of the guardrails, it was assumed that a three man crew could install three 3.658-m long guardrail sections in one hour, costing one man hour per 3.658-m section. An additional labor expense is the drilling of the holes in the reinforced glulam. It was assumed that using a CNC machine, all of the holes in the reinforced glulam could be drilled in a maximum of 20 minutes. The cost of the labor involved was estimated based on a millwright, $47.71 per man hour (Ogershock, 2002). Using these estimates the installed cost of the reinforced glulam guardrail was estimated at $115/m. All of the costs are summarized in Table 3.1.

Raw Material	Units	$/Unit	Total, $
Treated Glulam	m	15.65	15.65
FRP	m	37.20	37.20
FPL-1 Epoxy	kg	33.00	4.51
SIA E2119 Adhesive	liter	20.20	8.55
Steel Plates	kg	2.20	9.65
Labor			
Bond FRP to Glulam	man-hours	33.40	0.35
Bond Steel to FRP	man-hours	33.40	6.09
Machiene Bolt Holes	man-hours	47.71	4.35
Installation	man-hours	33.40	9.31
		Total :	114.79

Table 3.1 Cost Estimate Summary

Chapter 4

FLEXURAL TESTING

4.1 Introduction

In order to evaluate the stiffness and flexural capacity of the reinforced hardwood glulam guardrail sections under bending loading, two three-point bending test were performed. The tests were performed on 1.829-m specimens, specimens 8 and 9.

4.2 Test Setup

The specimens which were used for these tests were cut directly out of the reinforced glulams which were fabricated in 3.658-m billets as described in Chapter 3. The specimens, which were tested in three-point bending, were 1.829-m long. The specimens were supported on two vertical supports with the center of the pivots on the supports spaced 1.676-m apart. One of the supports allowed two degrees of rotational freedom. The other support allowed only one degree of rotational freedom. The reaction supports are seen in Figure 4.1:

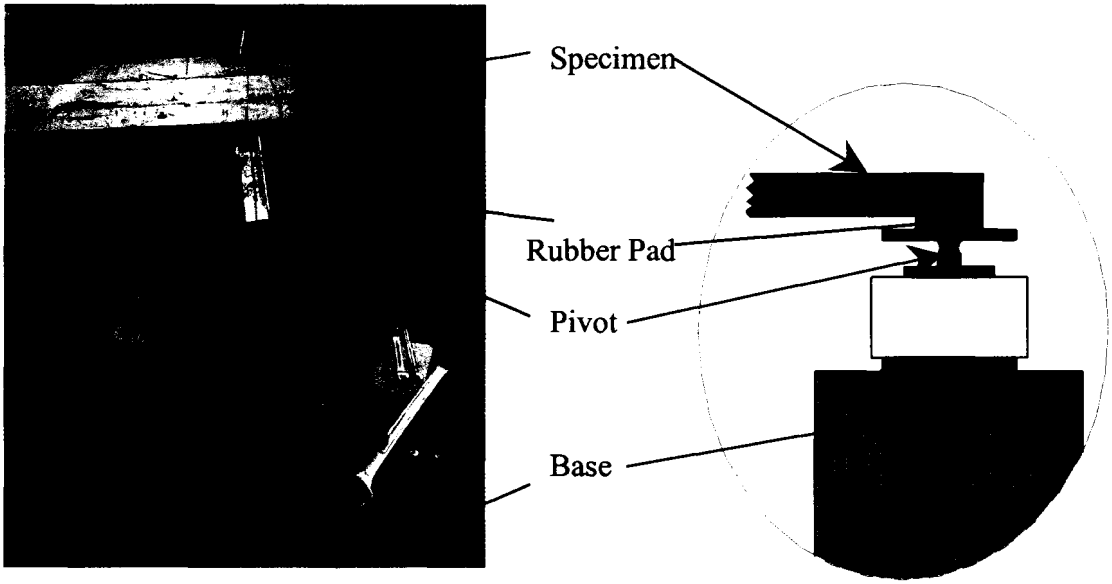

Figure 4.1 Specimen Supports

The specimens were supported on a 152-mm long, 13-mm thick rubber pad centered on the supports in order to ensure that the support centerline remained at the pivot point under large loads.

The load was applied at the center of the span with a 500 kN actuator mounted below the floor. The actuator was attached to a loading frame above the floor with a section of 36-mm Dywidag bar. A 100 kN load cell was mounted on the load frame. A radiused hardwood load head with a pivot was mounted on to the 100 kN load cell. This setup is shown in Figure 4.2.

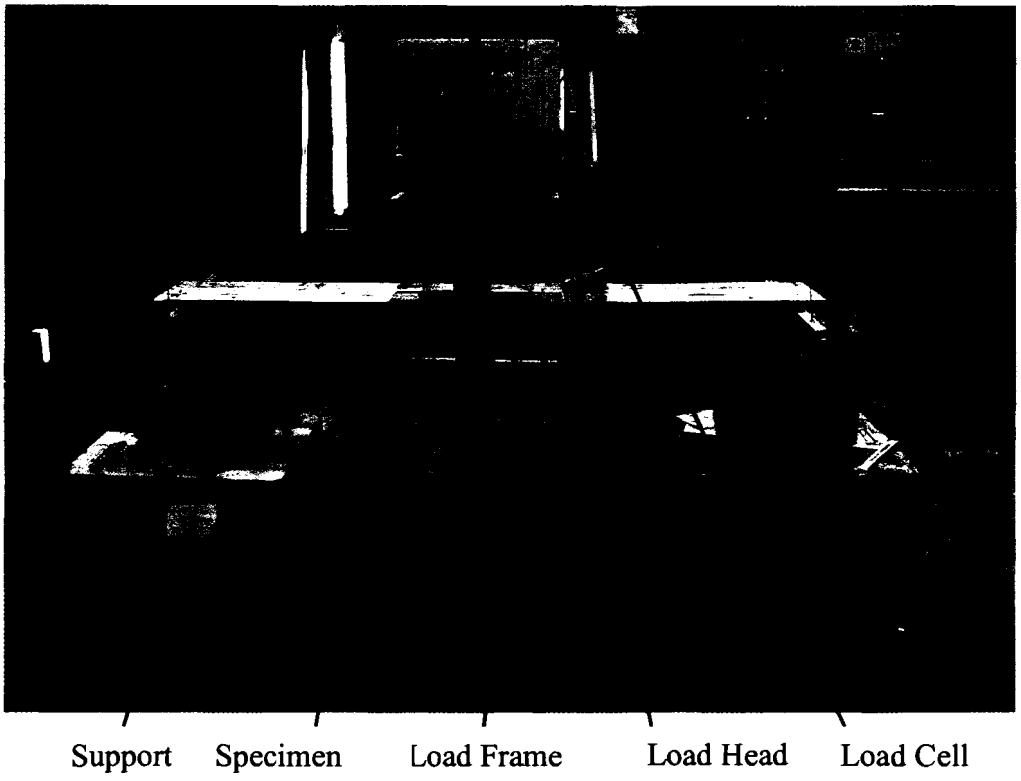

Figure 4.2 Test Setup

There was also a rubber pad placed between the load head and the specimen to raise the load head above the specimen to ensure that the point of load application remained at mid-span.

4.3 Instrumentation

The instrumentation which was used on the three point bending test was a 100 kN load cell to record load, LVDT's which recorded position, and strain gauges to record the strain in the FRP. The load and displacement of the actuator were output by the Instron controller as an analog output. This analog output was recorded in the data acquisition computer by a National Instruments PCI-6031E, 16 bit data acquisition card as a non-referenced single ended signal. The actuator displacements did not exactly measure the displacement of the beam at the center due to crushing of

the rubber pads under the load head and on the supports. However, the effects of this crushing were removed from the data by quantifying the compressive response of the rubber pads as discussed later in this chapter.

4.3.1 LVDT's

The displacement of the beam was recorded with a pair of LVDT's at 152-mm off mid-span. The vertical displacements of the specimens at the pivot of the supports were also recorded with four LVDT's, one on each side of the beam. The signals were read as a non-referenced single ended signal into a National Instruments PCI-6031E data acquisition card. The data which was recorded from the LVDT's which were 152-mm off mid-span were not useful because at high displacements the LVDT mounting brackets twisted significantly and caused the rods to bend and catch in the LVDT's .

4.3.2 Strain Gauges

The strains in the FRP were measured with four Measurements Group CEA-06-125UW-350 strain gauges bonded to the FRP of the specimens with MBond –200 epoxy. Two pairs of gauges were used: one at the center of the beam and one at 152-mm from the mid-span of the beam. This is shown in Figure 4.3:

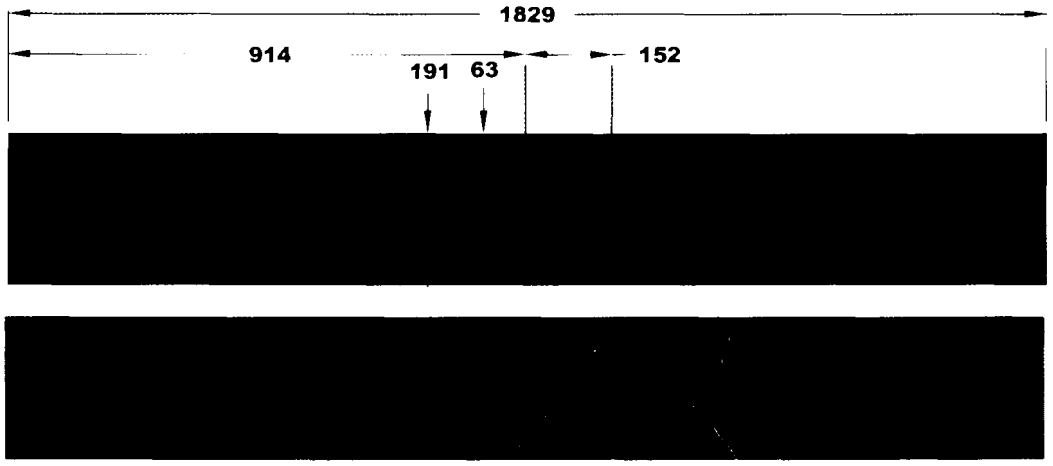

Figure 4.3 Strain Gauge Locations (all dimensions in mm)

The strain gauges were conditioned using a Measurements Group P2100. The analog outputs of the P2100 were read as non-referenced single ended signals by the data acquisition computer using a National Instruments PCI-6031E data acquisition card. The four gauges read by the P2100's were calibrated by reading approximately 30 seconds of zero values, approximately 15 seconds of positive calibration values, approximately 15 seconds of zero values, and approximately 15 seconds of negative values. This cycle was repeated once. All of the recorded zero values were averaged to find the voltage at zero strains. The voltage of zero strain was then subtracted from the calibration values. The absolute value of the adjusted calibration values was averaged in order to get the calibration voltage of each strain gauge. The number of strains that was approximated by the stint in the P2100's is 1000 μ strains at a gauge factor of 2.0. The gauge factor for the gauges used was 2.11 and the resistance of the wires was negligible. The number of strains approximated by the stint was therefore the ratio of the assumed gauge factor divided by the actual gauge factor and multiplied by 1000 μ strains. This value was 948 μ strains. This value was then

divided by the average calibration voltage to get the relation between voltage and strain.

4.4 Test Results

Two three point bending tests were performed on specimens 8 and 9. The tests were performed in displacement control, with a rate of 13-mm/min. Both of the specimens performed similarly. The load-displacement relations for specimens 8 and 9 are shown in Figure 4.4:

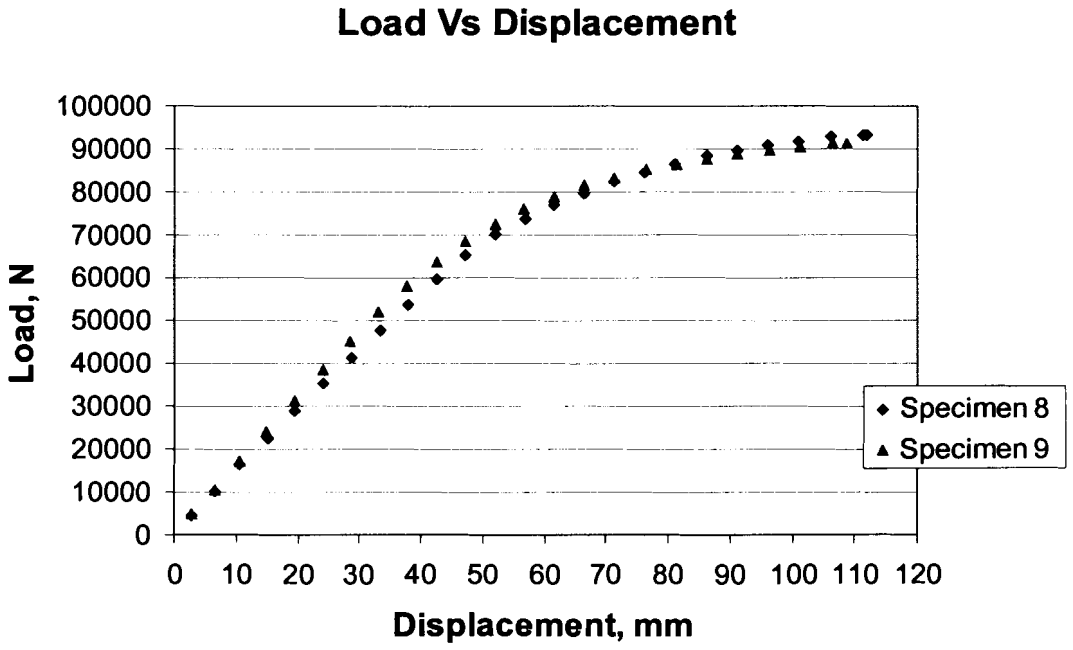

Figure 4.4 Pure Bending Load-Displacement Relations

The displacements shown in Figure 4.4 are the Instron load head displacements, corrected to account for the rubber pads placed under the actuators and on the supports. The effects of the 13-mm pads on the supports were removed from the Instron displacement by subtracting the average of the four LVDT readings at the pivots of the beam from the Instron actuator displacement. To account for the crushing of the load head and rubber pad under the load, head a test was performed to

find the relation between load and displacement in the rubber pad and load head. The test was performed by placing the rubber pad on an incompressible base and applying load through the load head to find the load-displacement relation. This test does not exactly model the system because there is a high degree of curvature in the actual beam in the area of the load head, however it was a reasonable approach to the problem. The load-displacement response obtained from the rubber pad and load head is shown in Figure 4.5:

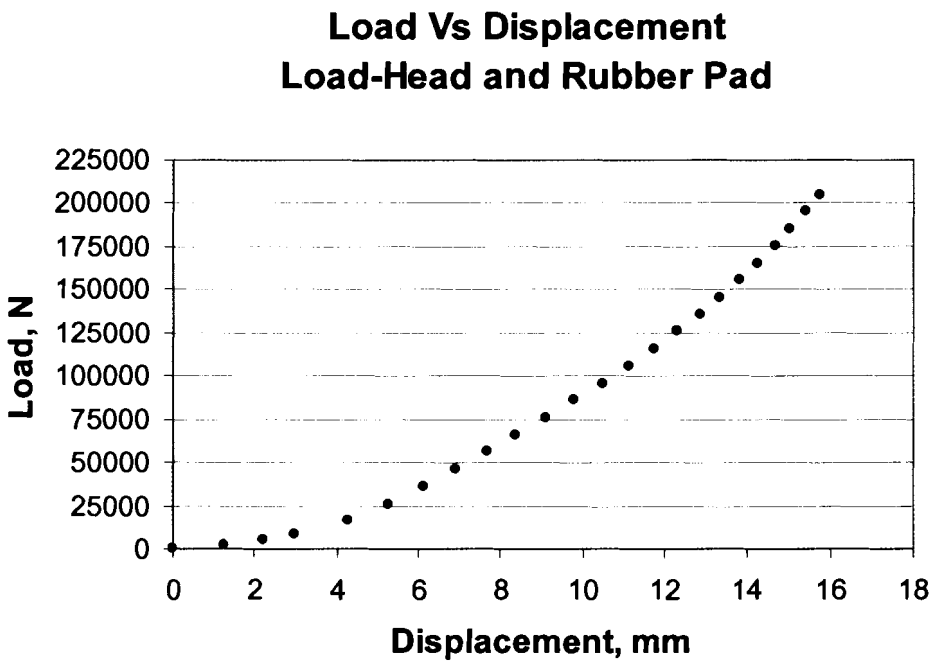

Figure 4.5 Load-Head and Rubber Pad Load Displacement

The maximum load which was applied to the load head and rubber pad was consistent with the maximum load which was applied to the specimens through all of the tests performed. All of the reported displacement values in this chapter and in Chapter 6 have been corrected to remove the effects of the load head and rubber pad.

The maximum load for specimen 8 was 93 kN with a displacement of 111-mm. The maximum load which specimen 9 achieved was 91 kN with a displacement

of 109-mm. The failure loads and displacements for the two tests were within 3%. The behavior of the load-displacement curve is nonlinear due to the high percentage of FRP (4.7%) causing significant compressive yielding in the wood at the high loads. The yielding behavior is also evident in the load-strain relation shown in Figure 4.6:

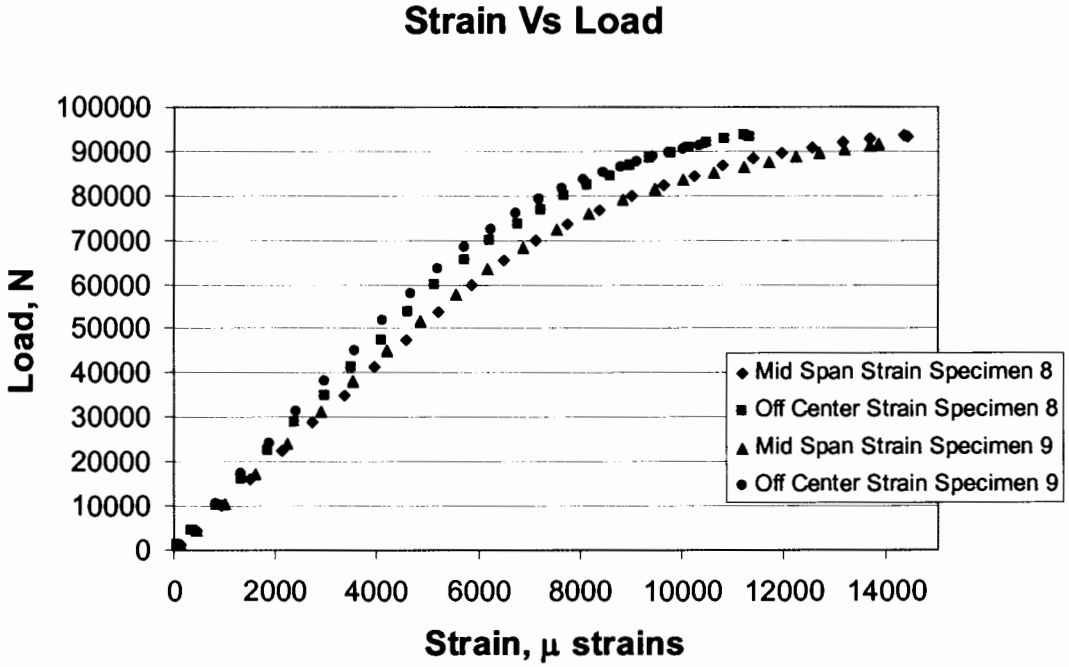

Figure 4.6 Pure Bending Load-Strain Relations

The specimens showed very similar load-strain behavior. The strains which were observed did not approach the failure strains for the FRP, 23000 μ strains. The effect of the compressive yielding in the wood is also evident in the non-linearity seen in Figure 4.6.

The failure mode of the specimens was also similar. The tensile laminations of the reinforced glulam failed. This failure resulted in the separation of the FRP from the glulam portion of the beam. However, the failure was not in the FPL-1 epoxy; instead the failure was an inter-laminar shear failure in the FRP. Several layers of FRP remained attached to the FPL-1. See Figure 4.7:

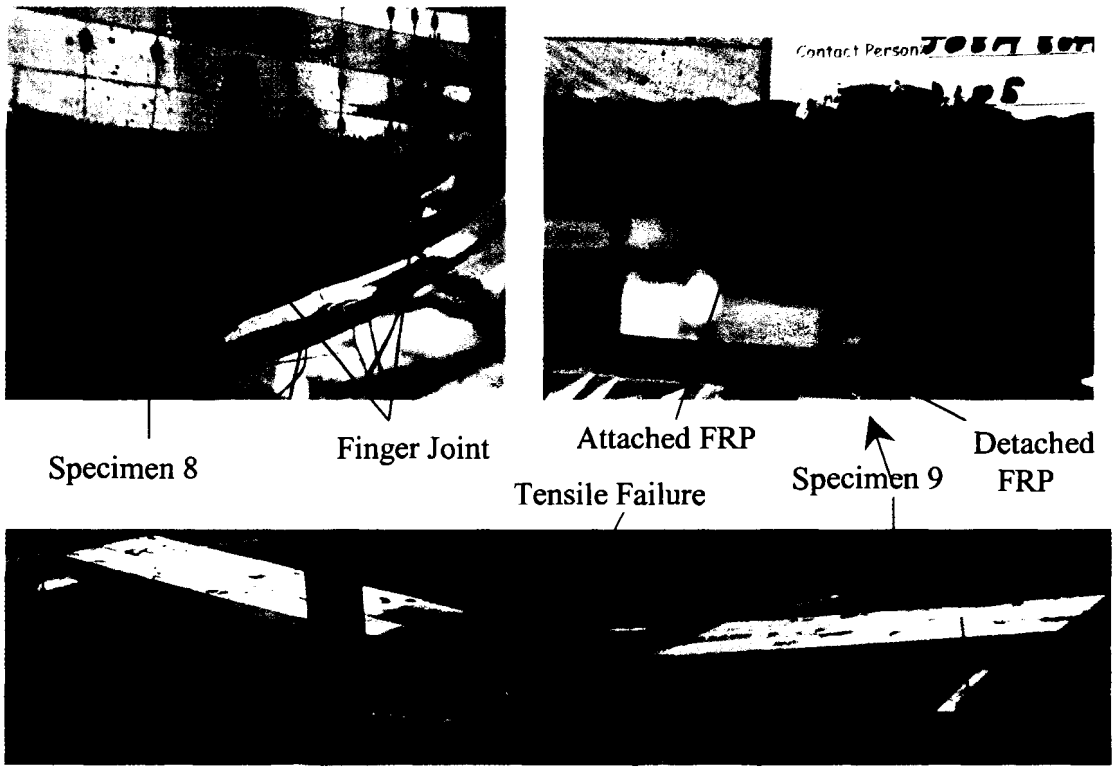

Figure 4.7 Beam Failures for Specimens 8 and 9

The FRP delamination was a result of the tensile failure in the wood. The tensile failures occurred at defects in the wood, which were near the center of the beam. The tensile lamination in specimen 8 failed at a finger joint approximately 75-mm off center. Specimen 9 did not tensile fail at a finger joint. The tensile failures which occurred in specimen 9 failed a larger area of the glulam. The tensile laminates did not fail on center. For both specimens, the failed tensile lamination pried the FRP away from the glulam. The FRP delamination was only observed in the half-span of the glulam in which the tensile failure occurred in both of the tests performed.

4.5 Analyses

In order to have accurate input for the modulus of elsticity, area, and moment of inertia for further modeling, the stiffness of the rail section was quantified. The modulus of elasticity of the wood glulam was calculated from the three point bending

test data. The moment of inertia was found by the transformed section analysis method, once the modulus of the wood was known. From the load-displacement relation seen in Figure 4.4, the bending rigidity, *EI*, of the reinforced hardwood glulam guardrail section was calculated using the standard equation for the displacement at the center of a simply supported beam with a concentrated load applied at the center:

$$\delta_c = \frac{P \cdot L^3}{48 \cdot EI} \tag{4.1}$$

Where δ_c is the mid-span deflection, P is the applied vertical load, L is the span length, E is the modulus of the wood, and I is the transformed section moment of inertia. The bending rigidity, EI was solved for to get the following relation:

$$EI = S \cdot \frac{L^3}{48} \tag{4.2}$$

In equation 4.2, S is the slope of the linear range of the experimental load-displacement curve. An average EI was determined for both specimens 8 and 9. The average EI was evaluated by finding S as a secant slope between 9 and 53 kN of applied vertical load. This load range was used because the load-displacement was most linear in this range; compressive yielding in the wood becomes significant only at loads greater than 53 kN.

The modulus and moment of inertia, E and I, were then calculated using the transformed section method. An initial guess for the modulus was used, then the corresponding moment of inertia was found by the transformed section method. A new modulus was then calculated by dividing the average EI, found from the data, by the moment of inertia calculated by the transformed section analysis. The process

was repeated until the modulus did not change significantly. The modulus was found to be 10.3 GPa, the transformed area was found to be 0.023-m^2, and the transformed moment of inertia was found to be $14x10^6mm^4$.

4.6 Conclusions

Both of the three point bending tests performed yielded similar results. The failure load of specimen 8 was 93 kN, with a displacement of 111-mm. The failure load of specimen 9 was 91 kN, with a displacement of 109-mm. Both tests displayed a nonlinear load–displacement and load-FRP strain relations. This is due to the compressive yielding which occurs in the wood at the higher loads. The FRP-glulam bond was verified under high loads, in both tests layers of FRP remained bonded to the glulam after the failure of the specimens. From the load-displacement results and a transformed section analysis, the modulus of the wood was found to be 10.3 GPa which was 8% less than the published value for red maple (Wood Handbook, 1999) of 11.3 GPa which was used in the modeling discussed in Chapter 2. The modulus found in the experiment may be less than the published modulus due to the gaps, which were present in the brickwork glulam. The spaces would not be present in a commercially produced glulam. The area was found to be 0.023-m^2 and the transformed moment of inertia of the guardrail section was found to be $14x10^6mm^4$.

Chapter 5

GUARDRAIL FIELD SPLICE CONNECTION

5.1 Introduction

During a vehicular impact, a guardrail system experiences a complex variety of loadings. Using the Barrier VII analysis tool it has been shown that rail impacts induce not only large bending moments in the rail, but also large tensile forces. This tensile force must be transferred throughout the entire length of the rail system and distributed into the posts. In order to transfer the tension between the reinforced glulam rail sections and allow for easy installation, a specialized splice connection was developed. In order to satisfy field serviceability requirements the splice connection between rails must allow the replacement of individual rail sections.

This chapter will deal with the development, fabrication, and testing of the splice connection. An additional topic discussed is the effect of bolt load creep in bolted glulam connections.

5.2 Design of Splice Connection

It is necessary to develop a splice connection to connect rail sections together due to the impracticality of fabricating a single rail section for long guardrail runs. The reinforced glulam guardrails will be fabricated in 3.658-m lengths, which is an industry standard when the conventional 1.829-m post spacing is used. These 3.658-m rail sections must be connected together to form a continuous rail. The rails must also be attached to the posts in order to transfer energy from the rail into the soil. Due to serviceability requirements placed on the reinforced glulam guardrail system,

it is necessary to connect the rails together in a manner which allows rail sections to be easily added or removed from the system when they become damaged. This requires the use of field-boltable connections to transfer tension through the splice. The simulations of Chapter 2 indicate that the tensile force in the connection can reach 240 kN. It must also be noted that the FRP acts as a continuous tension ribbon, once the rail has failed. The FRP carries the majority of the tensile load. This requires that the splice connection effectively transfer the tension between adjacent pieces of FRP.

Unfortunately, both wooden glulams and the unidirectional FRP used in the reinforced glulam have relatively low shear strength. This limits the load which can be transferred through a bolted connection. In order to carry the large tensile force, a unique connection had to be developed.

It is possible to increase the shear capacity of the FRP reinforced glulam bolted connection by varying the fiber orientations of the laminate, however this reduces the tensile strength and the stiffness of the rail, which was undesirable. It is also possible to add additional angled FRP between layers of wood or on the exterior of the laminate to increase the shear capacity as demonstrated by Soltis (1998) and Chi-Jen (1998). This process essentially increases the shear strength in the connection area, thus increasing the bolted connection capacity. However, this process is labor intensive, costly, and only provides a small increase in shear capacity for the increase in cost. For these reasons it was necessary to explore alternative methods to transfer the tensile force between glulam rail sections.

One such alternative method uses bonded hardwood dowels to distribute the tensile force between members. This method was developed by Japanese timber engineers (Komatsu, 1998). The bonding of hardwood dowels between rail sections allows the transfer of force through shear in the adhesive. The capacity of the connection is determined by the adhesive and the length of the bond. However, the bonding of hardwood dowels is not immediately applicable to the design of a splice connection due to the fact that the glulam does not carry the majority of the tensile load in the rail and large bond lengths would be needed to develop the tensile force. There are also inherent difficulties with performing the alignment and bonding of the dowel connections in field installations.

However, the concept of a bonded connection is useful. It is possible to use FRP plates epoxied into slots in the rail, which could be field cut, to obtain a splice connection (Drake, 1998). This method, however, involves field bonding an FRP plate into the beams. This process is labor intensive and sensitive to error in the bonding conditions. The need to prime the wood before bonding also restricts the usefulness of such a technique. Replacing damaged rail sections would be complicated and expensive due to the bonded inserts. Due to the complications associated with installation and maintenance and the added cost of the process, the use of bonded FRP plates was not feasible.

5.2.1 Splice Connection Details

The ideal bolted connection would combine the ease of a bolted connection and distribute the tension into the rail as shear across a large area into the rail section. Boone (2002) demonstrated that it is possible to transfer large tensile forces between

metal and FRP through shear in a thick epoxy bond line. The final design combines the concept of the thick epoxy bond, with the bolted connection by bonding a steel plate to the FRP and bolting the steel plate to a steel splice plate which is bolted to the post and the adjacent rail. The splice connection is fabricated in the shop which allows the rail sections to be easily bolted into place in the field. The variables which were considered in the design of the splice connection were connection length, adhesive type, metal plate size, surface preparation, and the size and number of bolts used. Figure 5.1 shows the general configuration of the splice connection:

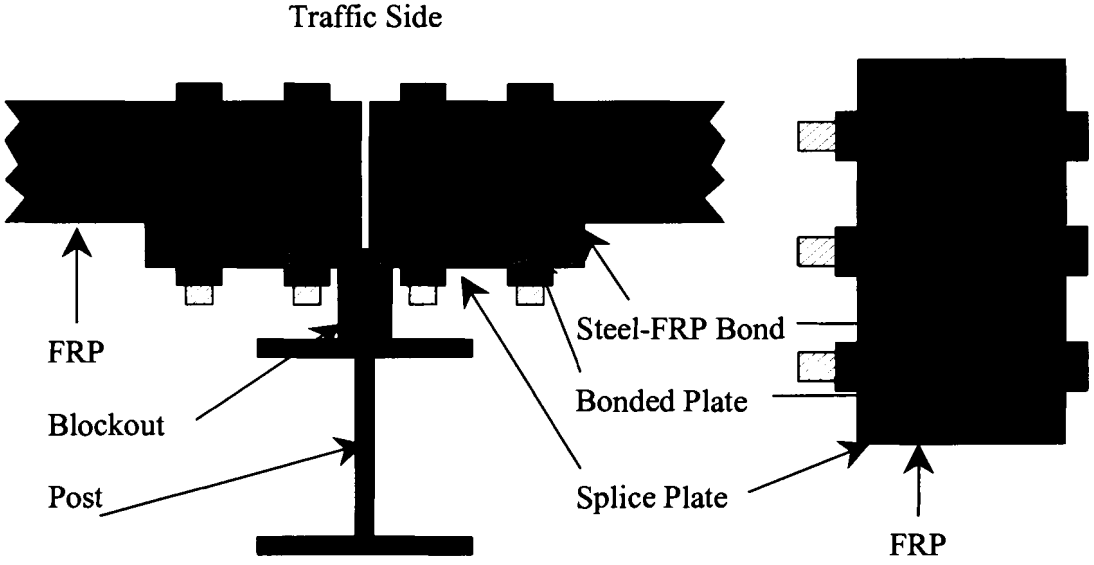

Figure 5.1 Splice Connection Concept

The first step in the development of the guardrail system connection was to select the material to bond to the FRP and the surface treatment of that material. Prior research by Boone (2002) evaluated aluminum bonded to E-glass vinyl ester FRP. The FRP which was used in the guardrail section is an E-glass epoxy and the

metal which was selected for the splice connection is steel due to its low cost, high strength, machineability, availability, and wide use in civil infrastructure applications.

In order to achieve a high strength bond, it is necessary to apply a surface treatment to the steel before it is bonded. The purpose of a surface treatment is to eliminate oxides from the bonding surface, as well as to add texture to increase mechanical interlocking of the epoxy and the steel. While steel is less sensitive to the development of oxides than aluminum, the same surface treatments developed by Boone (2002) for aluminum were considered: hand sanding, grit blasting, and acid etching. While Boone (2002) showed that acid etching provides the highest quality bond, it is not well suited for implementation on this project due to the high cost of implementation. Hand sanding was also ruled out due to the large amount of labor involved and its lower bond strength. Grit blasting was used as the surface preparation for the splice connections. Grit blasting the steel allows for a high strength bond with minimal additional labor and expense. One disadvantage of using grit blasting or hand sanding is that the surface has a limited life before it oxidizes. With aluminum, the maximum surface life was three hours. While steel oxidizes slower than aluminum, the same three hour surface life was assumed to apply to the steel to ensure bond quality. After grit blasting, the surface was wiped with acetone to remove dust and contaminates. It is also necessary to apply a surface treatment to the FRP. Due to the relatively thin size and relative softness of the FRP, the FRP cannot be grit blasted. However, the FRP is easily hand sanded to provide a fresh and textured surface. After hand sanding, the FRP was also wiped with acetone to

remove dust and contaminates from the surface. The same three hour surface life was assumed to apply to the FRP.

Once the splice material and surface preparation were selected, it was necessary to select an adhesive for the bonding. There were four requirements which the adhesive must meet. First, the adhesive must provide a capacity of greater than 240 kN, the predicted tensile load as discussed in Chapter 2, with a reasonable bond area. Second, the adhesive must be able to withstand impact loading and exhibit a non-brittle failure mechanism. Third, the adhesive must not degrade under exterior exposure conditions. Finally, the adhesive must be of reasonable cost. Based on the work of Boone (2002), Sovereign Specialty Chemicals, SIA Adhesives E2119 epoxy was selected for use in the splice connection. This adhesive is rated to withstand impact loadings. The E2119 adhesive also does not exhibit a brittle failure mode, instead it yields and plastically deforms. This plastic deformation benefits the overall rail system by yielding rather than causing a catastrophic connection failure. The E2119 epoxy also provides a high strength bond, at most reasonable bond line thicknesses, and is not sensitive to small variances in the bond line thickness. All of the E2119 epoxy which was used in this study was donated by Sovereign Specialty Chemicals.

Once the epoxy was selected, the appropriate bond length and bolt pattern needed to be determined. When determining the number and size of the bolts it was important to consider the ease of field installation of the guardrail system as well as the capacity. The standard W-beam guardrail system uses eight 13-mm diameter AASHTO M180 bolts to connect the rail sections. Due to the thickness of the steel

W-beam, the steel W-beam will locally yield before the bolts fails in shear. The design of the splice connection for the reinforced glulam guardrail splice connection uses six 19-mm bolts. Due to the capacity of the bond section A490 (grade 8) bolts were used. The ultimate design strength of the 19-mm diameter A490 bolts, assuming threads in the slip plane, is 88 kN per bolt per AISC (2001). The combined capacity for all six bolts is 528 kN, which is in excess of the loads predicted. For the purpose of determining the strength of the FRP-steel bond, 13-mm thick plates were bonded to the FRP. Once the size and number of bolts were determined, the length of the splice plate needed to be determined.

Due to uncertainty in the design of the bonded bolted connection, the strength of the bond could not be accurately calculated. Geometric constraints were used to set the lower limit for the size of the plate. The minimum size of the steel plate which was bonded to the FRP was determined to be 152 X 254 X 13-mm. The 254-mm is the depth of the guardrail cross-section and the 152-mm is the width required to ensure typical bolt spacing and edge distance requirements. Splice lengths of 229-mm and 305-mm were also initially considered. However, due to the performance of the 152-mm bond length, it was unnecessary to test the longer splice bond lengths, since the 152-mm splice length approached the capacity of the bolts, as discussed later in this chapter. The splice plate configuration which was tested is shown in Figure5.2:

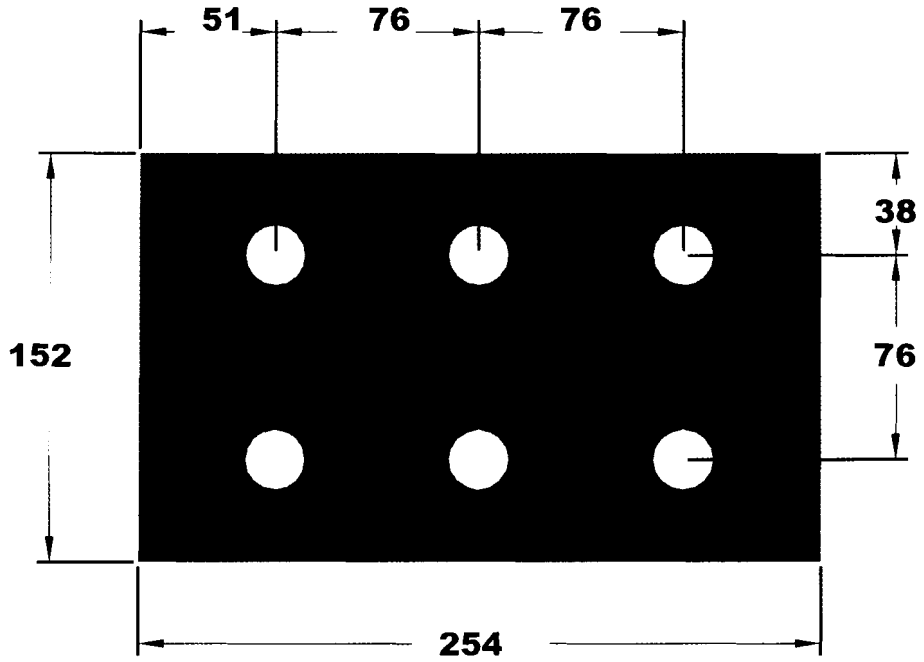

Figure 5.2 Splice Connection Bolt Locations

The bolt hole layout shown in Figure 5.2 on the 152-mm X 254 X 13-mm plate was the same for all of the connection specimens fabricated. The diameter of the holes for the tension testing specimens was 22-mm to allow for alignment with the fixture. The hole diameter for the combined bending and tension testing described in Chapter 6 was 19-mm to hold the tighter tolerances required for the testing.

An additional variable, which has a significant effect on the performance of the splice connection, is the torque load in the bolts. This torque is important because the failure mode of the bolted-bonded connection is yielding and failure of the steel-FRP epoxy bond. This failure is caused by two different stresses: the shear stress due to the tensile force and the peeling stresses due to the moment induced by the eccentricity of the load and the asymmetry of the connection. The use of bolts through the bond reduces the peeling stresses in the bond by compressing the bond and increasing the loads required to cause a peeling failure. The peeling stresses are

dependent on the bolt torque, with lower bolt torques leading to higher peeling stresses. However, bolt torque is difficult to predict in a wooden-bolted connection due to creep in the wood perpendicular to the grain.

The creep losses perpendicular to the grain of a wooden glulam can be quite large. An application where creep perpendicular to the grain is apparent is in stress laminated bridge decks. In stress laminated bridge decks bolt load losses have been observed as high as 60% (AASHTO, 1991). However, these stress laminated bridge decks are almost always fabricated using softwood. The visocelastic properties for hardwoods are not as well qualified as they are for softwoods. Also, there are many factors which contribute to creep in stress laminated decks which are not present in the guardrail bolted connection, such as gap reduction between boards. In addition the stress-laminated decks systems consider a force applied to either a steel end plate, or a set of hardwood laminations, (AASHTO 1998) which distributes the force across the width of the deck. The bolts in the guardrail system apply a force on the wood side of the system over a much smaller area. However, on the steel side of the system, the force is essentially an evenly distributed load. Therefore, the stress distribution throughout the thickness is not as constant as is the case with the stress-laminated decks.

Due to the lack of understanding in the subject, a projected value of the bolt force value was selected for testing based on the 1991 AASHTO Guide Specifications for the Design of Stress-laminated Wood Decks (1991) which states that the initial stress, P_i, be 2.5 times the desired prestress, P. The AASHTO relationship is based on the research of long-term prestress loss with steel tendons that have a long-term

prestress loss of 60% of the initial stress. This relationship is assumed to be a worst-case approximation to the creep load for the guardrail connection. Thus, the relationship which was used was as follows where T_i is the initial bolt torque and T is the final bolt torque:

$$T_i = 2.5\ T \qquad 5.1$$

The initial torque, T_i, was selected to be 136 N-m. This value is a typical torque value for a 19-mm bolt, and caused crushing of the glulam in the area of the bolts and washers. This initial torque yields a calculated minimum bolt torque of 54 N-m.

5.2.2 Fabrication of Splice Connection Specimens

The splice connections were fabricated in a separate step from the reinforced glulams. The specimens which were tested in tension were fabricated by using 838-mm reinforced glulams cut from the 3.658-m billets glulam. The splice plates were bonded to each end of the reinforced glulam as shown in Figure 5.3:

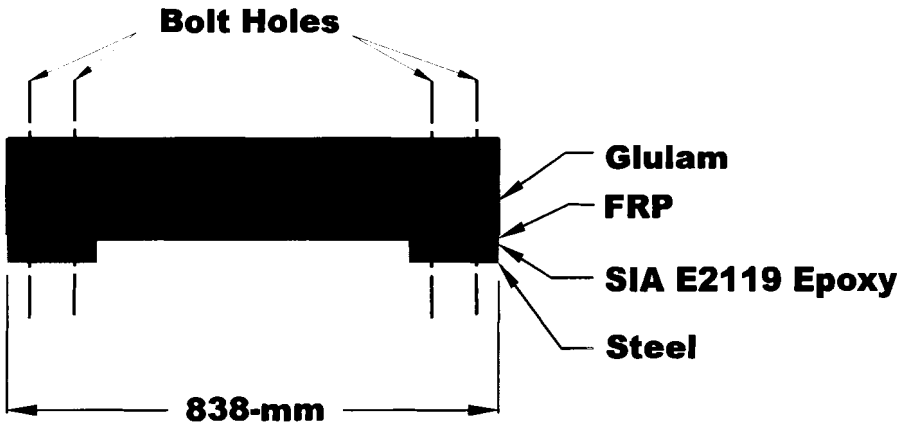

Figure 5.3 Splice Connection Tension Test Specimen Layout

The first step in the fabrication of the splice connection tension test specimens was to mill the bolt pattern into the steel plates, leaving approximately 2-mm of steel left in the bottom of the hole with a 22-mm center cutting end mill. Next, the plates were

grit blasted, on the non-milled side, and the FRP was hand sanded. After the surface treatment was applied, 162-g of SIA E2119 epoxy was applied to each splice plate. The steel plates were pressed onto the FRP and left to cure. The specimens were allowed to cure for three days. Then the holes were milled through the remaining steel and the FRP using the 22-mm center cut end mill. The holes through the wood were drilled with a 22-mm spade bit.

5.3 Connection Testing Program

The testing, which was performed to qualify the field splice connection, consisted of three ASTM D1101 tests and seven splice connection tension tests.

5.3.1 Test Matrix

In order to determine the capacity of the field splice connection seven tensile tests were conducted on the splice connection. To evaluate the effect of the bolt relaxation on the capacity of the connection, one trial test was performed, two tests were performed for an initial bolt torques of 136 N-m, two tests were performed for initial bolt torques of 54 N-m, and two were performed at an initial bolt torque of 27 N-m.

5.3.2 Tension Test Setup

The tests which were performed to determine the capacity of the splice connection were performed on the 1780 kN Baldwin-Satec test frame in the Hybrid structures lab in the basement of Boardman Hall. These tests consisted of an eccentric tension load which was applied through a bolted connection to the splice plate, which is consistent with the actual rail system. The length of the test specimen is 838-mm. The specimen was bolted to a connection plate which was gripped by the

Baldwin test frame. The layout and dimensions of the connection plate are shown in Figure 5.4:

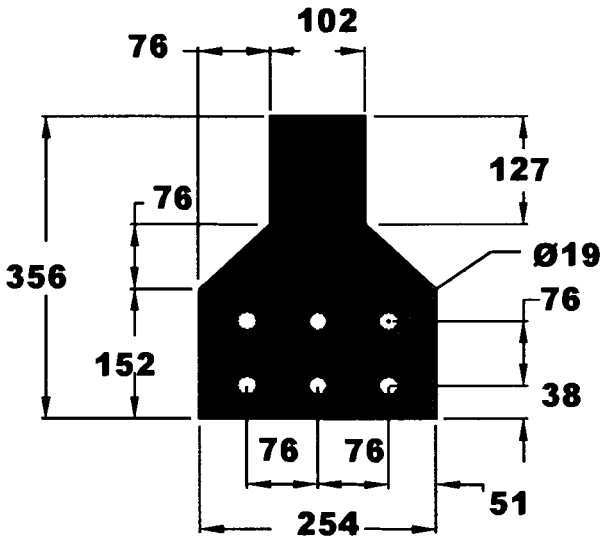

Figure 5.4 Connection Plate

The connection plates bolted into the Baldwin as shown in Figure 5.5. The connection plate was fabricated from 25-mm steel plate. The connection plates are designed to fit into the tension grips on the Baldwin test frame. The tension grips on the Baldwin test frame are manual tension wedge grips. The specimens were placed into the grips and hand cranked tight. Then load was applied to the specimen to maintain grip on the connection plates. On the Baldwin test frame, the top support moves up while the lower crosshead remains fixed.

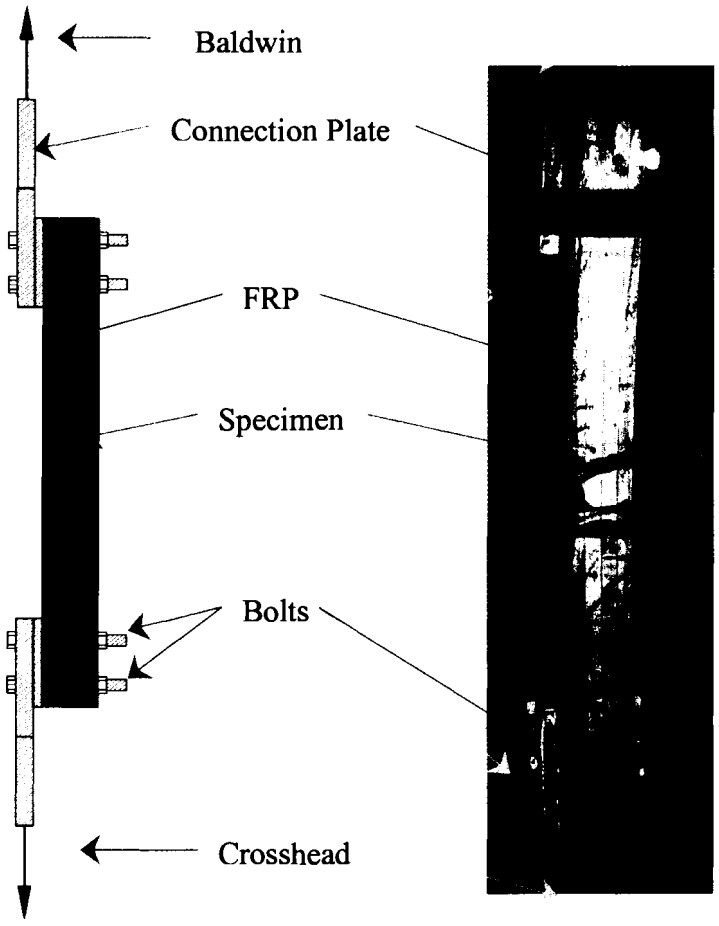

Figure 5.5 Tension Test Setup

The tests were run in load control with a load rate of 22000 N/min until the load approached the anticipated failure load, then the system was switched to displacement control. An equivalent load rate of approximately 22000 N/min was also maintained during the displacement control portion of the test. Due to safety concerns with the load approaching the failure load of the bolts, the load limit was set at 500 kN. The shear capacity of the six Grade 8 bolts was 528 kN. In order to limit the risk to personnel and equipment in the event of bolt shear failure, a safety frame was constructed around the specimen to deflect the bolts in the event that they sheared during the test.

5.3.3 Instrumentation

Load, crosshead position, and the strain at four locations on the FRP were recorded for the tensile test. The load and crosshead position were recorded from the Satec controller on the Baldwin test frame directly. The load was output by the controller as a linear voltage from 1-10 V and the relationship between voltage and load was 1V equals 4.448 kN. The controller output did not span enough of the test range to provide any useful data. Also, the controller was inconsistent in the internal recording of data. It was not possible to modify this load range with the equipment available. For some tests the data which was recorded was unrecognizable and for others the data was clear. Further, for these reasons a data acquisition system was used to record the strains and the crosshead position. An attempt was made to correlate the load data recorded by the Satec controller to the data acquired by the data acquisition system by using both time and position. However, this proved impossible, due to the variation in time step between the Satec data points and repeated position readings in the controller data. For this reason the load was manually recorded from the Satec controller screen display every 30 seconds. This load data was then correlated via time to the displacement and strain data acquired by the data acquisition system.

Due to inherent difficulties in measuring strains in wood, the strains were only measured in the FRP reinforcement. The strains were measured using Measurements Group CEA-06-125UW-350 strain gauges. These strain gauges have a resistance of 350 ohms, which is necessary to prevent excess heat generation in the gauges. This is necessary due to the inability of the FRP to disperse the thermal energy, which can

cause the FRP-gauge bond to perform poorly. For each test, four gauges were bonded to the FRP. Both the wood and FRP should each carry a portion of the tensile load. The tensile load was transferred into the FRP through the steel-FRP. A portion of the load was then transferred into the wooden glulam through the wood-FRP bond. It takes a finite length of bond for the load transferred from the FRP into the wood to fully develop. The length through which the load was transferred was unknown. The intent of using four gauges at two different positions was to qualify the shear lag effect of this tension transfer. This shear lag effect proved to be unrecognizable in the results. The gauges were located at 1/3 and 2/3 of the unbonded half length of the specimens. See Figure 5.6:

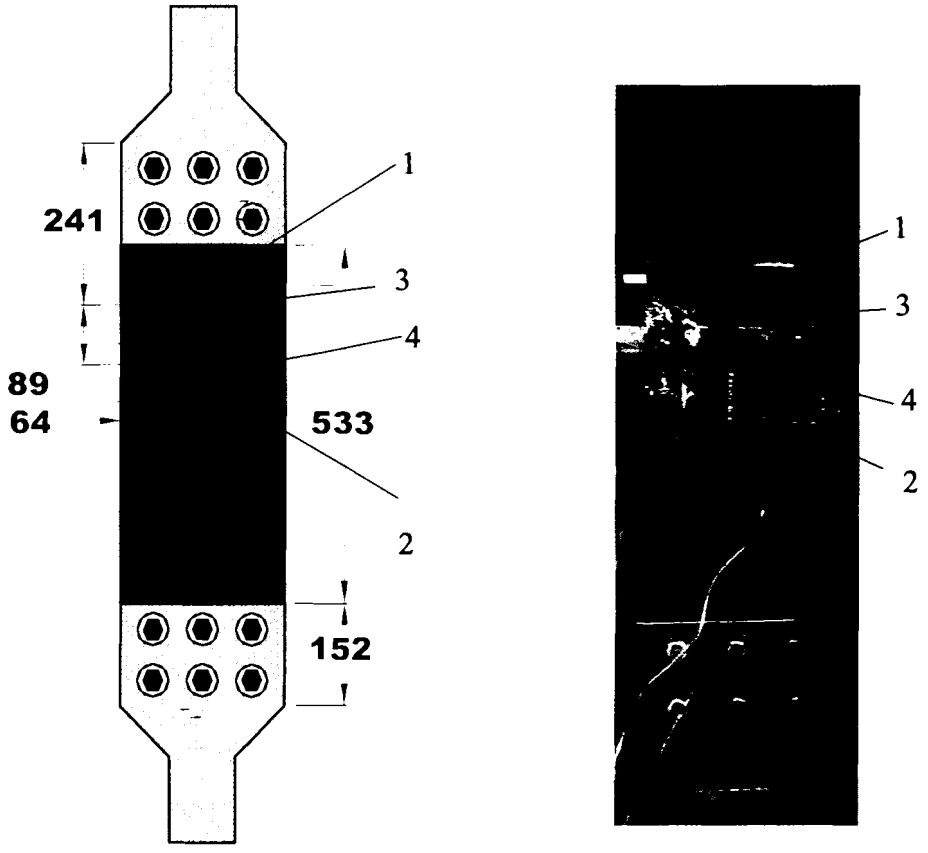

Figure 5.6 Strain Gauge Locations (Dimensions in mm)

The gauge numbers appear in Figure 5.6, as they are referenced in the results section of this chapter. These gauges were centered on each of the strips of FRP, 64-mm from the edge.

5.4 Test Results

The results of the six specimens which were tested are reported individually in three separate sections, grouped by initial bolt torque: 136 N-m, 54 N-m, and 27 N-m.

5. 4.1 Test Results for 136 N-m of Initial Bolt Torque

The first three tests were performed using an initial bolt torque of 136 N-m. The first test was a preliminary test and was designed to evaluate the instrumentation and test set up. The capacity of the splice connection was estimated at 410 kN based on the work of Boone (2002). The test setup was designed for 410 kN. Grade 5 bolts were used on the first test, which was terminated when the load reached 423 kN, at which point the load on the bolts became critical. The specimen did not fail at this load. This test was also performed with different instrumentation than the other tests. The strain gauges were at 1/3 the length of the specimens, symmetric about the center of the beam to test the symmetry of the beam and connections. These proved that the beam did in fact perform symmetrically. Other valuable information regarding the strain levels and gain settings for the strain gauges were obtained from this test.

The second tension test performed at an initial bolt torque of 136 N-m varied from the first test in several ways. Based on the results of the first tension test, the displacement rate was increased to better approximate the desired load rate of 22 kN/min. Due to an error in programming the increased displacement rate into the controller, the displacement rate slowed too small to cuase the specimen to increase in

load at a substantial rate, so the specimen stopped loading at 333 kN. Therefore, the test was stopped, the error was corrected, and the test was then rerun with the proper actuator settings until failure. Specimen 2 remained linearly elastic and no significant damage was incurred from the first loading cycle. The load rate which was used was, 22 kN/min until 333 kN, then a displacement rate of 0.25-mm/min displacement control. The load rate which resulted from the displacement rate of 0.25-mm/min was approximately 4 kN/min, less than the target load rate of 22 kN/min. The displacement rate was increased for the later tests to more closely approximate the 22 kN/min target load rate. Position was recorded by the data acquisition system in addition to the strains. Three of the gauges were damaged in the installation of the specimen into the Baldwin test machine. Only one strain gauge survived the installation of the test specimen, the load-strain relation from the surviving gauge can be seen in Figure 5.7:

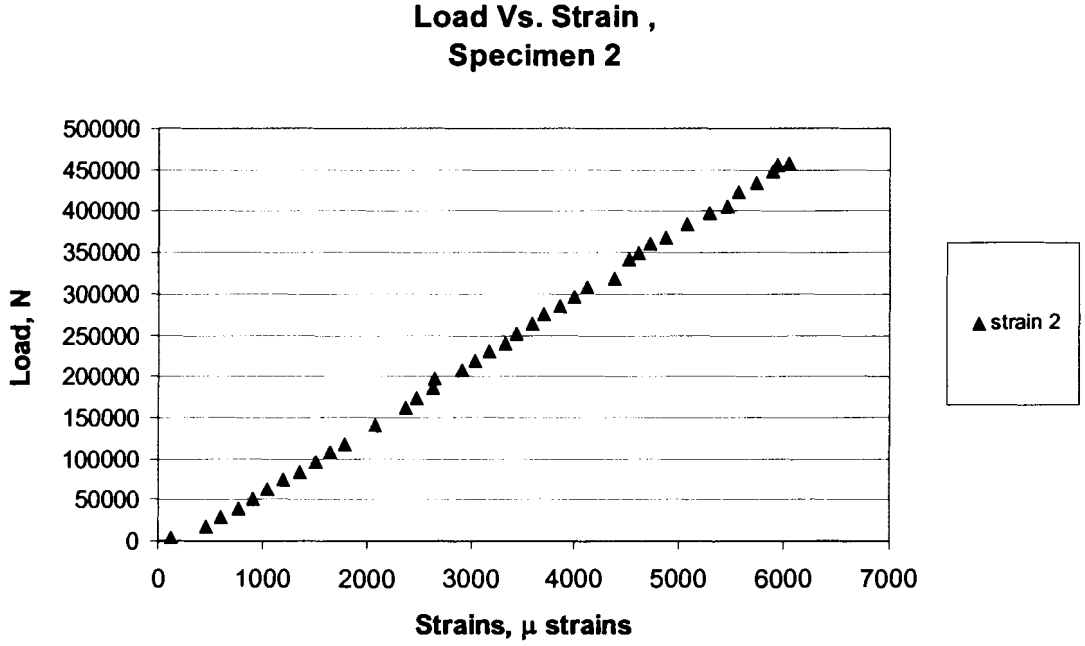

Figure 5.7 Specimen 2 Strain-Load Relation

As seen in Figure 5.7, the load-strain relation was linear. The slope of the load-strain relation was used as a means to compare the stiffnesses of the connections between tests. It is not possible to use load-deflection for direct comparison between tests because the amount of slippage in the Baldwin test frame varied from test to test. The slippage of the connection plate was increased by damage, plastic deformation, due to the large moments induced by the eccentricity of the tensile load. The load-strain relation was compared across a constant interval for all tests. To limit the effects of signal noise and gauge damage the load–strain relation was evaluated between the loads of 45 kN and 333 kN. The slope of the load-strain relation for the second test was found to be 0.0125 strains/N. Figure 5.8 shows the full results of the second tension test:

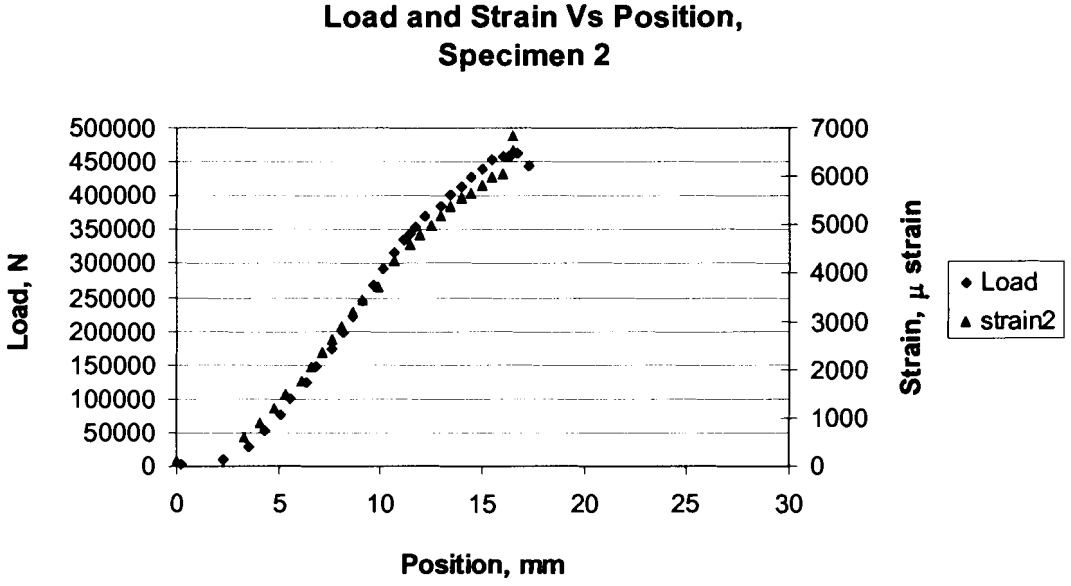

Figure 5.8 Load and Strain with Respect to Position, Specimen 2

Figure 5.8 shows the nonlinear load deflection relation of the rail section and connection. The nonlinearity of the load-displacement relation can be explained by breaking the curve into sections. The first section displays a smaller increase in load per increase in displacement, due to the slippage being eliminated from the system.

The second region is the region that displays linear load-strain and load-displacement relations. The final region consists of the nonlinear load-strain relation. The behavior of the final region was dominated by the behavior of the steel-FRP epoxy bond, which behaves non-linearly and yields. The yielding of the steel-FRP epoxy bond can be observed in the permanent plastic deformations which occur in the connection. The bond failed when areas of the epoxy failed. It is not possible to observe this failure because the plate is still attached to the FRP after failure. The strain results show the increase in strain up to a point near the maximum load, 462 kN. The strains spike at the peak of the curve, which is due to slip between areas of the FRP caused by localized failures of the FRP-epoxy bond, which causes areas of fiber to be loaded or unloaded. This variation in the distribution of loading caused transverse failures in the FRP. These failures allowed sections of fiber to slip past each other. The strain gauge was on a slip plane and the gauge sheared apart. Figure 5.9 shows this slip plane behavior:

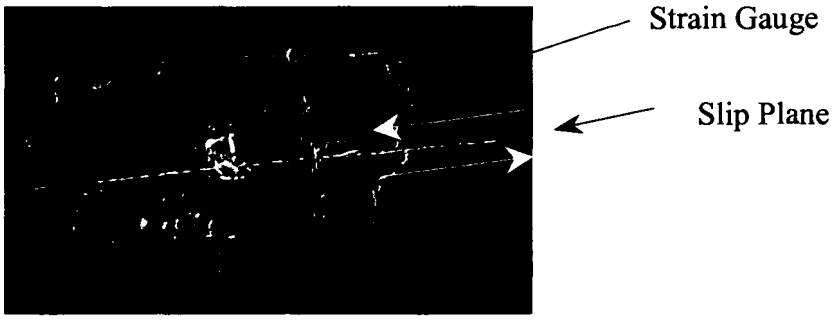

Figure 5.9 FRP Slip Plane

This shearing motion, seen in Figure 5.9, causes the strain reading to increase rapidly, and eventually to reach the maximum value when the gauge is completely sheared. The arrows indicate the direction of the shear movement.

The failure of the FRP, in shear parallel to the fiber direction was unexpected. However, the failure of the bolted connection occurred as anticipated with a plug-type tear out in the reinforced glulam, which occurred due to yielding of the steel-FRP bond. This plug-type failure was evident when looking at the ends of the tensile specimens. Figure 5.10 shows the end of specimen 2 and its bolt tear out:

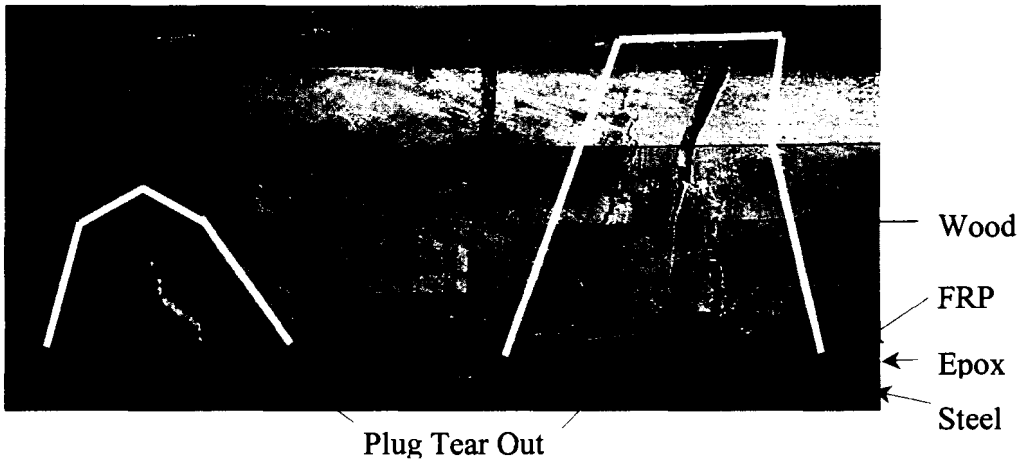

Figure 5.10 Bolt Tear Out

Figure 5.10 shows the plug tear out failure in the wood-FRP composite. It is important to note that despite the plug failure the connection remained intact and still carried a significant load.

The third test which was performed at an initial bolt torque of 136 N-m, specimen 3, was the only test performed with an initial bolt torque of 136 N-m which was performed with one loading cycle until failure. The load rate, which was used until a load of 333 kN, was 22 kN/min. From 333- kN until failure, a displacement rate of 0.5 mm/min was used. This displacement rate yielded an approximate load rate of 18 kN/min. For this test a new system was used to protect the strain gauges while installing the specimen into the testing frame, and all four of the strain gauges

survived the installation of the specimen. Load-displacement data was also obtained from the Satec controller. In this test, the specimen did not smoothly ramp up to a peak load and then fail once. Instead, as the load approached 400 kN the connection slipped, losing some load, and then resumed gaining load. The slippages in the connection are clearly seen in Figures 5.11 and 5.12 by the anomalies in the load-position, load-strain, and position-strain curves. There were several small slippages before the peak load was reached. The load strain for this test is displayed in Figure 5.11:

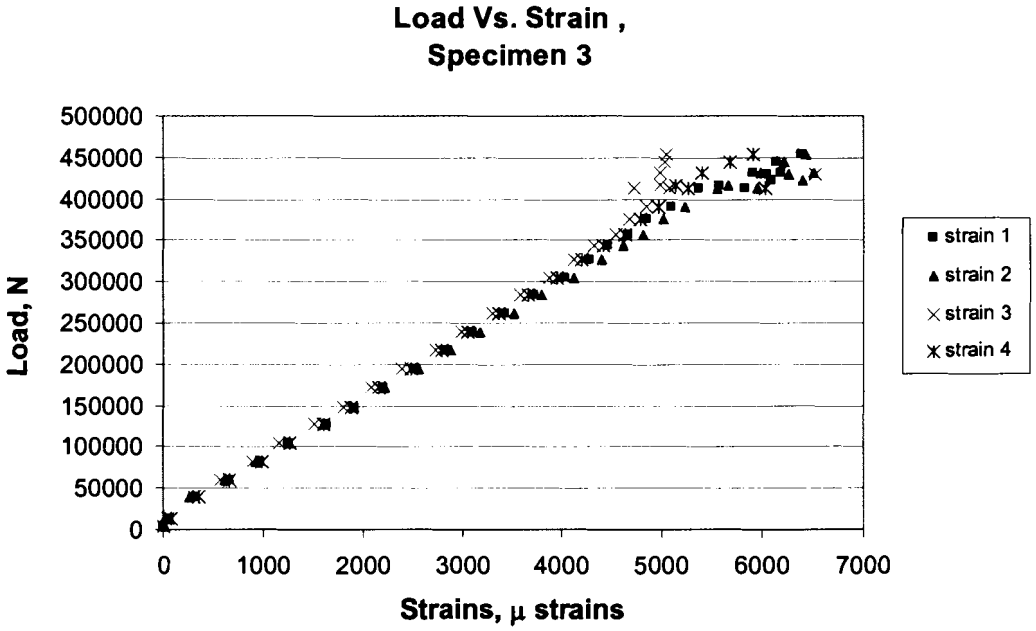

Figure 5.11 Specimen 3 Strain-Load Relation

As seen in Figure 5.11, the strain relation is linear until the first connection slippage. After the first connection slippage the load-strain relation became noisy due to the repeated load values, damage in the gauges, and an uneven redistribution of load across the cross-section. The load-strain relation was linear in the region before the yielding in the epoxy occurred. The average slope of the load-strain relation between

45 kN and 333 kN for all four gauges is 0.0138 μ strains/N. The maximum deviation from the average for any gauge is 4.5%.

It is important to note from Figure 5.12 that both strain gauges 3 and 4 encountered damage during the first slippages of the connection. This damage is due to longitudinal cracks in the FRP in the area of the strain gauges which occurred during the slippage similar to specimen 2. Strain gauge 4 failed totally. The strain gauges on the opposite side, 1 and 2, remained intact and follow the same shape as the loading curve. See Figure 5.12:

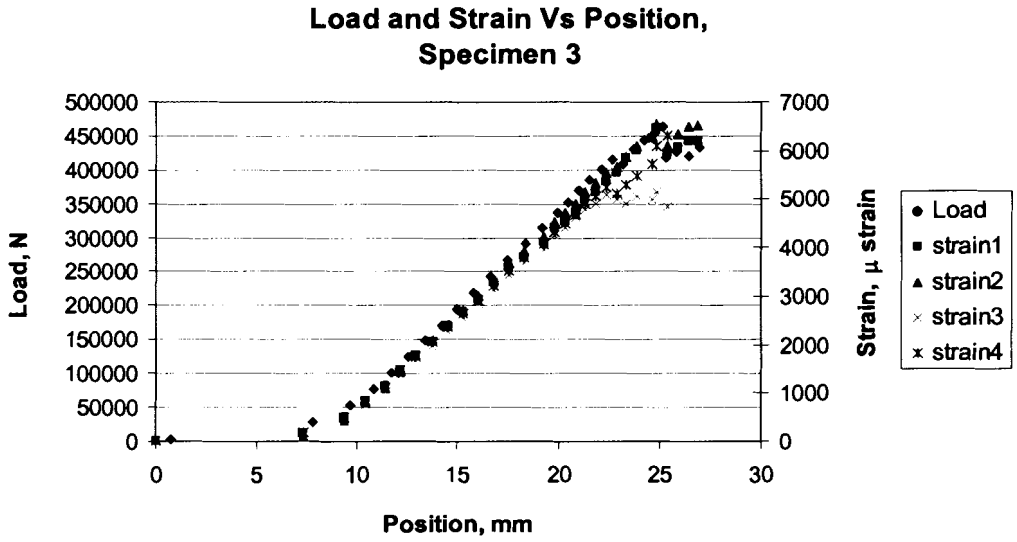

Figure 5.12 Load and Strain with Respect to Position, Specimen 3

In the period before the first connection slippage all four of the strain gauges yielded similar results.

Despite the slippages in the connection and the loss of load, the connection remained intact and still maintained substantial tensile capacity. The final failure was a yielding of the steel-FRP bond. The bond yielding resulted in bond slippage which in turn resulted in a shear plug-type of failure of the reinforced glulam as seen in the specimen 2. The ultimate load for specimen 3 was 463 kN.

The overall performance of the two tests which were performed at an initial bolt torque of 136 N-m was greater than anticipated. The average capacity was 463 kN, which is more than 1.9 times the anticipated design load on the connection (240 kN). In addition, results were very consistent with the maximum difference from the average being 440 N. Also, it is important to note that the moments which were induced in the specimens, due to the eccentric loading, approached the predicted failure moment with no significant effects noted other than the large curvatures induced.

5.4.2 Test Results for 54 N-m of Initial Bolt Torque

Two tests were performed with an initial bolt torque of 54 N-m. The first test which was performed with the initial bolt torque of 54 N-m, specimen 4, produced similar results to the previous test at 136 N-m of initial bolt torque. However, there was a smaller region with nonlinear behavior before the failure of the connection than was present in specimens 2 and 3. The load-strain relation is shown in Figure 5.13:

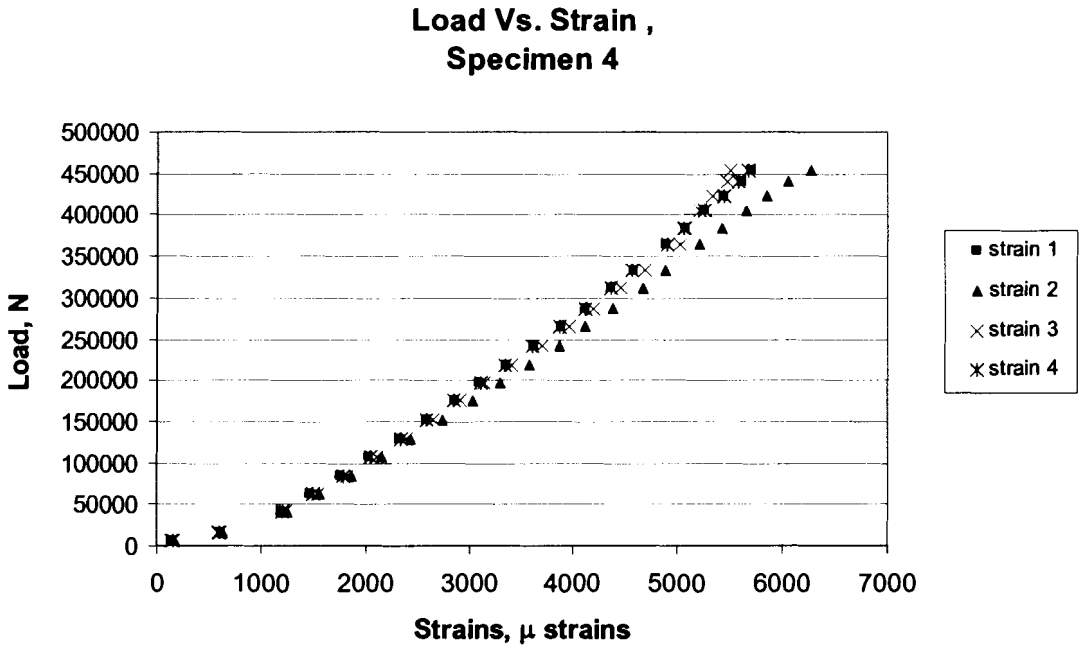

Figure 5.13 Specimen 4 Strain-Load Relation

The load-strain relationship was linear for the 54 N-m initial bolt torque and similar to the test performed at 136 N-m of initial bolt torque. The load-strain relation is shown in Figure 5.13. The average slope of the load-strain relationship between 45 kN and 333 kN was found to be 0.0118 μ strains/N. The largest variation from the mean slope was 5.4%. The effects of the nonlinear behavior of the steel-FRP bond were not as prevalent as in specimen 2, this is apparent in the nonlinear region of the load strain curve which does not lose load in region before failure. The abrupt failure of specimen 4 can be seen in Figure 5.14:

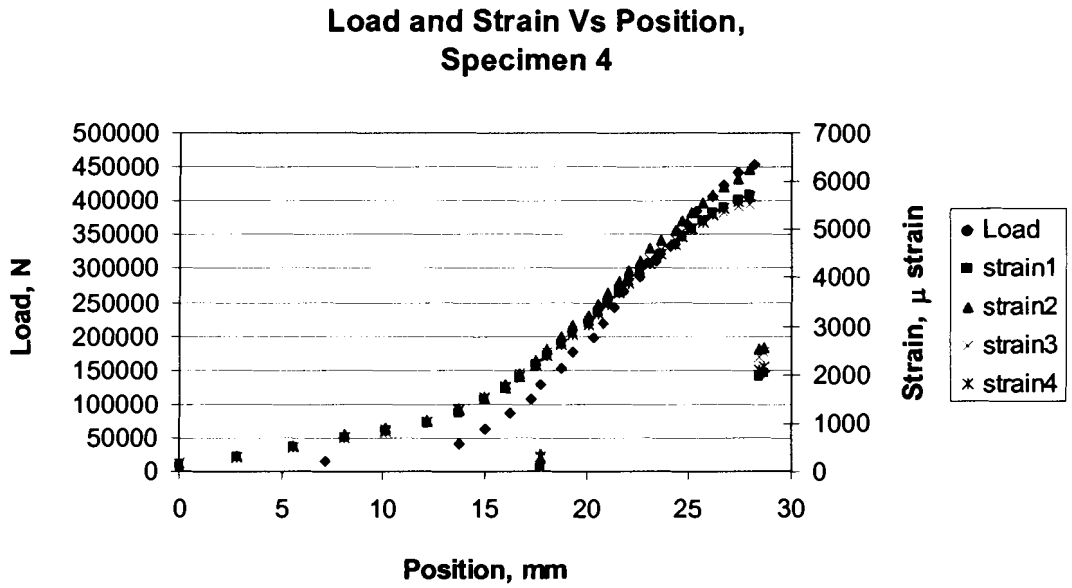

Figure 5.14 Load and Strain with Respect to Position, Specimen 4

Figure 5.14 also shows data for the unloading of the specimen. The maximum load for specimen 4 was 452 kN. This maximum load is 2.2% less than the average capacity of the specimens tested at 136 N-m of initial bolt torque. There were no large slippages in the connection preceding the failure in specimen 4, as occurred in the previous tests at 136 N-m of initial bolt torque. The failures which were observed were similar to those of the specimens tested at a higher initial bolt torque, with the steel-FRP bond yielding accompanied by a shear plug failure in the reinforced glulam. There were also longitudinal cracks in the FRP, similar to the previous specimens, caused by the redistribution of the load in the failure process.

The second specimen that was tested at an initial bolt torque of 54 N-m, specimen 5, contained a lower steel-FRP bond quality than any of the other specimens tested. Due to the lack of bond quality, there were decreases in the strength of the connection. The bond was observed to be of poor quality before the test was performed. The load-strain relation for the splice connection was still linear,

despite the lack in bond quality. The load-strain relation for specimen 5 is shown in Figure 5.15:

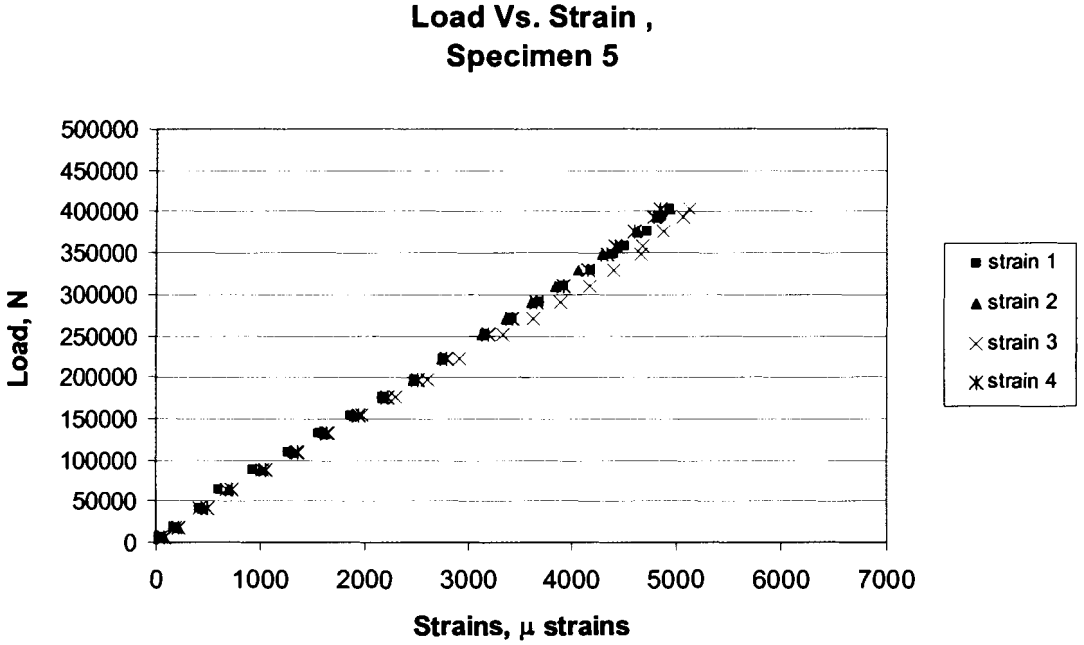

Figure 5.15 Specimen 5 Strain-Load Relation

The average slope of this load-strain relation between 45 kN and 333 kN for specimen 5 is 0.0129 μ strains/N. This is higher than the previous test performed at an initial bolt torque of 54 N-m. The difference in the load-strain relation could be due to several factors, including bond quality. The complete results for specimen 5 can be seen in the Figure 5.16:

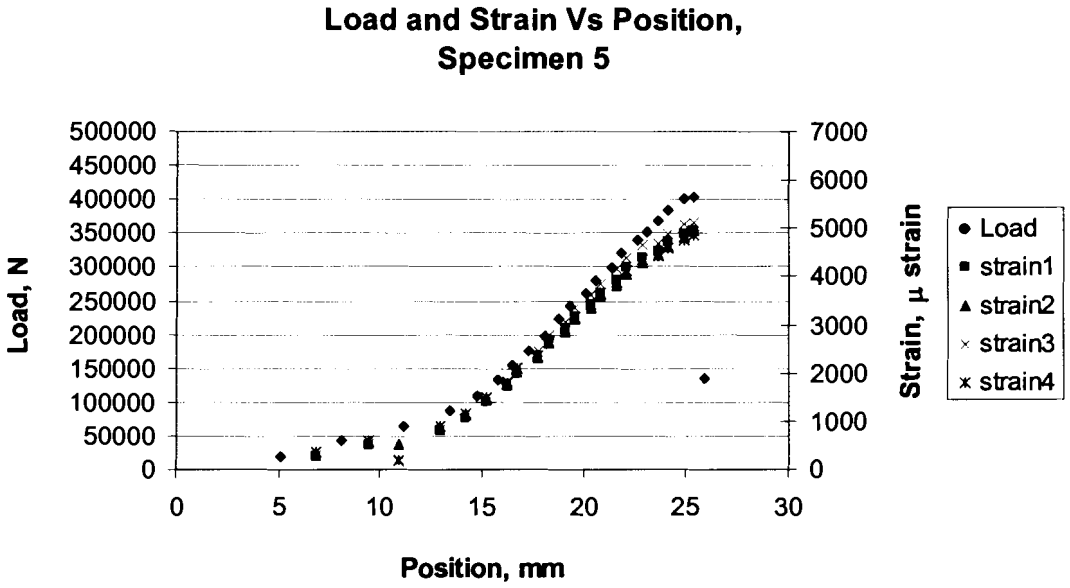

Figure 5.16 Load and Strain with Respect to Position, Specimen 5

The shape of the load-strain curve is similar to the shape of the previous specimen tested at this torque load, despite the decreased bond quality. The peak load which was carried by the connection, despite the bond quality problems, was 403 kN, which is an 11% decrease in capacity from the specimen 4, and approximately 1.67 times the required capacity of the connection. The failures which were observed were similar to the failures of the previously tested specimens, the slippage of the steel-FRP bond and resulting in plug-type shear failure around the bolts.

The overall performance of the connection tested with an initial bolt torque of 54 N-m was acceptable for the rail connection. The capacity and the failure modes of the connection are similar to those of the test performed with a higher bolt torque load. The average capacity of the connection was decreased to 427 kN, a 7.5 % decrease from the specimens tested at an initial bolt torque of 136 N-m, despite the poor bond quality of the second specimen.

5.4.3 Test Results for 27 N-m of Initial Bolt Torque

To determine the effect of extreme bolt relaxation due to creep losses in the wood on the tensile capacity of the splice connection, two tests were performed at an initial bolt torque of 27 N-m. This torque level represents almost total relaxation of the bolt load. The load rate which was used in these tests was 22 kN/min until 220 kN, then the tests were run in displacement control at 0.6 mm/min. This displacement rate yielded a load rate of approximately 22 kN/min. The first of the specimens tested at an initial bolt torque of 27 N-m, specimen 6, achieved a load of 392 kN. This is a significant decrease from the specimens tested at a higher initial bolt torque load. Specimen 6 also exhibits a linear load-FRP strain relationship. The relationship of load and FRP strain is shown in Figure 5.17:

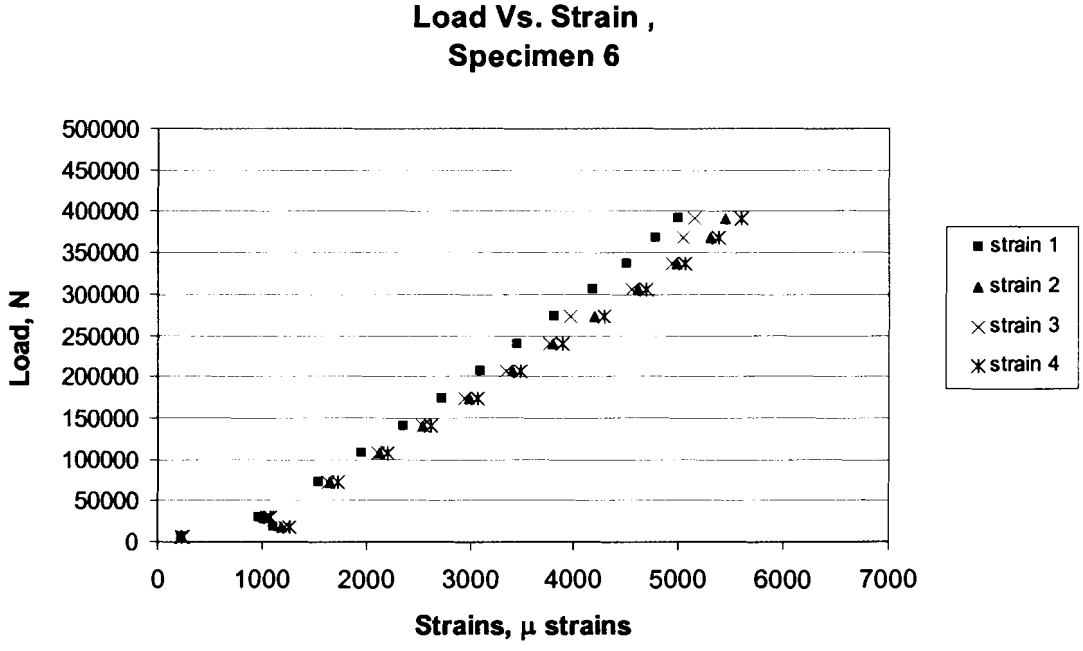

Figure 5.17 Specimen 6 Strain-Load Relation

As shown in Figure 5.17 the relationship between load and strain was linear, despite the low bolt torque. The average slope of the load strain relation between 45 kN and

333 kN for specimen 6 is 0.0120 μ strains/N. The connection still exhibited limited ductility during failure. This can be seen in the Figure 5.18:

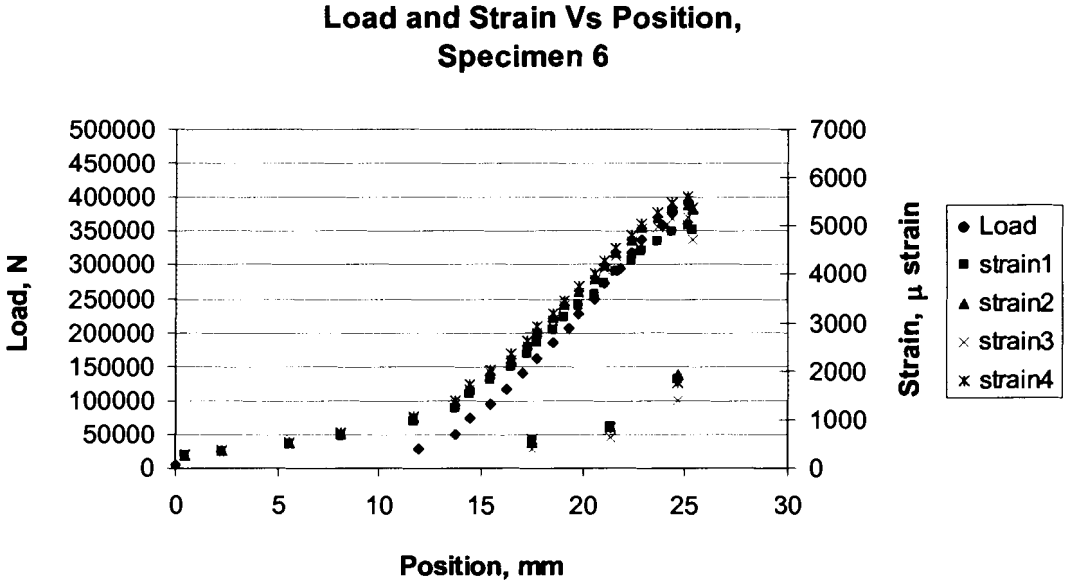

Figure 5.18 Load and Strain with Respect to Position, Specimen 6

Figure 5.18 shows the full results of the tests. All four of the strain gauges show similar results. The connection slightly yields before failure. The unloading of the specimen is also shown in the figure. The specimen still maintained a significant tensile capacity, in excess of 130 kN, after failure. The failure was observed to have more slippage of the steel-FRP bond and the associated plug-typed shear failure in the wood-FRP glulam than in the tests performed at higher levels of initial bolt torque.

The second test which was performed at an initial bolt torque of 27 N-m, specimen 7, achieved a maximum load of 376 kN, which was 4% less than the previous test. The load-FRP strain relation for specimen 7 was similar to the load-FRP strain relation for the first test performed at an initial bolt torque of 27 N-m. This load-FRP strain relationship is displayed in Figure 5.19:

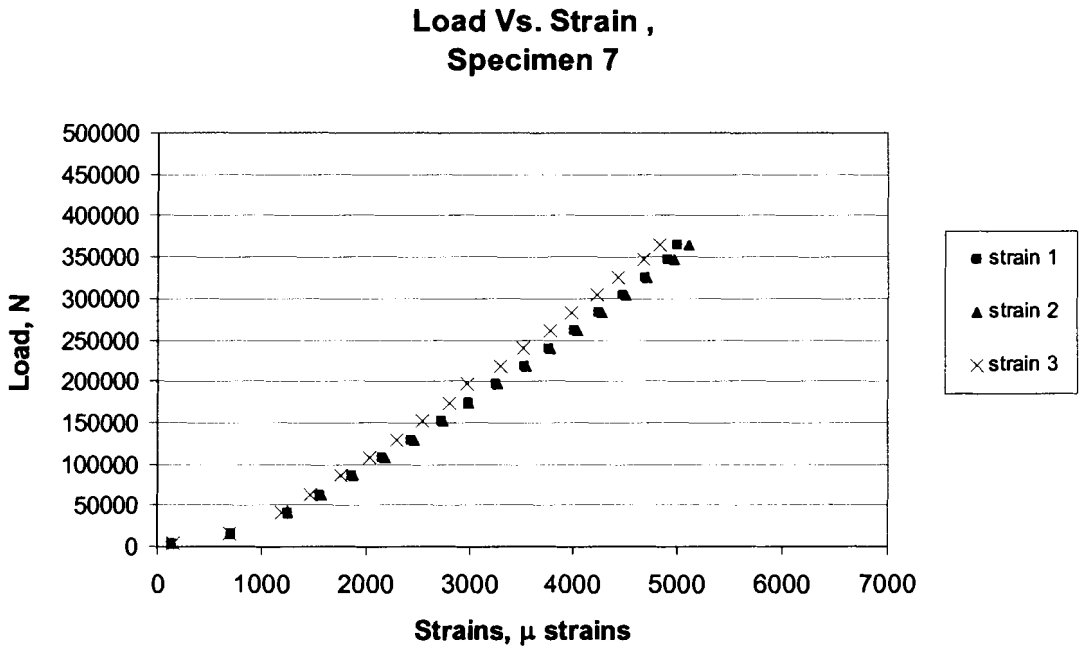

Figure 5.19 Specimen 7 Strain-Load Relation

Figure 5.19 shows the FRP strain-load relationship was linear. The average slope of the load-strain relationship between 45 kN and 333 kN for specimen 7 was 0.0118 μ strains/N. Only three of the strain gauges survived the installation of specimen 7. Specimen 7 also exhibited a similar failure mode to the previous specimens, the slippage of the steel-FRP bond, which results in a shear plug failure of the reinforced glulam. The system still maintains a significant capacity even after failure, in excess of 130 kN. The system also plastically deforms slightly before it fails. This yielding behavior is apparent in Figure 5.20:

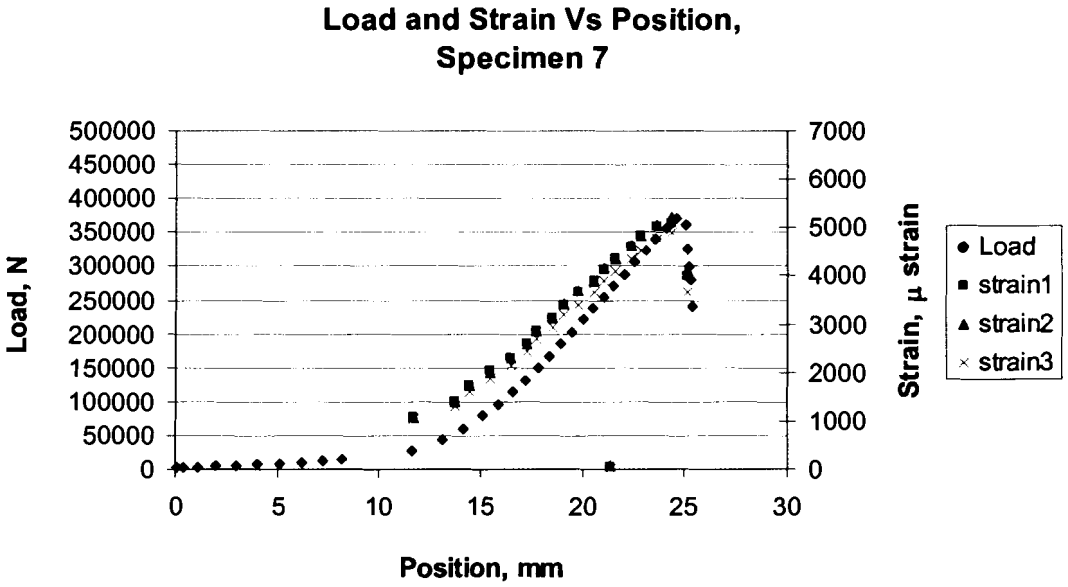

Figure 5.20 Load and Strain with Respect to Position, Specimen 7

Figure 5.20 shows the behavior of the specimen through failure and unloading. There is very good agreement between the three strain gauges which survived installation. The connection still exhibits limited yielding behavior despite the low initial bolt torque.

The average capacity for the two tests with 27 N-m of initial bolt torque was 383 kN, a 16 % decrease from the 136 N-m of initial bolt torque tests, and a 10% decrease from the 54 N-m of initial bolt torque tests. The average stiffness of the connection, load-FRP strain slope evaluated between 45 kN and 333 kN, is 0.0119 μ strains/N. There was more slippage present in the steel-FRP bond than was observed in the previous test performed at a higher initial bolt torque. This increased slippage results in a larger shear plug failure in the reinforced glulam. Peeling stresses played a larger role in the failure mode than in previous tests which resulted in the lower load capacity for the specimen. The overall results of the connection testing were within the acceptable limits for the guardrail system. Under 27 N-m of initial bolt torque,

which is very little bolt torque, the connection still maintained 1.6 times the anticipated tensile load on the splice connection in addition to retaining limited ductility.

5.5 Durability Testing

An additional set of tests which must be performed on the splice connection are durability/delamination testing. These durability tests are important to qualify the behavior of the splice connection and glulam under adverse exterior environmental conditions. The test which was used to qualify the durability of the bonding of the steel to the FRP and the FRP to the steel was the ASTM D1101 delamination test, as discussed in Chapter 3.

A total of three delamination specimens which included the bonded steel splice plate were tested. Also, three control specimens were tested without the steel splice plate. Due to limited material, the specimens tested under ASTM D1101 were cut from test specimen 1. Specimen 1 was tested under tension, however, it was never fully loaded and the failure which it encountered was a creep relaxation of the steel-FRP bond. This bond failure did not damage the reinforced glulam portion of the specimen. In order to test the durability of the connection, the specimens were specially made. It was not possible to fabricate a 152-mm wide splice and cut it into two, 76-mm wide specimens due to the heating associated with cutting the steel. Therefore, 76-mm sections of reinforced rail were cut and a 76-mm piece of steel was bonded onto the reinforced glulam. The locations of the specimens in the billet is displayed in the Figure 5.21:

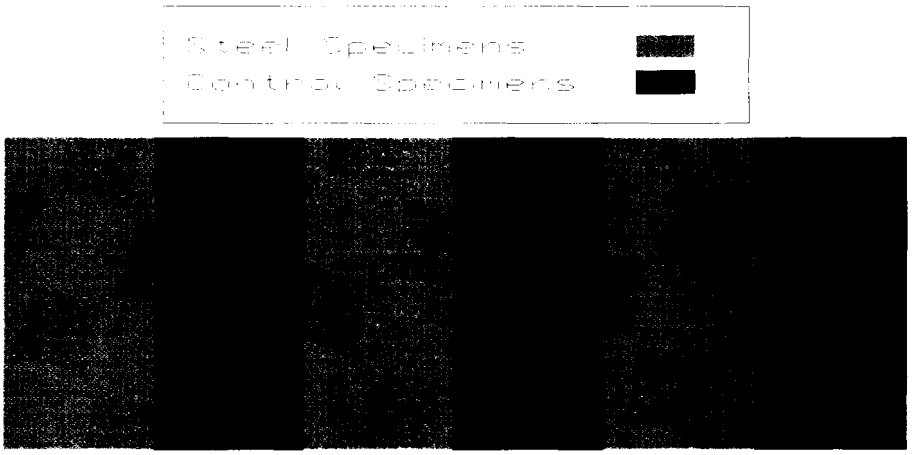

Figure 5.21 Splice Connection Delamination Specimen Layout

The splice specimens which were tested for the ASTM D1101 were fabricated with the same adhesive and procedures as discussed earlier in this chapter. The effects of the ASTM D1101 test are displayed in the Figure 5.22:

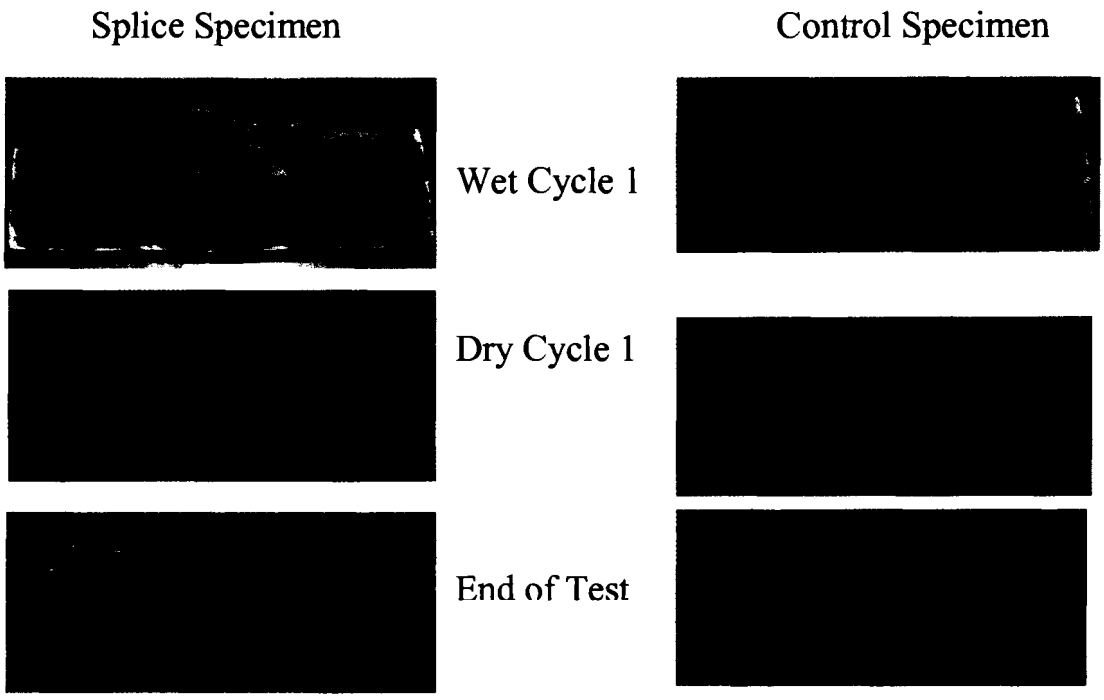

Figure 5.22 Effects of ASTM D1101

The results of the ASTM D1101 test were better than anticipated. All of the specimens passed the ASTM D1101 test method A. There was minimal delamination of the FRP-steel bond. In the control specimens, there were similar delaminations to those seen in the previous specimens which were tested under the ASTM D1101, with limited delamination in the areas of gaps in the wooden glulam. There was no measurable delamination. The steel-FRP bond and the FRP-glulam bond work to smooth the stress discontinuity between the wood, FRP, and steel. The steel constrained the system and did not allow the wood to bend under the hygrothermal loading. The end of the cross section instead curves in to the point where the FRP was bonded. This difference in curvature is caused by the addition of steel to the system is seen in Figure 5.22:

Steel Reinforced Control

Figure 5.23 End Curvatures of ASTM D1101 Specimens

Overall, the addition of steel to the reinforced hardwood glulam decreases the delamination of the FRP from the wood. There was also no delamination of the steel

from the FRP in the test. The bonded steel splice connection passed the ASTM D1101 test.

5.6 Summary and Conclusion

The testing of the rail splice connection showed that the splice connection has significant capacity for use in the reinforced guardrail system, even with minimal bolt torque. The capacity decreased by only 16% with the drop in bolt torque from 136 to 27 N-m. Also, the percentage of load carried by the FRP decreased as bolt torque load decreased, as evident from the 17% decrease in the load-FRP strain curve between the initial bolt torques of 136 and 27 N-m. An initial bolt torque of 27 ft-lbs corresponds to a very loose connection and yet both of the tests which were performed maintained a tensile capacity of above 360 kN, 1.6 times the predicted load in the splice connection. The bonded steel splice connection also passed the ASTM D1101 durability test and therefore the splice connection will be suitable for exterior exposure. The bonded steel plate splice connection has been proven capable of carrying tension between two rail sections and appears to be acceptable for use in the reinforced hardwood glulam guardrail system.

Chapter 6

COMBINED BENDING AND TENSION TESTING

6.1 Introduction

In order to quantify the response of the reinforced hardwood glulam guardrail under crash conditions, the rail design must be evaluated under simultaneous bending and tension. In an actual guardrail impact, tension is induced as a result of the large lateral deformation of the system and the restraint of the rail by the post. From the Barrier VII modeling discussed in Chapter 2, it was found that the amount of tension which was developed in the system is dependent on the stiffness of the guardrail sections. This chapter presents a program to test the rail design under combined bending and tension loading. The test results of the combined bending and tension testing are also reported in this chapter. First, a novel fixture was designed that produces controlled tension in the rail due to the shortening of the rail in flexure. Second, the test setup and instrumentation are discussed. Finally, the results of the testing program are reported.

6.2 Design of the Combined Bending and Tension Reaction Fixture

Producing bending simultaneous with tension can be accomplished in several different ways. The obvious solution would be to use two actuators, one to apply a vertical load, producing bending, and the second applying axial tension. However, this approach would require complex actuator controls and actuator mounts for the horizontal actuator. The more practical alternative chosen utilized a three member truss supporting each end of the specimen as shown in Figure 6.1:

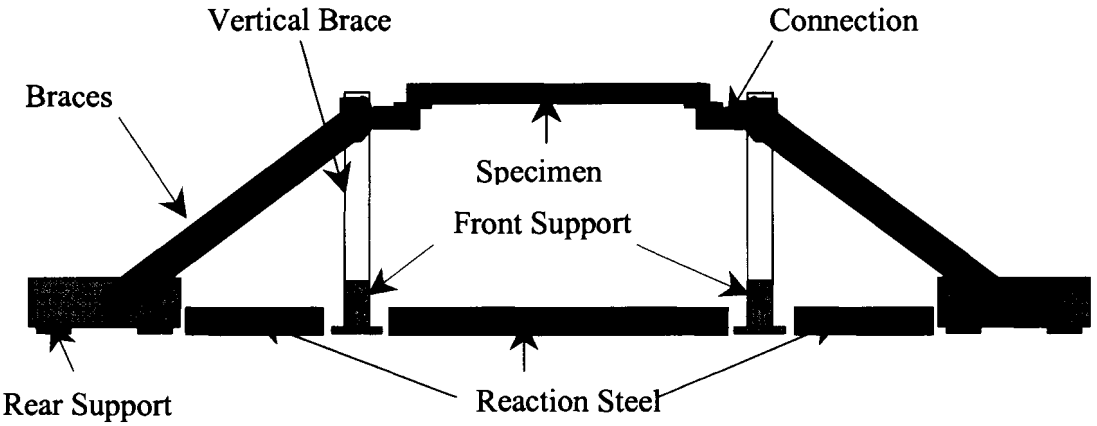

Figure 6.1 Combined Bending and Tension Reaction Fixture

As the rail shortens, due to flexure, the trusses act as springs at each end of the rail, inducing tension in the rail. The challenge with this approach lies in analyzing the system appropriately and sizing the braces so that the desired tensile force is produced for a given applied vertical load.

6.2.1 Modeling

In order to develop a model of the combined bending and tension test, the shortening of the beams during flexure must be determined. The equation for the differential shortening of an element assumes small deformation theory and negligible axial strain is defined as:

$$d\Delta = dx - ds \cdot \sqrt{1 - \left(\frac{dv}{dx}\right)^2} \qquad 6.1$$

In Equation 6.1 $d\Delta$ is the change in length of the differential element in the x direction, dx is the undeformed length of the element in the x direction, ds is the deformed differential length of the element, and v is the displacement in the y (vertical) direction of the element. In Equation 6.1 ds is often assumed to be approximately equal to dx. However, due to the large tensile loads and relatively low

axial stiffness of the reinforced glulam, the axial deflection could be significant. Therefore, *ds* is computed as:

$$ds = dx - \frac{P \cdot dx}{A \cdot E} \tag{6.2}$$

Where P is the axial load, A is the area of the element, and E is Young's modulus. The modulus, E, is a constant value for a linearly-elastic material. The reinforced glulam is only linear-elastic until the first tensile failure of a lamination. Therefore, the model is only valid until the first tensile failure occurs. Equation 6.2 is substituted into the expression for the differential element deflection and integrated to yield Equation 6.3:

$$\Delta = L + \left(1 - \frac{P}{A \cdot E}\right) \cdot \int_0^L \sqrt{1 - \left(\frac{dv}{dx}\right)^2} \cdot dx \tag{6.3}$$

Where L is the length of the element, and Δ is the total change in length in the x direction of the element. The radical in Equation 6.3 is eliminated by using the binomial theorem and the quantities are separated and integrated to yield the result in Equation 6.4:

$$\Delta = -\frac{P \cdot L}{A \cdot E} + \int_0^L \frac{1}{2} \cdot \left(\frac{dv}{dx}\right)^2 \cdot dx \tag{6.4}$$

In order for Equation 6.4 to be relevant, it has been placed into the context of structural analysis. Structural analysis begins with a two-noded element of length L. The element exists in the global coordinates system x and y. The element is shown in Figure 6.2:

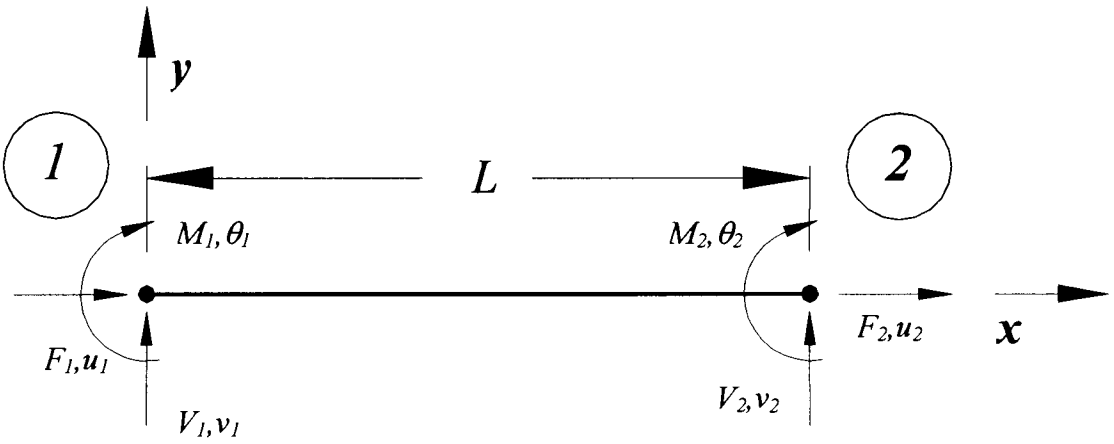

Figure 6.2 2D Beam Element

The elements are constructed with nodal forces in the x and y directions and a moment. The displacements at the nodes are: u in the x direction, v in the y direction, and θ is the angle of rotation, positive counter clockwise. See Figure 6.2. The vector of element displacements, U, is defined as:

$$U = \begin{bmatrix} u_1 \\ v_1 \\ \theta_1 \\ u_2 \\ v_2 \\ \theta_2 \end{bmatrix} \tag{6.5}$$

The element displacements in the y direction are defined by shape functions and nodal values. Third order shape functions are used to approximate the displacements of the elements (McGuire, 2000). These shape functions are then multiplied by the vector of nodal displacements for the elements. The displacements in the y direction, v, are defined as:

$$v = N \cdot U \tag{6.6}$$

The vector of nodal displacements, U, is not a function of the element x coordinate. Therefore, the derivative of the displacements in the y direction are functions of the derivatives of the shape functions multiplied by the nodal displacement vector:

$$v' = N' \cdot U \tag{6.7}$$

Substituting Equation 6.7 into Equation 6.4:

$$\Delta = -\frac{P \cdot L}{A \cdot E} + \int_0^L \frac{1}{2} \cdot U^T \cdot N'^T \cdot N' \cdot U \cdot dx \tag{6.8}$$

Since the vector of nodal deflections is not dependent on x, the relationship becomes:

$$\Delta = -\frac{P \cdot L}{A \cdot E} + \cdot U^T \int_0^L \frac{1}{2} \cdot N'^T \cdot N' \cdot dx \cdot U \tag{6.9}$$

The integral is defined as the geometric stiffness matrix, k_g, which is commonly known from geometrically nonlinear structural analysis (McGuire, 2000). Equation 6.9 becomes:

$$\Delta = -\frac{P \cdot L}{A \cdot E} + \cdot U^T \cdot k_g \cdot U \tag{6.10}$$

To find the total displacement for the rail, the axial displacement of each element is summed, where n is the total number of elements:

$$\Delta_T = \sum_{i=1}^{n} \left(\frac{P \cdot L_i}{A_i \cdot E_i} + U_i^T \cdot k_{gi} \cdot U_i \right) \tag{6.11}$$

Once the method of calculating the displacements had been found, the system was modeled using geometrically nonlinear structural analysis code written in MATLAB to quantify the level of shortening which the beam would encounter. The complete algorithm is given in the next section.

6.2.2 Combined Bending and Tension Reaction Fixture

The combined bending tension fixture was designed based on a three member triangular truss at each end of the beam. These trusses were mounted to the floor.

This method was chosen because it was simple, allowed for the high stiffness needed to induce the tension, and it could be easily modified to increase or decrease the stiffness and the tension which is induced in the system. See Appendix 1 for detailed drawings of the final fixture design. The full span of the rail specimen and connection was 2.438-m between the pins. The specimens which were tested had a total length of 1.829-m. The model considered the specimen to be 1.676-m long, the distance between the centerlines of the splice connection. The remaining length, 762-mm, connects the rail specimen to the truss. The centerline of the beam was also 29-mm above the centerline of the pins. The 29-mm dimension applies to the redesigned test fixture used on the three successful bending-tension tests; the original eccentricity was approximately 132-mm as discussed later in this chapter. The fixture was modeled as a beam with an applied force at the end. See Figure 6.3:

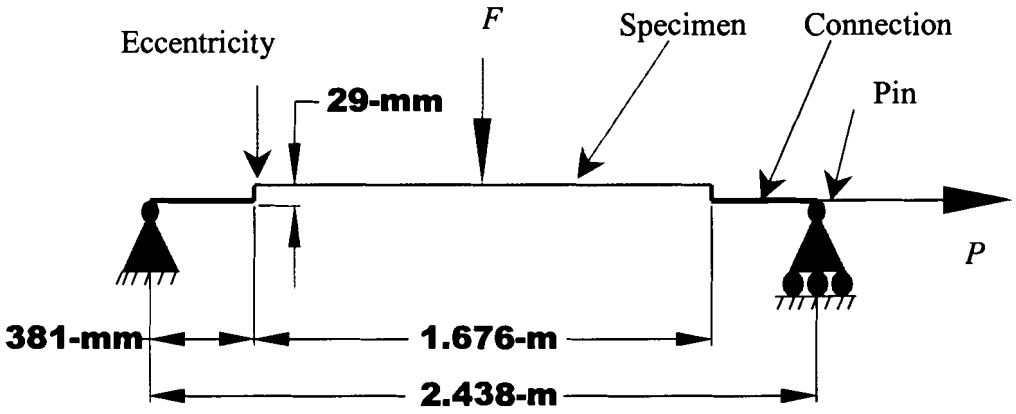

Figure 6.3 Model of Combined Bending-Tension Test

The 2.438-m length was modeled with three different sections. The first type of element used was the connection from the pin to the beam. This region consists of three 127-mm elements from the center of the pin to the center of the bolt pattern of the splice connection. These connection elements were modeled with an average

moment of inertia and area for the length of the section. A 29-mm long vertical element was used from the centerline of the pin to the neutral axis of the beam. This vertical element represents the eccentricity of the connection. The vertical element had a large moment of inertia and area. The third area of the test setup which was modeled is the specimen. The 1.676-m length was modeled with 76-mm long elements. The elastic modulus of the reinforced glulam was found from the pure bending test to be 10.3 GPa, as discussed in Chapter 4. The moment of inertia was calculated using the transformed section method as 14×10^6-mm^4. The area was found by the transformed section method to be 0.023 m^2.

The majority of the curvature occurs in the specimen. The connections bend minimally under the loads for which the section was modeled, although the connection does rotate significantly. The vertical load, F, was applied at the center of the beam, and the axial load, P, was applied at the roller end of the fixture. The second order structural analysis code used here does not account for actual shortening of the elements, therefore the elements could not be used as springs to apply the axial force. The axial force, P, was computed using one half of the shortening of the beam multiplied by the net horizontal stiffness of the brace members, which act as springs. Each side of the fixture has two braces. The net stiffness which result from these braces, which accounted for the 27° inclination, was 259 kN/mm.

The structural model was evaluated using structural analysis code which was developed in the CIE 640 Advanced Structural Analysis class at the University of Maine. This code was written in MATLAB and has been verified on a number of linear and nonlinear test problems as part of the course. A top-level program was

written to find the shortening of the beam and the equivalent induced force, which used the results from the structural analysis of the guardrail.

The algorithm used to solve the system is:

Define the Properties, Connectivities, and Nodes

Tolerance = 0.1%

While Error <= Tolerance

$P_{old} = P_{new}$

Apply P and F

Solve $R=0$

$\Delta = shortening(U)$

$$P_{new} = k \cdot \frac{\Delta}{2}$$

$$Error = abs\left(\frac{P_{new} - P_{old}}{P_{old}}\right)$$

End

Solving $R=0$ represents performing the geometrically nonlinear structural analysis algorithm; R is the residual force vector. When R is zero, the system is solved, and the vector of nodal displacements and member forces are output. These nodal displacements are used to calculate the shortening of the beam, Δ. The target values for the sizing of the braces were a tensile force of 178 kN induced in the rail due to a 58 kN applied vertical load. These target values were based on preliminary analyses using Barrier VII, similar to those discussed in Chapter 2. However, these models used incorrect material properties and did not include the hinged elements in the system, and were therefore only used for the design of the braces. The actual axial load which was induced in the system was 240 kN. The initial modeling of the combined-bending tension fixture predicted that with 58 kN of applied vertical load,

the tension which is induced in the rail was 148 kN. This 148 kN load is 17% lower than the target value of 178 kN. There was an error in the computations of the original model which resulted in the original model being stiffer than the final model. However, the final model results agree very well with the actual test data, as reported later in this chapter.

6.3 Combined Bending and Tension Test Setup

6.3.1 Combined Bending and Tension Specimens

In order to develop significant tension in the system, it is necessary to hold the tolerances on the specimen layout tight. Small amounts of slippage in the connections will reduce the tension that is induced in the rail. In order to minimize the misalignment of the specimens and gaps in the system, a special fixture was used to fabricate the specimens and the bolt holes were the precise size of the bolts. The overall length of the specimen is 1.829-m. The length of the glulam used was 1.822-m. This is to allow the specimen to fit into the fixture. The reinforced glulam is bonded to a 152-mm by 254-mm by 13-mm thick steel plate. The fixture which was developed to ensure the alignment can be seen in Figure 6.4:

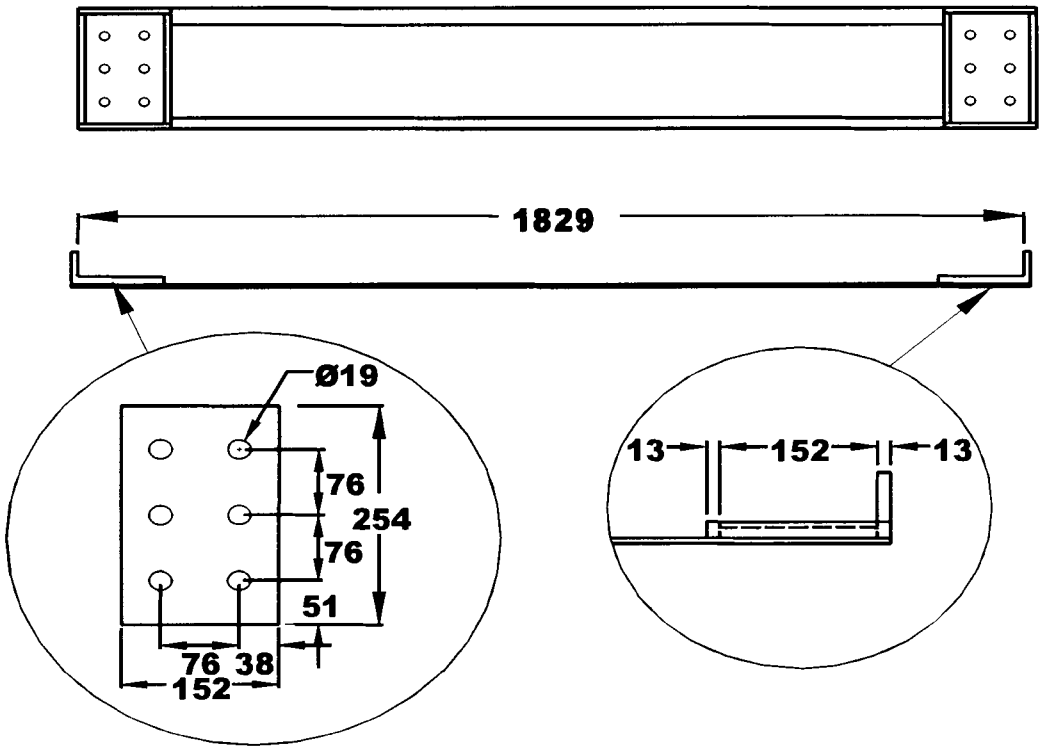

Figure 6.4 Specimen Alignment Fixture (all dimensions in mm)

The specimens were fabricated by first grit blasting the steel, then placing 162-g of epoxy on the steel plates, as described in Chapter 3, and placing the steel plates into the fixture. Next, the reinforced glulam was sanded and placed on top of the epoxy covered plate in the fixture. Then approximately 21 kPa was applied to the reinforced glulam as it was moved to ensure a quality bond by removing air from the bond line and to squeezing out excess epoxy. Finally, the reinforced glulam was aligned on the fixture and left to cure for three days. The bonds were visually inspected to determine bond line defects. There was excess epoxy squeezed out on all of the specimens fabricated. Further, none of the specimens were found to have failed due to poor bond quality. The alignment fixture with a glulam in place is shown in Figure 6.5:

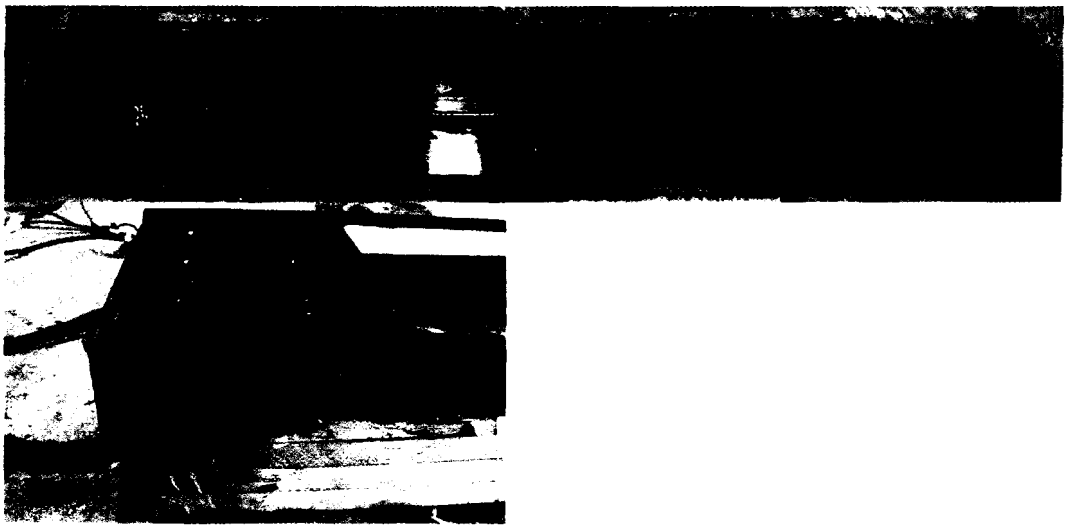

Figure 6.5 Alignment Fixture

6.3.2 Combined Bending and Tension Test Setup

The test setup for the combined bending-tension tests was the reaction fixture which was designed to apply tension from the shortening as previously discussed in this chapter. The reaction frame is shown schematically in Figure 6.1 and detailed dimensions of the reaction fixture can be found in Appendix 1. The rear supports were bolted to the reaction floor using two-36-mm Dywidag bars. The front supports were bolted to the reaction floor using 25-mm rods. The reaction frame was held together with 51-mm pins of 4140 steel, with a yield strength of 968 MPa. The test fixture was fabricated by Alexander's Welding and Machine, Inc. of Greenfield, Maine. Three pieces of C12X20.9 channel were bolted to the reaction floor to make the system self reacting. The center piece of channel was bolted to the floor with two 25-mm threaded rods, at one third of the length from the ends. The end pieces of channel were connected to the reaction floor with one 25-mm rod each, at the center of the channel. There were gaps between the ends of all three of the reaction steel channels and the truss supports. These gaps were designed to be eliminated with

shims prior to testing, causing the entire truss to become self-reacting in the horizontal direction. On one end of each piece of channel a 13-mm plate was placed, and at the other end a slightly wider shim was hammered into place. The shims were cut to different widths to remove all of the slack from the system. The shims were hammered into place with a sledgehammer to ensure that all of the gaps in the system were removed. The specimens were loaded with a 500 kN actuator mounted beneath the floor. This actuator was connected to a reaction frame on which a 250 kN load cell was mounted with a radiused load head attached to the load cell. The load head rested on a 25-mm rubber pad placed on the beam to distribute the load. The setup is seen in Figure 6.6:

Figure 6.6 Combined Bending and Tension Test Setup

6.3.3 Instrumentation and Data Acquisition

The instrumentation which was used to acquire the data for the combined bending-tension test was similar to that used in the pure bending test. The load and

position were acquired from the Instron controller. These were read using a National Instruments PCI-6031E, a 16 bit data acquisition card. The signal was read as an analog referenced single ended signal. The displacement that was output by the Instron controller was not the actual displacement of the beam. Included in the displacement of the actuator was the displacement of the fixture, which was quite small, and the compression of the rubber pad and the load head, which was significant at high loads. At 180 kN vertical load, the deflection of the load head and rubber pad was found to be 15-mm. Four Measurements Group CEA-06-125UW-350 strain gauges were bonded to the FRP of the specimens with MBond –200 epoxy. Two pairs of gauges were used: one at the center of the beam and one at ½ of the length between the center of the beam and the end of the steel plate. The strain gauge locations are shown in Figure 6.7:

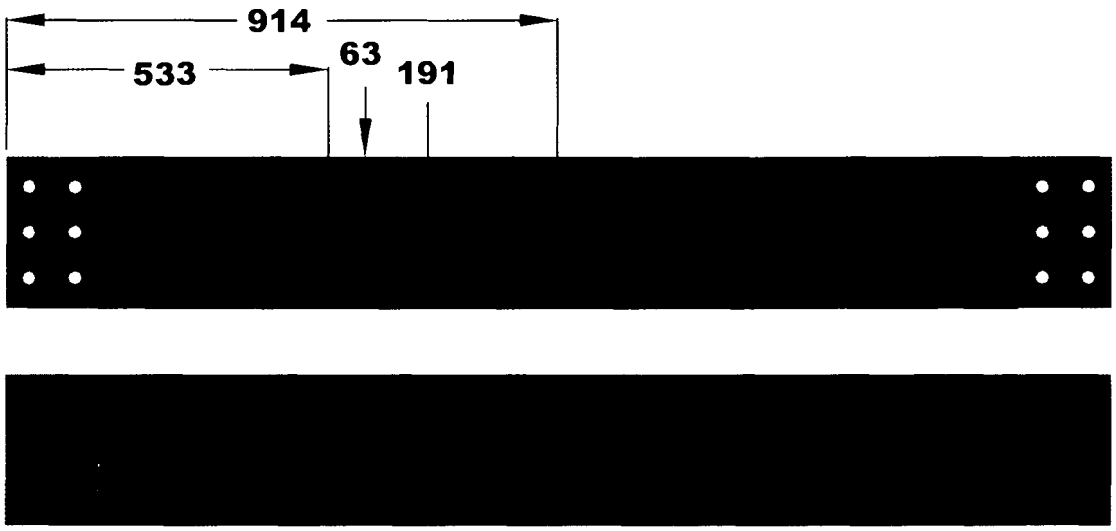

Figure 6.7 Strain Gauge Locations

Eight additional gauges were used in the combined bending and tension test. These gauges were used on the braces of the reaction frame. There were two gauges on each of the four braces. These gauges were centered longitudinally and vertically

on the braces. One gauge was placed on each side of the braces. The strain measured in the steel braces was used to calculate the tension force in the system. The strains measured in the braces were significantly smaller than those measured in the FRP, which required a more refined system to record the data. It was determined that the building ground created large variances in the signals, as high as 0.1V, which had the potential to contaminate the readings of the strains measured in the steel braces. To eliminate the effect of the building ground on the results of the tests, a laptop computer running on battery was used to record four of the gauges on the braces and the four gauges mounted on the FRP. Eight Measurements Group P3500's were used with a quarter bridge configuration to read these strains. These strain conditioners run on battery power and are therefore not affected by the building ground. The strains were output from the P3500's as an analog output into a National Instruments Daq-1200, 12 bit data acquisition card. The National Instruments Daq-1200 data acquisition card had a maximum of eight channels of input, which was why only eight gauges were recorded in this manner.

The remaining four strain gauges were conditioned using a Measurements Group P2100 in a quarter bridge configuration. This strain conditioner was connected to the building power supply so there was the possibility of induced error. The analog outputs of the P2100 was read by the same National Instruments PCI-6031E data acquisition card as load and position. The signal was read as an analog referenced single ended signal which minimized the effect of the ground noise. The total data acquisition setup is shown in Figure 6.8:

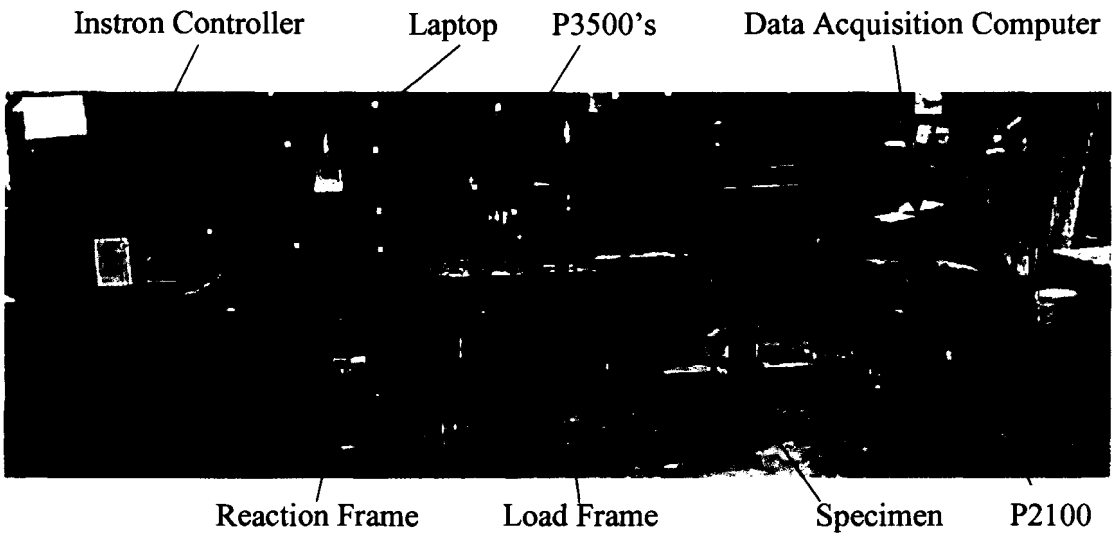

Figure 6.8 Combined Bending Tension Test Setup

This data acquisition setup proved to provide reliable data. The strains recorded by the P3500's were calibrated using the data acquisition system. The gauge factor was set for the gauges used. To eliminate the effect of noise in the system, the data acquisition system was used to record zero values for the system. The zero values were recorded for approximately 30 seconds, then the calibration button was pressed on the P3500's, which applies a stint that is the equivalent of 5000 μ strains at a gauge factor of 2.0. The P3500's display the number of micro strains which result with the gauge factor and the added resistance of the wires. This calibration value was recorded from the P3500's. The voltages resulting from the calibration were recorded by the data acquisition system for at least 30 seconds. Then zero values were recorded for approximately 30 seconds, calibration values were recorded for approximately 30 seconds, and zero values were recorded for approximately 30 seconds. All of the zero values were averaged to find the voltage at zero strain. The value at zero strain was subtracted from the calibration values, then the calibration values were averaged to find the voltage at the calibration strain.

Finally, the calibration value was divided by the voltage to determine the number of micro strains per volt. This calibration value was determined for all eight of the gauges read by the P3500's.

The strains from the P2100's were calibrated in a slightly different manner. The four gauges read by the P2100's were calibrated by reading approximately 30 seconds of zero values, approximately 15 seconds of positive calibration values, approximately 15 seconds of zero values, and approximately 15 seconds of negative values. This cycle was repeated once. All of the recorded zero values were averaged to find the voltage at zero strains. The voltage at zero strain was then subtracted from the calibration values. The absolute values of the adjusted calibration values were averaged to get the calibration voltage of each strain gauge. The number of strains that was approximated by the stint in the P2100's was 1000 μ strains at a gauge factor of 2.0. The gauge factor of the gauges used was 2.11 and the resistance of the wires was negligible. The number of strains approximated by the stint was therefore the ratio of the assumed gauge factor divided by the actual gauge factor multiplied by the 1000 μ strains stint value. This value was 948 μ strains. This value was then divided by the average calibration voltage to get the relation between voltage and strain.

6.3.4 Preliminary Test and Fixture Redesign

Two preliminary tests were performed to qualify the response of the system. The first test was a trial specimen with the glulam portion of the rail made from douglas fir with the same stiffness as the guardrail specimens. The second preliminary test was performed with an actual rail specimen. Due to the height of the neutral axis of the specimens above the centerline of the pins, which was 132-mm in the original test setup, the two trial specimens experienced arching instead of

bending. This produced the opposite of the desired result in the reaction fixture. The arching action caused compression in the braces, which moved the rear supports away from each other, and caused gaps in the shimmed reaction frame as large as 25-mm. In order to lower the center of gravity of the specimens, the connection pieces were flipped, such that the surface previously bolted to was facing the floor. The angle was cut out to allow for clearance of the beam, steel bars were welded to the outside of the connection specimen to provide additional stiffness, and spacer blocks were fabricated to keep the specimen clear of the angles. The dimensions of this redesign can be seen in Appendix 1. The redesigned fixture can be seen in Figure 6.9:

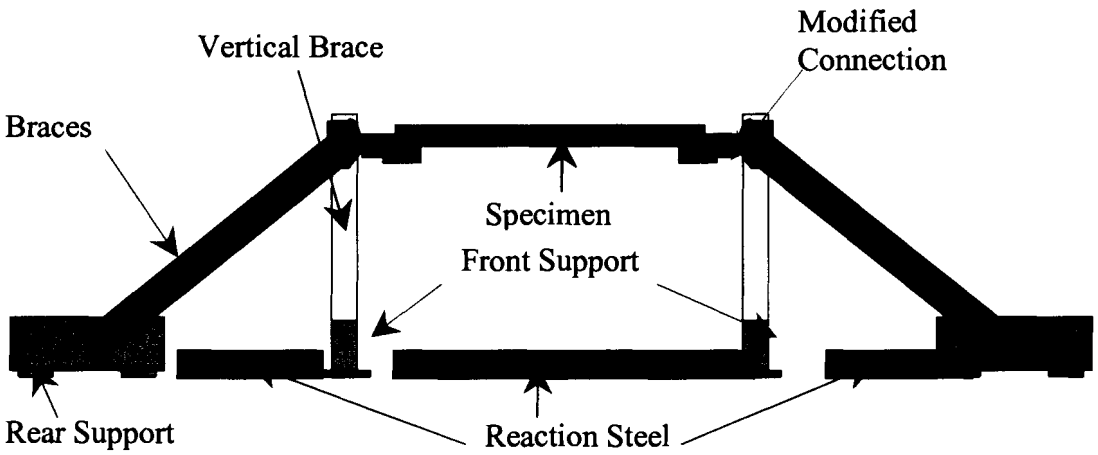

Figure 6.9 Modified Combined Bending and Tension Reaction Fixture

These modifications moved the neutral axis of the beam to approximately 29-mm above the center of the pins. This proved to be enough of a reduction in the eccentricity to eliminate the effect of arching on the system. The restraints did produce tensile forces in the specimens due to the shortening of the guardrail in flexure.

6.4 Testing

A total of three combined bending-tension tests were performed. These tests were performed using the modified bending-tension test fixture. The tests were performed in displacement control with a displacement rate of 13-mm per minute. All bolts were torqued to 136 N-m to reduce slippage in the connection. In all three tests the wood exhibited a tensile failure at between 80 and 95 kN of applied vertical load. The specimens continue to gain load after the tensile failure due to the bolted connection.

6.4.1 Specimen 11 Testing

The first successful test, which was performed on the modified bending tension fixture, was on specimen 11. This test was performed in two separate tests. The fixture had been designed to withstand a maximum applied vertical load of 130 kN and 260 kN of axial load. However, the specimen did not fail under these loads. The first test was stopped when the applied vertical load reached 118 kN with an axial load of 276 kN for safety reasons. The specimen did encounter a tensile lamination failure during the first loading of the specimen at 91 kN of applied vertical load. The fixture was reevaluated for the higher loads and it was deemed safe for the fixture to sustain a vertical load of 178 kN and an axial load of 489 kN. The specimen was retested. In the second test the specimen exhibited a reduced stiffness in the beginning of loading due to the previous partial failure of the wood in tension. However, both loadings did attain a common point in the region where the tensile lamination fails. The load-displacement relation for specimen 11 is displayed in Figure 6.10:

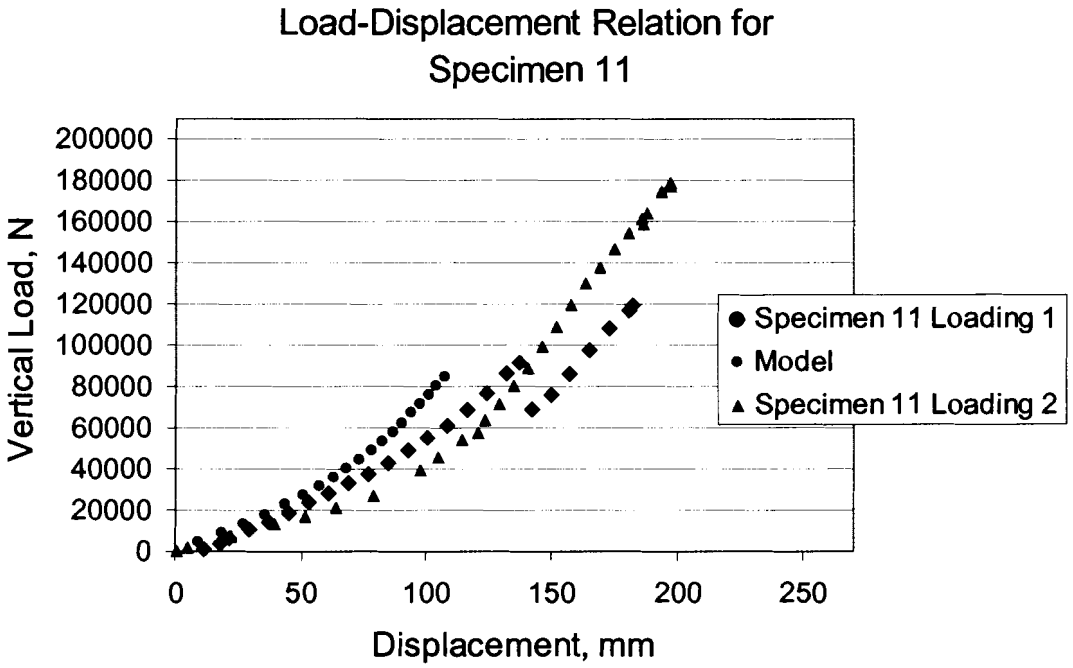

Figure 6.10 Specimen 11 Load-Displacement Relation

The beginning of the curve is the first loading, which continues to the point at which the tensile failure occurs in the glulam at 91 kN. Then the curve drops to the string of points which is separate from the rest of the curve and continues until 119 kN. The second loading is the line of points which continues up to 179 kN and is linear. The failure of the tensile lamination was observed to be a failure of a finger joint at 110-mm from the center. This failure caused delamination of the FRP. The delamination was not a failure of the glulam-FRP bond, however, since several layers of FRP were still attached to the glulam and FPL-1 epoxy. As the load approached the maximum, the FRP at the locations of the bolt holes broke free of the steel-FRP bond and delaminated from the rest of the FRP. This was due to the smaller area in which tension can be developed in the FRP near the bolt holes. When the test was stopped, the position of the actuator was held at a constant position. After 96 seconds, the steel-FRP bond underwent a significant creep relaxation which led to the

load dropping rapidly. The SIA E2119 epoxy has been observed to be prone to creep failures at high loads. (This would not be a factor in an actual guardrail due to the limited duration of the impact loadings.) The applied vertical load to induced axial load relation for specimen 11 is shown in Figure 6.11:

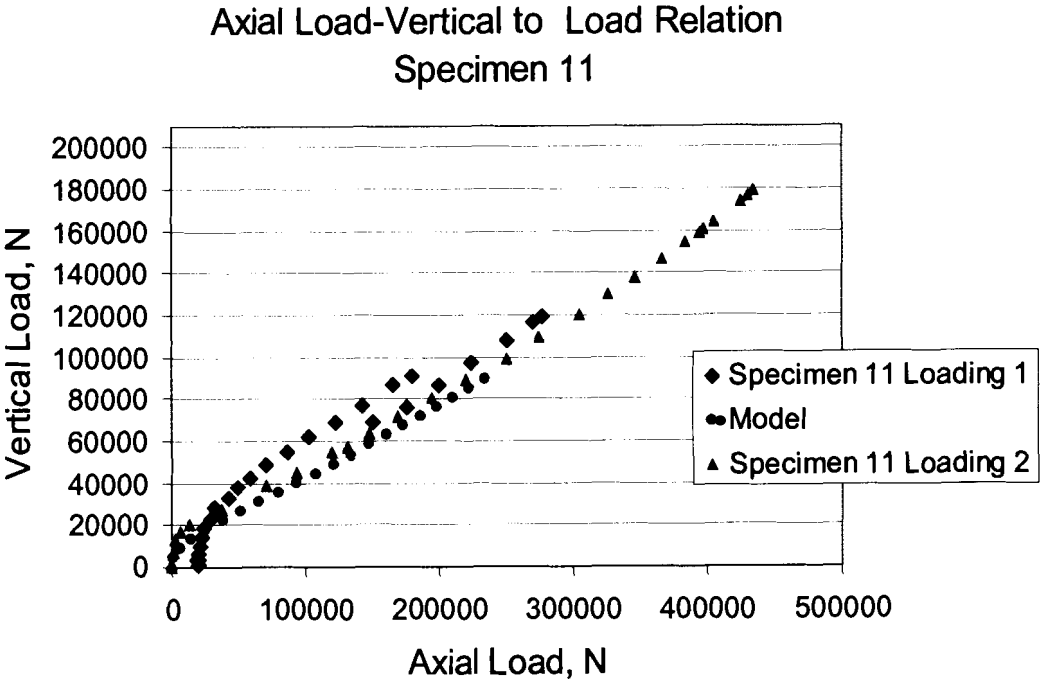

Figure 6.11 Specimen 11 Induced Axial Load to Applied Vertical Load Relation

The maximum axial load induced during the second loading of the beams was 435 kN. Based on the published value of the average elastic modulus of the Gordon Composites GC-67-UB FRP in the fiber direction and under tensile loads, 40 GPa, the maximum stress attained by the FRP was 595 MPa, 62% of the published ultimate capacity. The relationship between applied vertical load and the strains measured in the FRP is shown in the Figure 6.12:

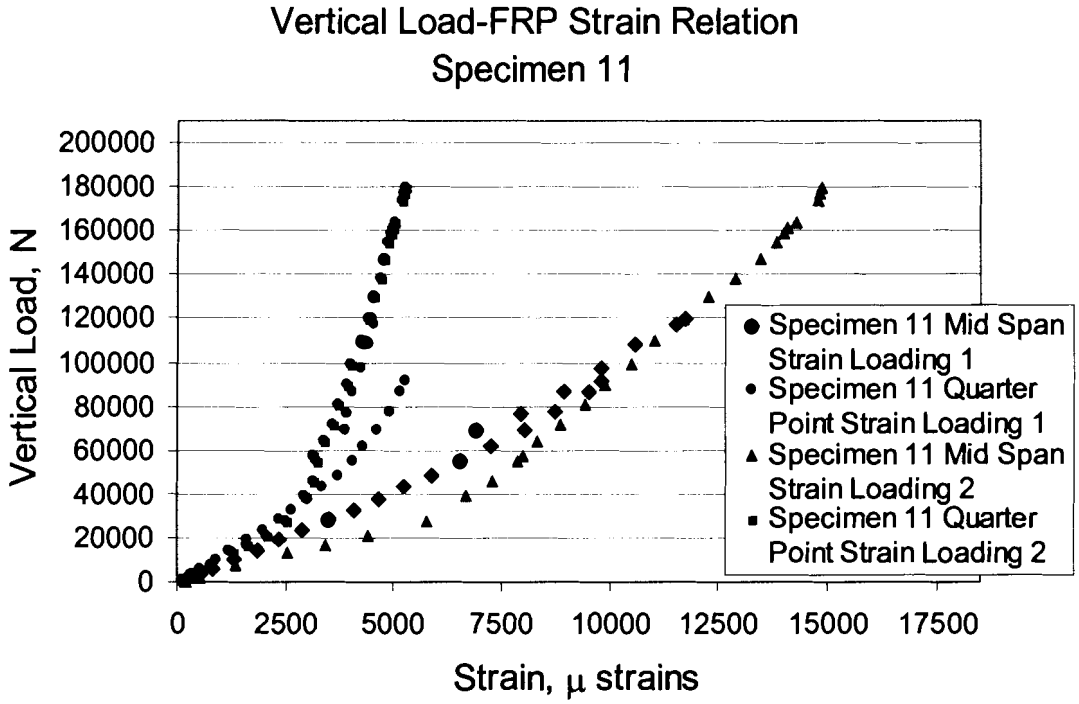

Figure 6.12 Specimen 11 FRP Strain to Applied Vertical Load Relation

The strains in the FRP show a nonlinear behavior. In regions where the tensile lamination in the glulam failed, there are multiple strain values for a given load. Despite the loss of bond between the glulam and the FRP specimen 11 attained a peak applied vertical load of 179 kN, with an induced tensile load of 435 kN. This load was significantly higher than the expected capacity of the system. Further, specimen 11 did not fail under the loads. Despite the creep failure, the specimen was intact and still retained significant capacity.

6.4.2 Specimen 12 Testing

The second combined bending-tension test was performed on specimen 12. The specimen was shimmed and loaded until the applied vertical load was 44 kN. The specimen had not achieved a significant axial load at this point, so the load was removed and larger shims were added to the system to remove the gaps in the system.

The test was then restarted and did develop axial load in the beam. The load-strain relation is similar to the relation on specimen 11 and is shown in Figure 6.13:

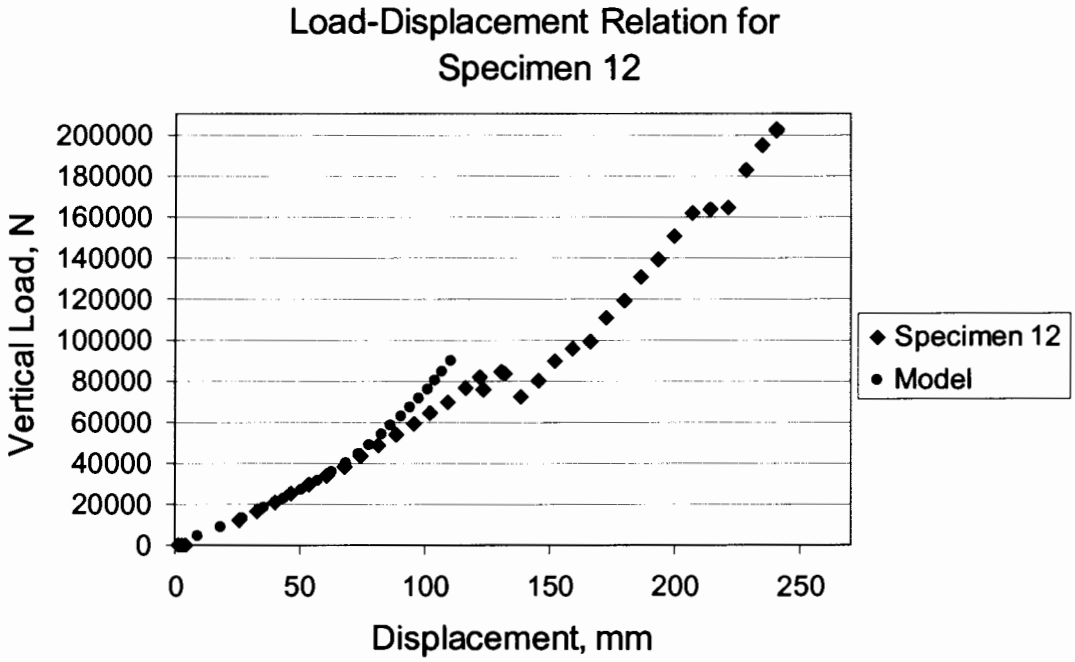

Figure 6.13 Specimen 12 Load-Displacement Relation

The applied vertical load to displacement relationship for specimen 12 is not as smooth as specimen 11. This relation is closer to the specimen 13 than specimen 11 but there is still good agreement between all three tests. The wood encountered a tensile failure at an applied vertical load of 83 kN. The maximum vertical load applied was 202 kN. The maximum axial load induced was 461 kN. The relationship between the applied vertical load and the induced axial load is seen in Figure 6.14:

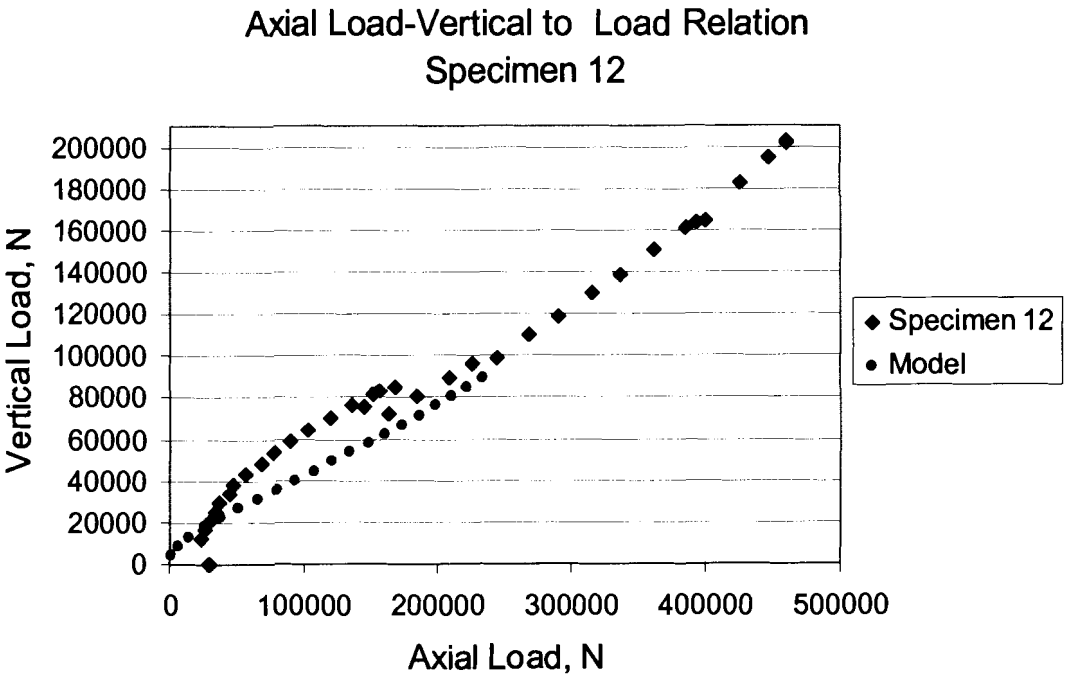

Figure 6.14 Specimen 12 Induced Axial Load and Applied Vertical Load

Figure 6.14 shows that the actual results of the test was closest to the model in the region of the curve after the failure of the tensile laminations. The failure mode of specimen 12 was not the same as specimen 11. The FRP did not delaminate, except inline with the three rows of bolt holes, where the FRP delaminated from the wood and pulled out of the steel-FRP bond. See Figure 6.15:

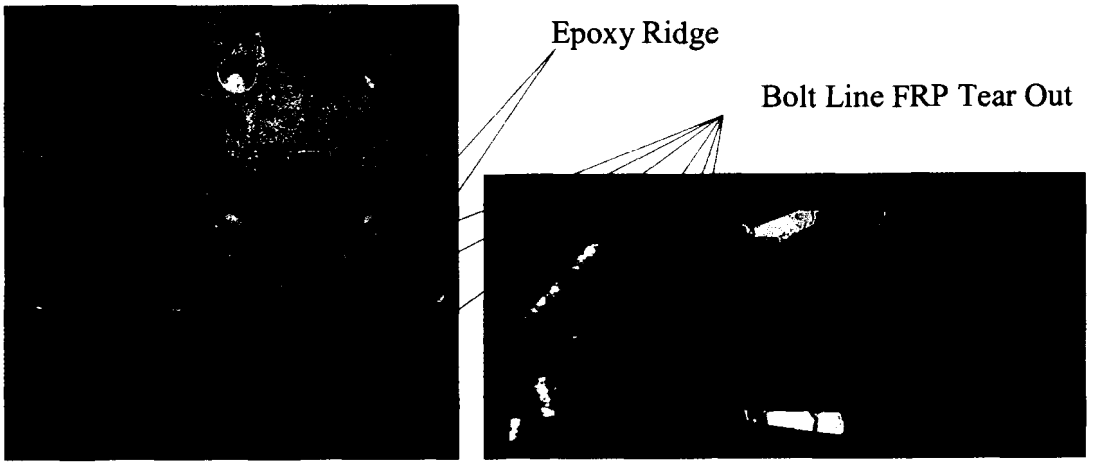

Figure 6.15 Specimen 12 Bolt Line FRP Tear Out

In Figure 6.15 there was a ridge of epoxy created by fabricating the specimen in the alignment fixture. This epoxy ridge moved only in the area of the bolt line, the rest of the epoxy remained in the original position. The applied vertical load to FRP strain relation for specimen 12 was similar to specimen 11 and 13, this relation is seen in Figure 6.16:

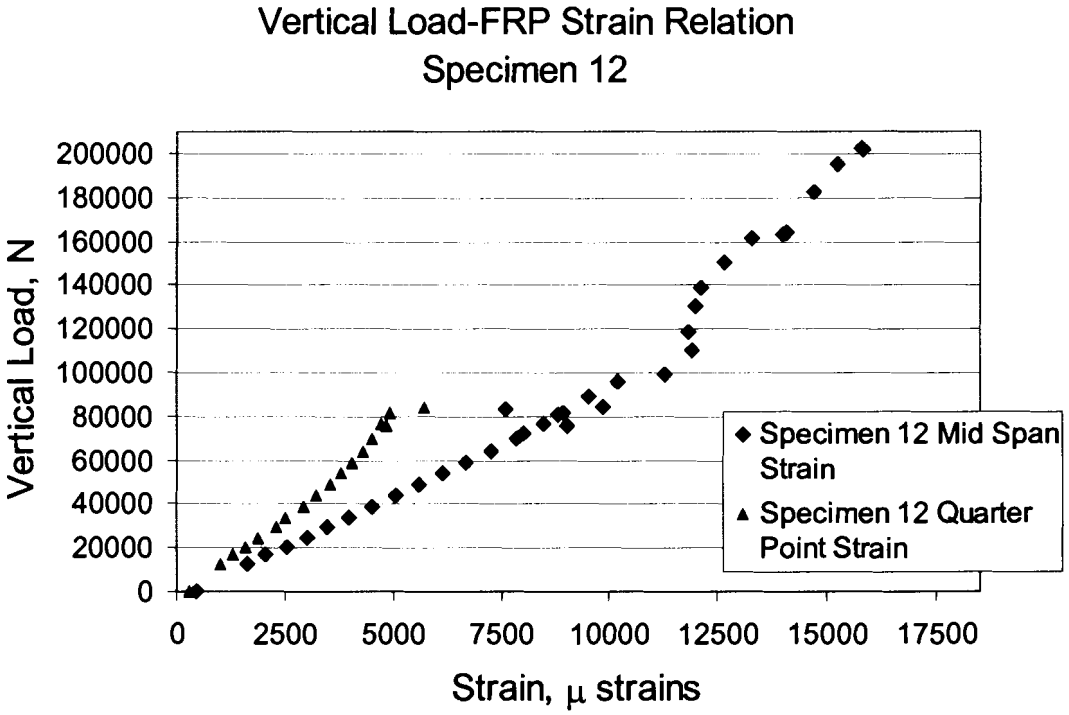

Figure 6.16 Specimen 12 FRP Strain to Applied Vertical Load Relation

The quarter point strain gauges clipped out due to damage encountered during the tensile failure of the glulam. The strains displayed are the average of each pair of strain gauges until one of the gauges is damaged, then the functioning strain gauge values are reported. Based on the published value of the average elastic modulus of the Gordon Composites GC-67-UB FRP in the fiber direction and under tensile loads, 40 GPa, the maximum stress attained by the FRP was 632 MPa, 67% of the published ultimate capacity.

The loads which were applied in this test exceeded the capacity of the reaction fixture, and the modified connections yielded in flexure. This created a slight tilt in the bolted connection area of the reaction frame, as well as elongating the fixture, which required additional shimming for the final test.

6.4.3 Specimen 13 Testing

The third combined bending-tension test which was performed on the modified bending-tension fixture, specimen 13, was different from the other two tests which were performed. However, the results were similar. Due to the yielding in the bolted connection which occurred in the previous test, this test showed limited arching at the beginning of the test. The effects of this yielding can be seen in Figure 6.17:

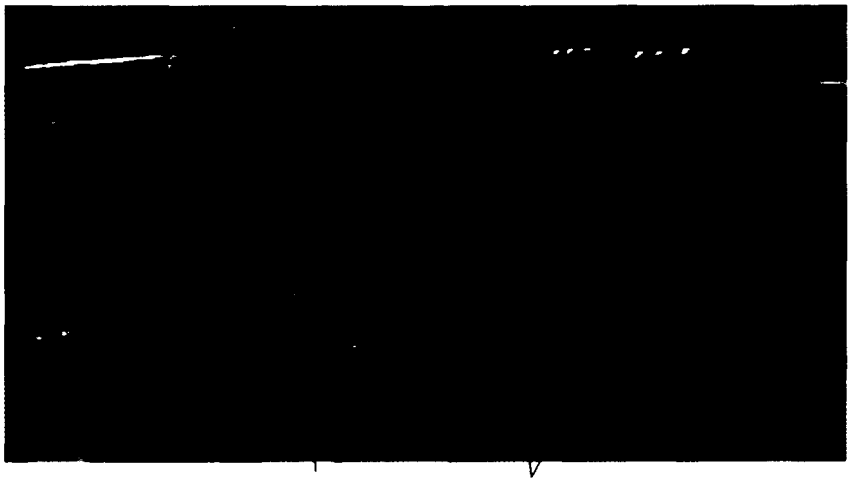

Figure 6.17 Yielded Connection

Due to the yielding in the fixture, additional shimming was needed in the system to remove additional gaps. The three machined shims were used and one of the 13-mm bearing plates was replaced with a 16-mm shim. The load-displacement relation for specimen 13 are displayed in Figure 6.18:

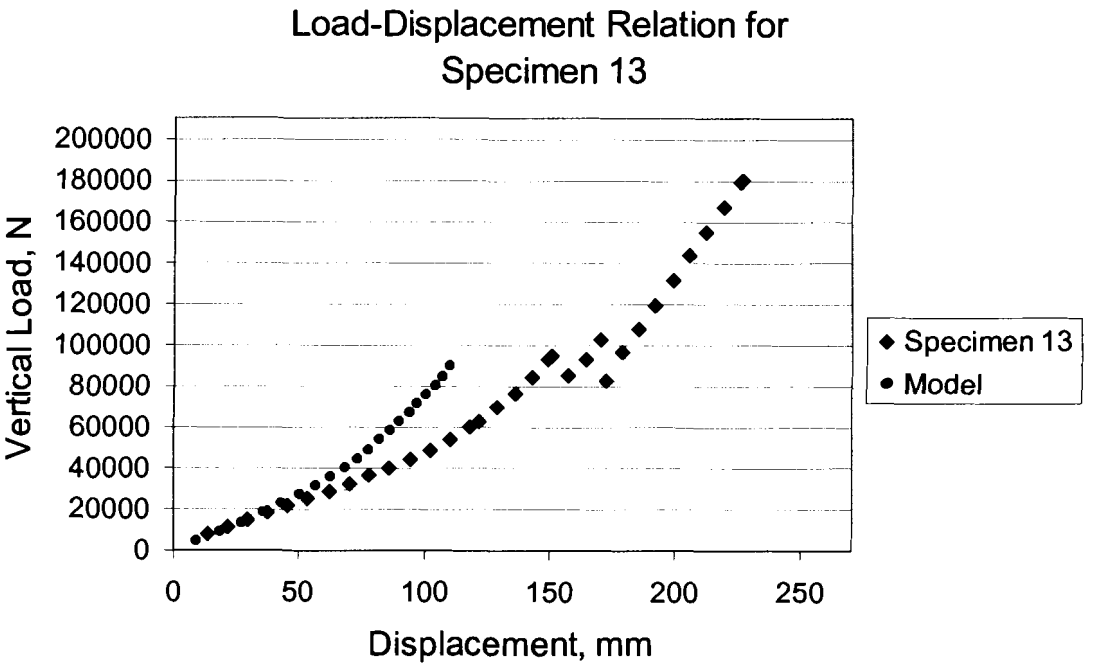

Figure 6.18 Specimen 13 Load-Displacement Relation

Specimen 13 exhibited two tensile failures. The glulam exhibited the first tensile failure at an applied vertical load of 94.5 kN. The second tensile failure in the wood occurred at 102 kN of applied vertical load. However, aside from the double tensile failure the results of specimen 13 are similar to those of specimens 11 and 12. The maximum applied vertical load for specimen 13 was179 kN, which resulted in an induced axial load of 422 kN. The induced axial load to applied axial load relation is shown in Figure 6.19:

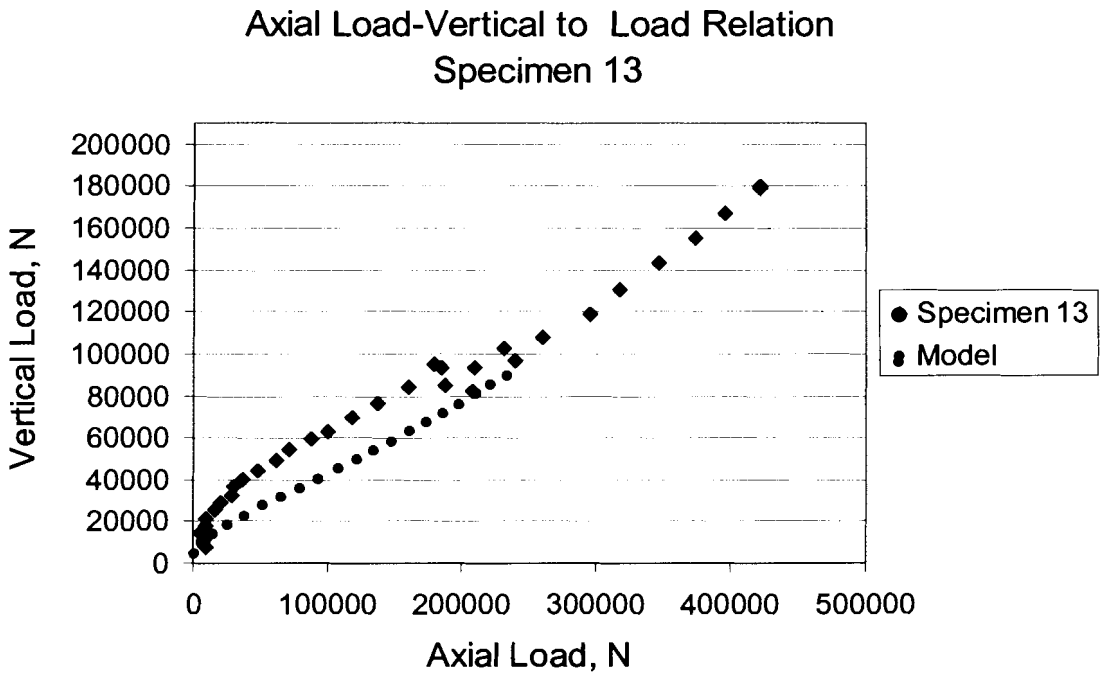

Figure 6.19 Specimen 13 Induced Axial Load to Applied Vertical Load Relation

The effects of the arching in the applied vertical load to induced axial load is evident in Figure 6.19, where the load decreased slightly from the shim induced load and then rose again once the beam had overcome the arching action. With the exception of the beginning of the test, the load-displacement, applied vertical load to induced axial load, and the load strains relations were similar to those of the previous test. Based on the published value of the average elastic modulus of the Gordon Composites GC-67-UB FRP in the fiber direction and under tensile loads, 40 GPa, the maximum stress attained by the FRP was 719 MPa, 76% of the published ultimate capacity. The load strain relation is seen in Figure 6.20:

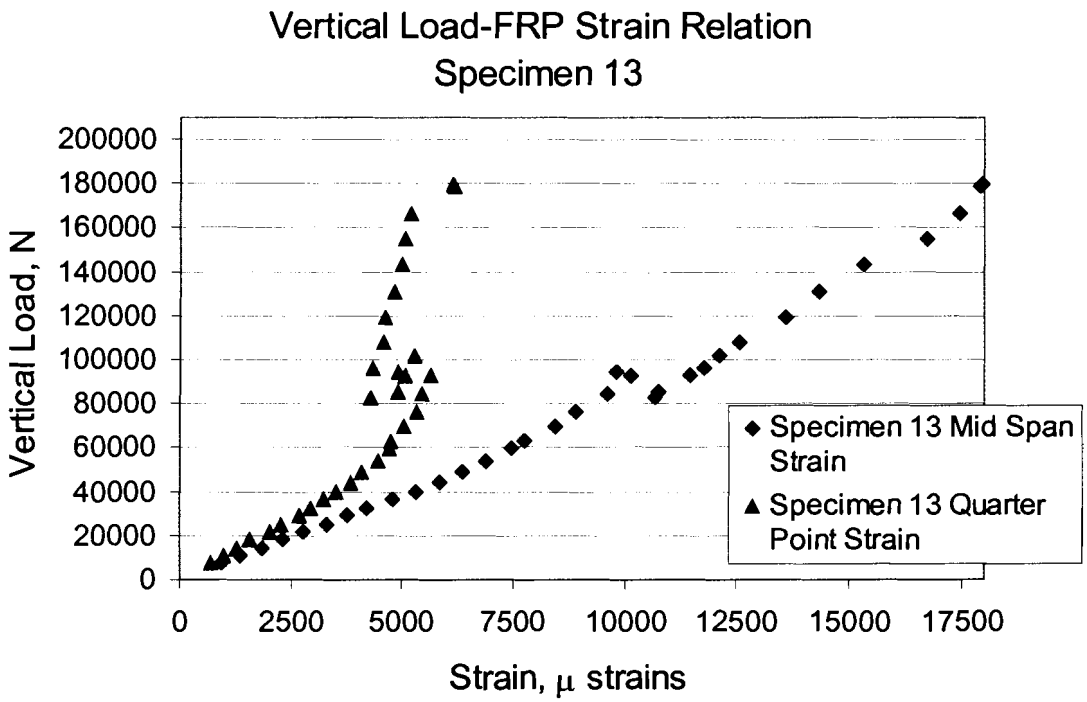

Figure 6.20 Specimen 13 FRP Strain to Applied Vertical Load Relation

Near the end of the test problems were encountered. The load head moved from the center of the beam, approximately 25-mm off center laterally. At the conclusion of the test, the loading frame was visibly tilted at an angle. No explanation was reached for the movement of the load head or the angle of the load frame. The shift in the load head did not greatly affect the response of the beam. However, a strip of FRP, approximately 6-mm, delaminated and detached from the connection on the outside edge of the specimen. This could be a result of the torsion induced in the rail. The FRP in line with all three bolt holes delaminated and pulled out of the steel-FRP bond. This, however, was not observed until the load was removed, see Figure 6.21:

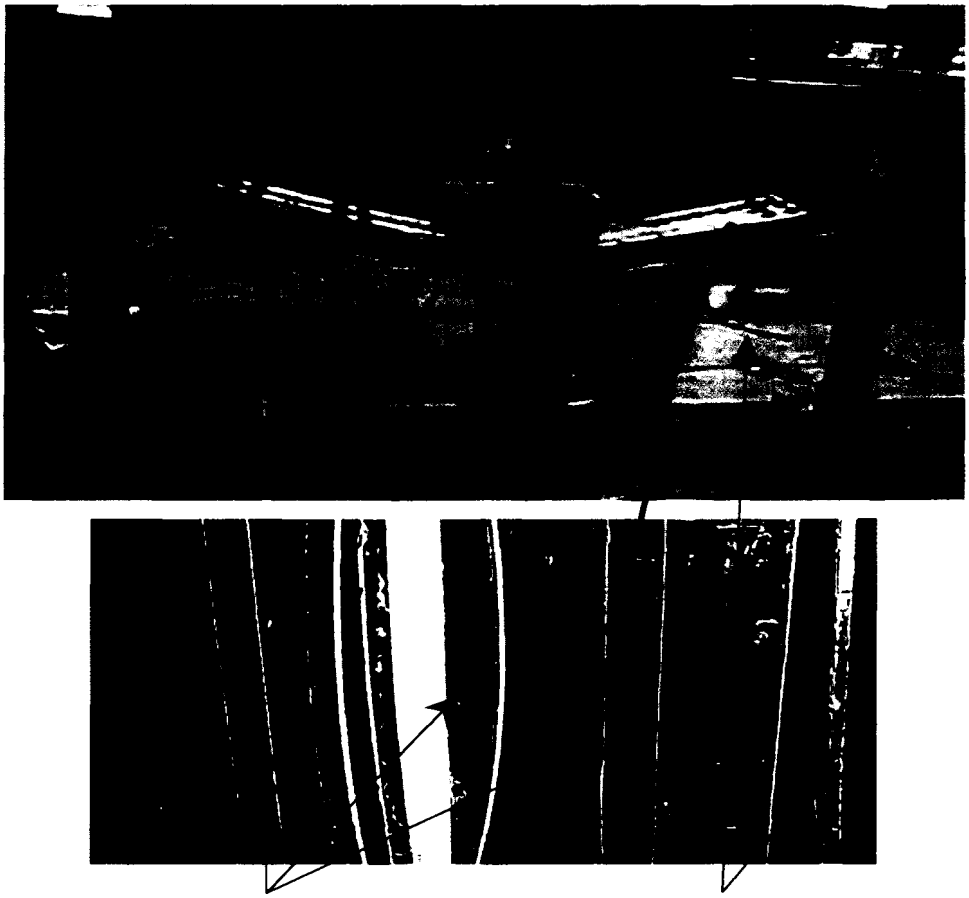

Figure 6.21 Delaminated FRP, Specimen 13

Despite the problem in the application of the load, the test results were similar to those of the previous test. The specimen did not fail under the loads applied.

6.5 Summary and Conclusions

Three successful combined bending and tension tests were performed. None of the specimens failed. All of the specimens were carrying the loads when the tests were halted. All of the tests were terminated due to load limits on the combined bending and tension test fixture. The critical results of the three tests are summarized in Table 4.1. The specimen stiffness is the secant stiffness between the vertical loads of 40 kN and 80 kN which typifies the linear response for all specimens prior to the tensile failure of the glulam.

Specimen	Vertical Load at First Tensile Failure (kN)	Axial Force at a Vertical Load of 170 kN (kN)	Maximum Vertical Load (kN)	Maximum Mid-Span Deflection (mm)	Specimen Stiffnesses (kN/mm)
11	91.2	411.2	179	197	0.3
12	83	417.7	202.2	241	0.42
13	94.5	404.3	179.3	226	0.36

Table 6.1 Results of Combined Bending and Tension Testing

The maximum applied vertical load was 202.2 kN and the resulting axial load of 461 kN far exceeds the anticipated loads on guardrails under impact as estimated using Barrier VII as discussed in Chapter 2. The maximum deflection of the rail between two posts was found from the Barrier VII modeling discussed in Chapter 2, to be 140-mm. The deflections which were endured by the rail sections were in excess of 1.4 times the predicted deflections. The largest deflection, 241-mm, occurred during the test of specimen 12. The deflection of specimen 12 is higher than in the other two tests due to specimen 12 being loaded more than the other specimens which caused yielding of the bolted connections. These tests therefore indicate that the rail system, as designed, has sufficient structural capacity to survive a vehicular impact, which indicates that the reinforced hardwood glulam should perform similarly to the steel W-beam. Additionally, the model predictions compared very well with the test results, which justifies the development of the test fixture and the chosen method of testing.

Chapter 7

SUMMARY AND CONCLUSIONS

7.1 Summary

A reinforced hardwood glulam guardrail system was developed. This guardrail consists of a 254-mm by 76-mm reinforced hardwood glulam reinforced on one face with 3.5-mm of unidirectional E-glass. The properties of the reinforced glulam design were evaluated using transformed section analysis, and the response of the guardrail system under vehicular impact was modeled with Barrier VII (Powell, 1973). The analyses indicate that the barrier deflections and vehicle accelerations are comparable with those of a standard steel W-beam guardrail system, and that tensile forces as high as 240 kN are present at the splice connections of the rail.

In order to carry the large tensile forces between the adjacent rails, a specialized field boltable splice connection was developed. This splice connection relies on a steel plate bonded to the E-glass reinforcement. This bond allows the load to be transferred into the FRP through shear in the steel-FRP bond. SIA Adhesives E2119 epoxy adhesive was chosen to bond the steel to the FRP.

Both the reinforced glulam and splice plate were tested for durability under exterior environmental conditions using the ASTM D1101 test. Through all of the delamination testing there was minimal quantifiable delamination. Both the reinforced hardwood glulam and the splice connection passed the ASTM D1101 test and appear to be suitable for exterior exposure.

Two three point bending tests were performed on the reinforced guardrail sections. The specimens tested in bending both behaved similarly and did in fact demonstrate nonlinear load-displacement response due to compressive yielding which occurred in the wood. The average failure moment for the bending test was 37 kN-m which is 3% less than the predicted yield moment.

The splice connection was tested under eccentrically loaded tension to model the real rail splice connection. The torque load in the bolts played a role in the behavior of the tensile specimens. The minimum bolt torque was predicted to be 54-N-m. Two specimens were tested at the initial bolt torques of 136-N-m, 54 N-m, and 27 N-m. The specimens tested at 136 N-m of initial bolt torque had an average capacity of 463 kN, the specimens tested at 54 N-m of initial bolt torque had an average capacity of 427 kN, and the specimens tested at 27 N-m of initial bolt torque had an average capacity of 383 kN, all of which are greater than the expected tension load of 240 kN.

In addition to tension, it was necessary to test the reinforced glulam guardrail and splice connection under combined bending and tension loading. To apply bending and tension loads simultaneously a specialized fixture was designed that induced tension due to shortening of the rail section under flexure. The fixture was a triangular truss which was bolted to the reaction floor and pin-connected to the splice connection. The truss was designed using 2nd order geometrically nonlinear analysis techniques. Three specimens were tested under combined bending and tension. All three tests were performed with an initial bolt torque of 136 N-m to eliminate slippage from the system. All of the specimens encountered tensile lamination

failures in the wooden glulam. However, the FRP backing did provide additional capacity and ductility. The largest vertical load which was applied was 202 kN, which induced an axial load of 461 kN. None of the specimens failed and all three specimens carried all of the applied loads at the conclusion of the test. The specimens demonstrated capacities in excess of the expected demands predicted from the models of the guardrail systems.

7.2 Conclusions and Recommendations

Testing and simple modeling indicates that the 76-mm deep reinforced hardwood glulam guardrail as designed is structurally sound for use in a guardrail system. Models of the reinforced glulam guardrail section indicate that it would perform similarly to a standard W-beam guardrail. However, further work is required before the system is ready for field implementation. Preservative treatments and their effect on the wood-FRP bond would need to be determined. Also, it may be beneficial to investigate alternate lamination schemes, such as horizontal stacked laminations. These methods are less expensive ways to obtain the 76-mm rail cross-section than the brickwork layup used in this study. A critical parameter which would need to be evaluated is the quality of the wood-FRP bond, which could be adversely affected by the use of horizontally stacked laminations. The cost of the installed reinforced hardwood glulam guardrail is estimated at $115/m. The predicted cost of the reinforced hardwood glulam is significantly less than the $150/m cost of the steel backed timber guardrail. It is recommended that crash testing of the reinforced hardwood glulam guardrail system be pursued once the remaining issues are resolved. It may be possible to reduce the cross-section, splice connection length,

and number of bolts in the splice connection. However, additional modeling would need to be performed to determine the effect of theses changes, as well as additional testing. It is also possible that the splice connection developed in this study has applications for heavy timber tension connections, which could be an additional area of future research.

REFERENCES

AASHTO, (1998). *AASHTO LFRD Bridge Design Specifications, SI Units, Second Edition* (1998). Washington, D.C.: American Association of State Highway and Transportation Officials.

AISC, (2002). *Manual of Steel Construction, Load and Resistance Factor Design*, Chicago: American Institute of Steel Construction Inc.

ASTM (a). (2002). *Standard Test Method for Integrity of Adhesive Joints in Structural Laminated Wood Products for Exterior Use*. ASTM D1101 Baltimore, MD: American Society for Testing and Materials.

ASTM (b). (2002). *Standard Specifications for Adhesives for Structural Laminated Wood Products for Use Under Exterior (Wet Use) Exposure Conditions*. ASTM D2559, Baltimore, MD: American Society for Testing and Materials.

Boone, M. J., (2002). *Mechanical Testing of Epoxy Adhesives for Naval Applications*, Master of Science Thesis, University of Maine.

Calcote, R. and Kimball, C.E. (1978). Properties of Guardrail Posts for Various Soil Types. *Transportation Research Record. No. 679*, pp. 22-25. Transportation Research Board, Washington, D.C.

Chen, C.-J. (1998). Mechanical Performance of Fiberglass Reinforced Timber Joints. In J. Natterer & J.-L. Sandoz (Eds.) *Proceedings of the 5th World Conference on Timber Engineering* (pp. 500-507). Montreux, Switzerland.

Dagher, H. J., and Lindyberg, R. (2003). Development of the AASHTO Specifications for FRP-Reinforced Glulam Beams. *Presented at the 82nd Annual Meeting of the Transportation Research Board.* January 12-16, 2003, Washington, D.C. (CD-ROM)

Drake, R., Ansell, M., Aram, J., Mettem, C., and Bainbridge, R. (1998). Non-Metallic Connections For Timber Structures. In J. Natterer & J.-L. Sandoz (Eds.) *Proceedings of the 5th World Conference on Timber Engineering* (pp. 557-584). Montreux, Switzerland.

Forest Products Lab, (1999). *Wood Handbook: Wood as an Engineering Material*, Madison, WI: Forest Products Lab.

Gordon Composites, Inc. (2001). http://www.gordoncomposites.com/UB_Specs.htm

Komatsu, K. (1998). Glued-in Hardwood Dowels as an Alternative Timber End-Jointing Device. *Otto-Graf Journal*, 9, 135-152.

Lohrey, E. C., Carney, J. F., III, Bullard, D. L., Jr., Alberson, D. C., and Menges, W. L. (1997). Testing and Evaluation of Merritt Parkway Guidrail. *Transportation Research Record. No. 1599*, pp. 40-47. Transportation Research Board, Washington, D.C.

Lopez-Anido, R., Gardner, D. J., and Hensley, J. L., (2001). Adhesive Bonding of Eastern Hemlock Glulam Panels with E-glass/Vinyl Ester Reinforcement. *Forest Products Journal,* 50, 43-47.

Maine Department of Transportation (2002). http://www.state.me.us/mdot-old/project/design/bt920900.htm

Maine Department of Transportation (2003). http://www.maine.gov/mdot/projects-design-old-site/bt1021300.htm

McGuire, W., Gallagher, R. H., and Ziemian, R.D. (2000). *Matrix Structural Analysis, Second Edition.* New York: John Wiley & Sons, Inc.

New York State Department of Transportation (2000). http://www.dot.state.ny.us/cmb/consult/eib/files/ei00022.pdf

NCHRP (1993). *NCHRP Report 350: Recommended Procedures for the Safety Performance Evaluation of Highway Features.* Transportation Research Board. National Research Council. Washington, D.C.

Ogershock, D. (2002). *2002 National Construction Cost Estimator*. Carlsbad, CA: Craftsman Book Company.

Patzner, G.S., Plaxico, C. A., and Ray, M. H. (1998). Effect of Post and Soil Strength on the Performance of a Guardrail Terminal. H. Murakami & J. E. Luco (Eds.) *Proceedings of the 12th Engineering Mechanics Conference* (pp. 170-173). La Jolla, California.

Powell, G. H. (1973). *Barrier VII: A Computer Program for Evaluation of Automobile Barrier Systems* (FWHA Report Number FWHA-RD-73-51). Springfield, VA: U.S. Department of Commerce, National Technical Information Service.

Rosson, B. T., Bierman, M. G., and Rohde, J. R. (1997). Assessment of Guardrail-Strengthening Techniques. *Transportation Research Record. No. 1528,* pp. 69-77. Transportation Research Board, Washington, D.C.

Soltis, L.A., Ross, R. J., and Windorski, D. F. (1998). Fiberglass-Reinforced Bolted Wood Connections. *Forest Product Journal*, 48 (9), 63-67.

Tuan, C. Y., Post, E. R., Ataullah, S., and Brewer, J.O. (1989). Development of Kansas Guardrail to Bridgerail Transition Designs Using BARRIER VII. *Transportation Research Record, No. 1233*, pp. 145-154. Transportation Research Board, Washington, D.C.

APPENDIX

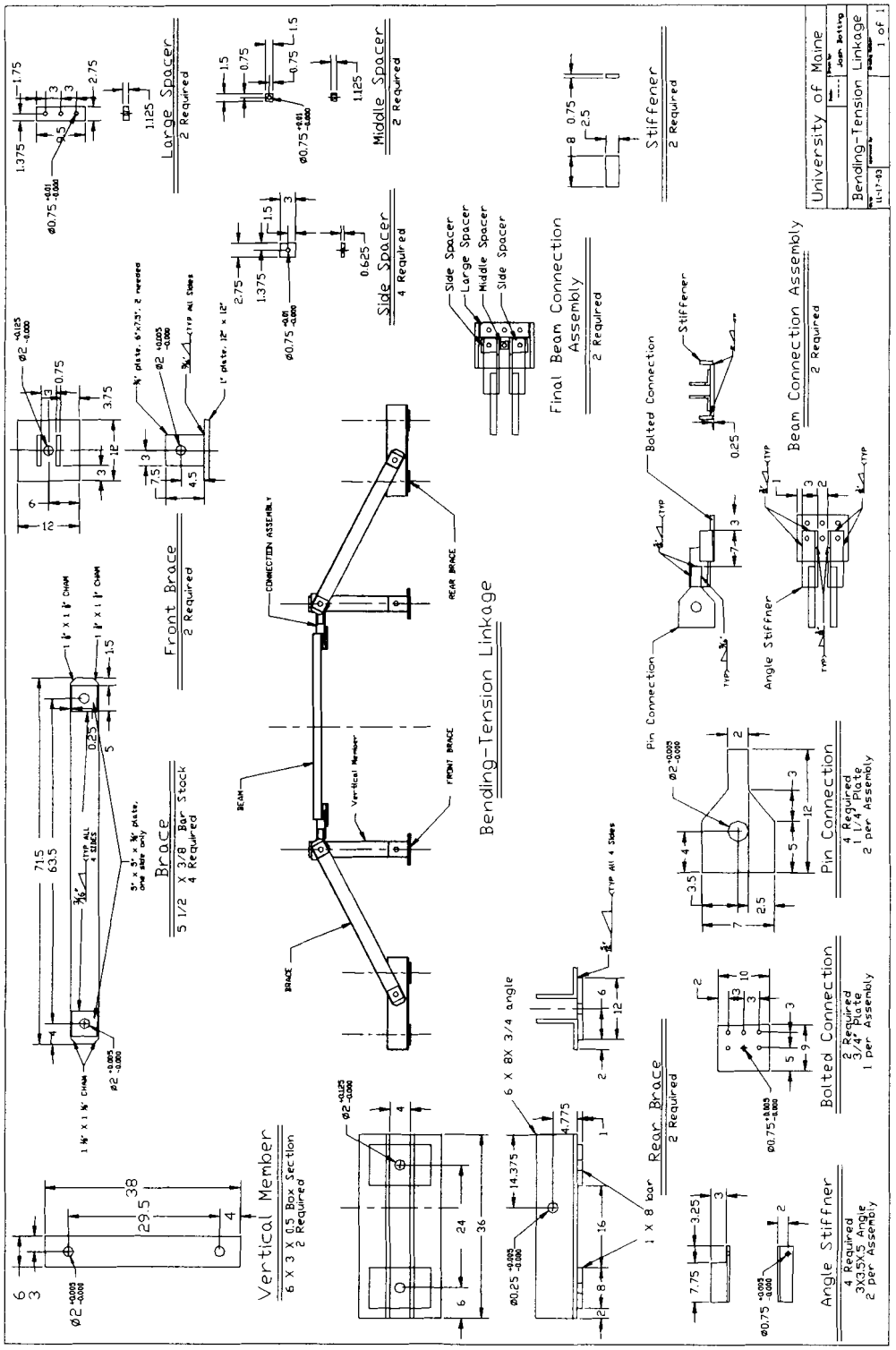

Figure A1 Combined Bending-Tension Linkage

BIOGRAPHY OF THE AUTHOR

Joshua Keith Botting was born on August 6, 1979 in Bangor, Maine. He was raised in Alton, Maine and graduated from Old Town High School in 1997. He then attended the University of Maine and graduated with a Bachelor of Science degree in Mechanical Engineering in May, 2001. During his time at the University of Maine, he was inducted into Pi Tau Sigma, the Mechanical Engineering honor society, as well as Tau Beta Pi, the engineering honor society.

Joshua is a candidate for the Master of Science degree in Mechanical Engineering from The University of Maine in December, 2003.